Trans-Planckian anisotropies in the cosmic microwave background

Nicolaas Ervik Groeneboom
Master's thesis
Institute of Theoretical Astrophysics
University of Oslo
Norway

Acknowledgments

Events were not intended to happen in this order, nonetheless they did. This thesis was seeded during February 2007, originally designed as supplementary lecture notes for a graduate course in cosmology. But things grew out of hand, and suddenly a chaotic primordial thesis script had developed. Hopefully, the primordial part has evolved into something more mature, but I'm afraid the chaotic components are still evident. However, for the likes of me, a manuscript can *never* be thoroughly completed, but rather converges logarithmically to a 100%. And as with all physics, the important thing is knowing when to introduce your cutoff Λ, whether it be 98% or 99.9%. Alas, I feel this cutoff is way too low. We will see more of Λ throughout this thesis. Anyways. There are people to mention.

Øystein Elgarøy: Supervisor. The man behind the idea. Always available, eager, interested, quick-witted and helpful. **Jostein Riiser Kristiansen**: Without this guy I would've been stuck with homotopy theory. For a nice introduction to cosmological software, intuitive descriptions and long discussions about this, that, things and stuff. And coffee. **Øystein Rudjord**: For using his critical hawk eye on sections where I went blind. **Hans Kristian Eriksen**: For not believing in my preliminary results, which were wrong. And nice discussions about likelihoods. **Ingeborg S. Ligaarden**: A silly freckled girl who happens to be my girlfriend. Luckily also a mathematician, albeit female. Endured much cosmological nerdy talk. **Frode Kristian Hansen**: The breakfast at Santemar hotel with that likelihood discussion. **Boudewijn & Vesla Groeneboom**: Gene suppliers.

Contents

0.1 Conventions 1
0.2 Preliminaries from general relativity 1
0.3 Mathematical preliminaries 2

I Introduction **7**

1 Introduction **9**
1.1 Introduction 9
1.1.1 Physical theories 9
1.1.2 Cosmology 10
1.1.3 Trans-Planckian effects 11
1.2 Primary goals 11
1.3 Chapter partitioning 11
1.3.1 Part I: Introduction 12
1.3.2 Part II: Evolving the universe 12
1.3.3 Part III: Trans-Planckian effects 12
1.4 A note on notation 13

2 Cosmology **15**
2.1 The Robertson-Walker metric 15
2.2 The Friedmann equations 16
2.3 De Sitter space 17
2.3.1 Definition 17
2.3.2 Embedding de Sitter space 18
2.3.3 Real-life de Sitter 18
2.4 Conformal time 19
2.4.1 Conformal time during inflation 19
2.4.2 Conformal Hubble parameter 20
2.5 The inflation model 20
2.5.1 The horizon problem 21
2.5.2 The flatness problem 21
2.5.3 The inhomogeneity problem 21
2.5.4 Introductory inflation 21
2.6 Chapter conclusions 22

3 Curved spaces and Symmetries **23**
3.1 Introduction . . . 23
3.2 Conserved currents . . . 23
3.2.1 Symmetries . . . 23
3.2.2 Symmetries in curved spaces . . . 25
3.3 Gauge transformations . . . 25
3.3.1 Introduction . . . 25
3.3.2 An example from QED . . . 26
3.4 The particle concept . . . 27
3.4.1 Flat Minkowski space . . . 27
3.4.2 Curved spaces . . . 28
3.5 The troublesome vacuum . . . 28
3.5.1 In and out mode-solutions . . . 29
3.5.2 The effect of a curved space . . . 30
3.6 Scalar fields . . . 30
3.6.1 Hamilton's principle and the equations of motion . . . 31
3.6.2 Equations of motion for a scalar field . . . 31
3.7 Chapter conclusions . . . 32

II Evolving the universe **33**

4 Inflation in the Robertson-Walker universe **35**
4.1 Giving birth to a universe . . . 35
4.1.1 The epoch of unified forces . . . 35
4.1.2 The epoch of Inflation . . . 36
4.1.3 Inflation consequences . . . 37
4.2 The equation of motion . . . 38
4.3 The slow-roll approximation . . . 40
4.3.1 Introduction . . . 40
4.3.2 The slow-roll parameters . . . 40
4.4 Quantizing a scalar field . . . 41
4.4.1 Fourier expansion . . . 41
4.4.2 Quantizing the harmonic oscillator . . . 42
4.5 Perturbing the inflaton . . . 42
4.5.1 Introduction . . . 42
4.5.2 Perturbing the inflaton . . . 43
4.5.3 Fourier expansion . . . 43
4.5.4 Rewriting to conformal time . . . 44
4.5.5 Bogoliubov-coefficients . . . 45
4.5.6 Horizon crossing . . . 46
4.6 Bunch-Davies vacuum . . . 46
4.7 Chapter conclusions . . . 47

5 Cosmological perturbation theory **49**
5.1 Introduction . . . 49
5.2 The primordial spectrum . . . 49
5.2.1 Gaussianity . . . 50
5.2.2 The power spectrum . . . 50
5.2.3 Harrison-Zel'dovich scaling . . . 51

5.3 Cosmological perturbation theory . . . 52
5.3.1 The decomposition theorem . . . 52
5.3.2 Perturbing the RW metric . . . 53
5.4 Tensor perturbations . . . 54
5.4.1 Golden recipe . . . 54
5.4.2 Solutions to the wave equation . . . 55
5.4.3 Conclusion . . . 55
5.5 The freedom of gauge . . . 55
5.5.1 The Bardeen potentials . . . 56
5.5.2 The Newtonian gauge . . . 56
5.5.3 Synchronous gauge . . . 57
5.6 The co-moving curvature . . . 57
5.6.1 Introduction . . . 57
5.6.2 The power spectrum of $\mathcal{R}$ . . . 58
5.6.3 From $\mathcal{R}$ to Ψ . . . 59
5.7 The Spectral Index . . . 59
5.7.1 Introduction . . . 60
5.7.2 The spectral index . . . 60
5.8 Conclusion and predictions . . . 61

6 Evolving the universe 63
6.1 Introduction . . . 63
6.1.1 The Boltzmann equation . . . 63
6.1.2 Evolving the primordial power spectrum . . . 64
6.2 Post-inflationary events . . . 66
6.2.1 The radiation-dominated epoch . . . 66
6.2.2 The matter-dominated period . . . 66
6.2.3 The cosmological constant-dominated period . . . 67
6.3 The geometry of space . . . 68
6.4 Chapter conclusions . . . 70

III Model testing 71

7 The angular power spectrum 73
7.1 Introduction . . . 73
7.1.1 The cosmic microwave background . . . 73
7.1.2 The Mollweide projection . . . 74
7.2 CMB analysis . . . 74
7.2.1 Spherical harmonics . . . 74
7.2.2 The angular power spectrum . . . 75
7.2.3 Gaussianity . . . 76
7.2.4 Theoretical and observed spectrum . . . 77
7.2.5 Cosmic variance . . . 78
7.3 Interpreting the angular power spectrum . . . 78
7.3.1 Acoustic oscillations . . . 79
7.3.2 The geometry of space . . . 79
7.3.3 The spectral index . . . 79
7.3.4 The baryon density . . . 80
7.3.5 The ISW-effect . . . 80

7.4 Simulating data . . . 81
7.4.1 Introduction . . . 81
7.4.2 The χ^2 distribution . . . 81
7.4.3 Method . . . 82
7.4.4 Results . . . 83
7.4.5 Simulating a map from a power spectrum . . . 83
7.5 Likelihood analysis . . . 84
7.5.1 Gaussian likelihood analysis . . . 84
7.5.2 Maximizing a Gaussian likelihood . . . 85
7.5.3 Cosmological model testing . . . 86
7.6 Software packages . . . 86
7.6.1 CAMB . . . 86
7.6.2 CosmoMC . . . 86
7.7 Chapter conclusions . . . 88

8 Paper review **89**
8.1 Introduction . . . 89
8.2 Note on inflation and trans-Planckian physics . . . 90
8.2.1 Introduction . . . 90
8.2.2 Bogoliubov transformation . . . 90
8.2.3 The adiabatic vacuum . . . 91
8.2.4 Interpretation of the adiabatic vacuum . . . 92
8.2.5 The modified primordial power spectrum . . . 92
8.3 Can MAP and Planck map Planck physics? . . . 92
8.3.1 What to look for . . . 93
8.3.2 Predictions for CMB measurements . . . 93
8.4 Chapter conclusions . . . 94

9 Trans-Planckian effects **95**
9.1 Introduction . . . 95
9.1.1 Generic effects . . . 95
9.1.2 WMAP data and trans-Planckian effects . . . 95
9.1.3 Simulated data and trans-Planckian effects . . . 96
9.2 The nature of the oscillations . . . 96
9.2.1 Introduction . . . 96
9.2.2 Verifying the code . . . 99
9.2.3 Verifying logarithmic oscillations . . . 100
9.3 Behaviour of ΔC_l for ϵ and ξ . . . 100
9.3.1 The behaviour of ΔC_l for varying ξ . . . 101
9.3.2 The behaviour of ΔC_l for varying ϵ . . . 102
9.4 Parameter estimation using WMAP data . . . 105
9.4.1 What to expect . . . 105
9.4.2 Results . . . 106
9.5 Increasing accuracy . . . 107
9.5.1 Results . . . 108
9.6 Parameter estimating with simulated data . . . 110
9.6.1 Adding “perfect” data to CosmoMC . . . 110
9.6.2 Verifying the likelihood code . . . 110
9.7 Estimating parameters for the HW universe . . . 111
9.7.1 Introduction . . . 111

9.7.2 Setup . . . 111
9.7.3 Results: ξ free . . . 112
9.7.4 Results: ϵ free . . . 113
9.7.5 Results: Both ξ and ϵ free . . . 115
9.8 Explaining the results . . . 116
9.8.1 Detailed likelihood analysis . . . 116
9.8.2 2D exact likelihood landscapes . . . 118

10 Conclusions and outlook **121**
10.1 Summary . . . 121
10.1.1 A comment on [1, 2] . . . 121
10.2 Conclusions . . . 122
10.3 Outlook . . . 122
10.3.1 Additional data sets . . . 122
10.3.2 Additional methods . . . 123
10.3.3 Modifying the likelihood algorithm . . . 123

A Self-references **125**
A.1 General notice . . . 125
A.2 Graphs and figures . . . 125
A.3 Code modification . . . 126
A.3.1 Modifying CAMB . . . 126
A.3.2 Modifying code . . . 127
A.3.3 Modifying CosmoMC . . . 127
A.3.4 Likelihood code modifications . . . 127
A.3.5 Additional changes . . . 128
A.4 Independent software . . . 128

B A note on trans-planckian physics **129**
B.1 Initial conditions . . . 129
B.2 The fluctuation spectrum . . . 130

C Can MAP and Planck map Planck physics? **133**
C.1 Parameter relations . . . 133

bibliography **134**

Units, conventions and preliminaries

0.1 Conventions

- A spatial vector **x** is denoted by a bold font lock. Some vectors, like the mode **k**, are denoted without font lock: k. The four-mode k^μ is defined as $k^\mu \equiv (\omega, k)$.
- We use units $\hbar = c = 1$ such that [length] = [time] = [energy]$^{-1}$ = [mass]$^{-1}$.
- The derivative is expressed as $\partial_\mu \equiv \frac{\partial}{\partial x^\mu}$ with respect to given space-time coordinates.
- A map $\phi \in C^k$ denotes that ϕ is continuous and k times differentiable.
- $\dot{x}$ denotes differentiation with respect to time dt, while x' denotes differentiation with respect to conformal time $d\eta$.
- For a covariant quantity Q_μ, $\not{Q}$ denotes the "dotting" with the gamma matrix $\not{Q} \equiv \gamma^\mu Q_\mu$.
- When mentioning the *Lagrangian*, we *always* mean the Lagrangian density, $\mathcal{L}$.
- We use Einsteins summation convention, and sum over all repeated indices: $\sum_0^3 x^\mu x_\mu \equiv x^\mu x_\mu$.
- Operators $\hat{O}$ are expressed without the hat: O.

0.2 Preliminaries from general relativity

These preliminaries are stated without further treatment. For a thorough introduction to general relativity, see [3] or [4].

The space-time of *special relativity* is an important space. It is a place where general relativity has no hold, and the concepts of particles and vacua thrive.

Definition 0.1. *The 4-dimensional **Minkowski** space $\mathcal{M}_4$ is the setting in which the theory of special relativity is formulated. It consists of 3 spatial and 1 time-like dimensions, and is a flat Riemannian manifold with a metric $\eta_{\mu\nu}$ with signature $(-,+,+,+)$ such that the line element is $ds^2 = \eta_{\mu\nu} dx^\mu dx^\nu = -dt^2 + d\mathbf{x}^2$*

Definition 0.2. *The connection coefficients (Christoffel symbols in coordinate basis)* $\Gamma^{\mu}_{\alpha\beta}$ *are defined as*

$$\Gamma^{\mu}_{\alpha\beta} = \frac{1}{2} g^{\mu\nu} \Big(g_{\nu\alpha,\beta} + g_{\nu\beta,\alpha} - g_{\alpha\beta,\nu} \Big)$$

and describes the covariant derivative of the basis coordinates:

$$D_{\mu} e_{\nu} = \Gamma^{\sigma}_{\mu\nu} e_{\sigma} \tag{0.1}$$

The curvature tensor will be important when studying the cosmological perturbations of the metric during inflation.

Definition 0.3. *The* ***Riemann curvature tensor*** *is defined by*

$$R^{\mu}_{\nu\alpha\beta} \equiv \partial_{\alpha} \Gamma^{\mu}_{\nu\beta} - \partial_{\beta} \Gamma^{\mu}_{\nu\alpha} + \Gamma^{\mu}_{\sigma\alpha} \Gamma^{\sigma}_{\nu\beta} - \Gamma^{\mu}_{\sigma\beta} \Gamma^{\sigma}_{\nu\alpha}$$

The ***Ricci curvature tensor*** *is the contracted Riemann curvature tensor*

$$R_{\mu\nu} \equiv R^{\sigma}_{\mu\sigma\nu}$$

The Ricci curvature tensor provides a way of measuring the degree to which the geometry determined by a given Riemannian metric differs from that of ordinary Euclidean 4-space.

Definition 0.4. *The scalar curvature (****Ricci scalar****) of a Riemannian manifold* $\mathcal{M}$

$$R = R^{\mu}_{\mu} \tag{0.2}$$

is a map $\mathcal{M} \to \mathbb{R}$ *that characterizes the intrinsic curvature of the manifold at every* $x \in \mathcal{M}$*. In two dimensions the scalar curvature completely characterizes the curvature of* $\mathcal{M}$*. For dimensions larger than 2, more information is needed.*

Definition 0.5. *A* ***reference frame*** *is defined as a continuum of non-intersecting time-like world lines in space-time. An* ***inertial reference frame*** *is a non-rotating set of free particles.*

0.3 Mathematical preliminaries

The reader is expected to be vaguely familiar with the mathematical context, but most mathematics in use will be revealed as the introduction evolves. Rigorous treatment is omitted, and the reader is advised to engage other sources of literature for a more detailed discussion [5, 6].

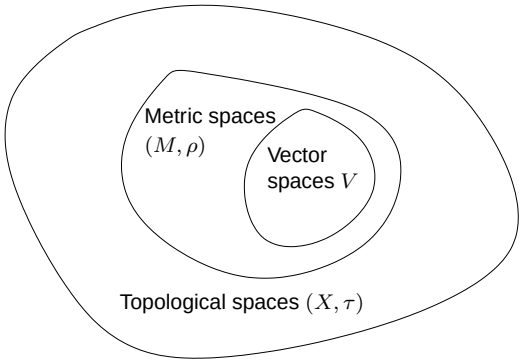

Figure 1: Hierarchy of spaces

The machinery of general relativity acts on spaces that possess the structure of a *metric*. Metric spaces are topological spaces equipped with a distance function. The distance function makes it possible to decide several relations between points in the space. A **topological space** can be thought of as a *set* with a notion of **closeness** of points; this ensures the property of **continuity**. All vector spaces are metric spaces, and all metric spaces are topological spaces, see figure (3.2.1).

Definition 0.6. *A **metric** on a set X is a function $\rho : X \times X \to \mathbb{R}^+$ with the following properties:*

1. $\rho(x, y) = 0$ *if and only if* $x = y$ *(positive definiteness).*
2. $\rho(x, y) = \rho(y, x)$ *for all* $x, y \in X$ *(symmetry).*
3. $\rho(x, z) \leq \rho(x, y) + \rho(y, z)$ *for all* $x, y, z \in X$ *(triangle inequality).*

General relativity acts on metric spaces that behave *nicely*. Space-time should be free of singularities, discontinuous areas and preferably possess smoothness allover. The Riemannian manifold is such a structure.

Definition 0.7. *A **manifold** is a topological space (M, τ) which has the following properties:*

1. *M is Hausdorff (any two points can be separated by two disjoint open sets).*
2. *M has a countable basis for the topology (A **basis** for a topological space τ is a collection B of open sets in τ such that every open set in τ can be written as a union of elements of B).*
3. *Any point $x \in M$ has an open neighbourhood that is locally homeomorphic to $\mathbb{R}^n$.*

Definition 0.8. *Let $\mathcal{M}$ be a manifold and $x \in \mathcal{M}$. Then a **tangent space** is a **real vector space** associated with each $x \in \mathcal{M}$ that intuitively describes all the possible directions a vector can pass through x. The dimension of the tangent space equals the dimension of the manifold.*

Definition 0.9. *A **Riemannian manifold** $(\mathcal{M}, \rho)$ is a real, differentiable manifold where each tangent space is equipped with a continuous inner product ρ. This gives rise to various notions such as curve lengths, volumes, angles and curvatures.*

All manifolds considered in this thesis are Riemannian manifolds. The Minkowski space-time $\mathcal{M}_4$ is especially a Riemannian manifold.

When probing the symmetries of the universe, we will encounter the notion of a *group*. A group can be thought of as a set closed under a reversible binary operation.

Definition 0.10. *A **group** $(G, *)$ is a set G that is closed under a binary operation $*$ such that the following properties are satisfied:*

1. *For all $a, b, c \in G$ we have $(a * b) * c = a * (b * c)$ (associativity of $*$).*
2. *There exist and element $id \in G$ such that for all $x \in G$ then $id * x = x * id = x$ (identity element id).*
3. *For each $x \in G$, there exists an $y \in G$ such that $x * y = y * x = id$ (y is the inverse of x).*

The symmetry groups mentioned in chapter two will mostly be continuous *Lie-groups*, reflecting the non-discrete symmetries of the universe.

Definition 0.11. *A **Lie group** is a group which is a finite-dimensional smooth manifold where the elements are smooth transformations. A Lie group is often represented by matrix algebra.*

The **gauge transformations** are smooth maps between Riemannian manifolds. We will encounter such transformations both in chapter 3 and chapter 5, when discussing cosmological perturbation theory.

Definition 0.12. *A **homomorphism** is a structure preserving map $\phi : A \to B$ such that $\phi(xy) = \phi(x)\phi(y)$. Two groups A and B are **isomorphic** if there exists a bijective homomorphism $\phi : A \to B$. This means A and B are structurally identical.*

Definition 0.13. *A **diffeomorphism** is an invertible C^∞ function that maps one differentiable manifold to another. It can be viewed as an isomorphism of two manifolds.*

Isometries are the elements of the Poincaré-group.

Definition 0.14. *An **isometry** is a distance-preserving isomorphism between two metric spaces. An isomorphism from a space $X \to X$ is called an **automorphism**.*

The Poincaré-group will be important when studying the symmetries of Minkowski space.

Definition 0.15. *The distance-preserving automorphisms (or isometries) of the Minkowski-space defines the **Poincaré-group** $P(1, 3)$. It is a 10-dimensional Lie group, and contains the **Lorentz group** as a subgroup. Another subgroup is the **translation group**, which is abelian.*

Definition 0.16. *The **Lorentz Group** is the (6-dimensional) group of all **isometries** of the Minkowski-space **which leaves the origin fixed**. The Lorentz group is isomorphic to $SL_2(\mathbb{C}) \oplus SL_2(\mathbb{C})$.*

Definition 0.17. *The **de Sitter group** $P(1,4)$ is the group of translations and rotations in five-dimensional Minkowski space. This group is a **minimal extension** of the Poincaré group $P(1,3)$.*

Definition 0.18. *A **generator** of a group G is an element $g \in G$ such that the repeated binary operation $g * g$ spans G. For instance, in the integer group $\langle \mathbb{Z}, + \rangle$ is generated by -1 and $+1$, as any element $n \in \mathbb{Z}$ can be expressed as a sum of $+1$ or -1. For continuous groups, we refer to the **infinitesimal generators** as elements close to the identity that repeatedly generates all the elements in the group.*

Definition 0.19. *A **killing vector field** is a metric-preserving vector field on a Riemannian manifold. Killing fields are the infinitesimal generators of isometries.*

The Riemannian manifolds considered have the following properties:

- Negative Ricci curvature implies there are no nontrivial Killing fields.
- Non-positive Ricci curvature implies that any Killing field is parallel. i.e. covariant derivative along any vector field is identically zero.

Definition 0.20. *The **special orthogonal group** $SO(n)$ is the group of all $n \times n$ orthogonal matrices over real numbers with determinant 1 where the group operation is matrix multiplication. $SO(n)$ is a subgroup of the general linear group $GL(n)$, and is a Lie group.*

Definition 0.21. *The **special unitary group** $SU(n)$ is the group of all $n \times n$ unitary matrices determinant 1 where the group operation is matrix multiplication. $SU(n)$ is a subgroup of the general linear group $GL(n)$, and is a Lie group. The simplest case $U(1)$ corresponds to rotation on the circle $\mathbb{S}^1$.*

Definition 0.22. *A representation of a Lie group G on a vector space V is a smooth group homomorphism $G \to Aut(V)$ from G to the automorphism group of V. If a basis for the vector space V is chosen, the representation can be expressed as a homomorphism into the general linear group $GL(n, K)$. This is known as a **matrix representation**, and means that the Lie group operations can be expressed as matrix operations.*

Definition 0.23. *We define the n-sphere as $\mathbb{S}^n = \{x \in \mathbb{R}^n \,\big|\, |x| = 1\}$.*

Definition 0.24. *A **Hilbert space** $\mathcal{H}$ is a real or complex inner product space that is a Banach space under the norm defined by the inner product. In quantum mechanics, it is the space where the quantum states are defined :*

$$\mathcal{H} = \{|\phi\rangle, |\psi\rangle, \dots\}$$

Definition 0.25. *The **gamma function** $\Gamma : (\mathbb{R} \backslash (-\mathbb{N})) \to \mathbb{R}$ is defined as*

$$\Gamma(n+1) = \int_0^\infty e^{-t} t^n \, dt$$

such that $\Gamma(n+1) = n\Gamma(n)$.

Note that $\Gamma(n) = n!$ for $n \in \mathbb{N}$, while $\Gamma(1/2) = \sqrt{\pi}$.

Part I

Introduction

Chapter 1

Introduction

1.1 Introduction

In this thesis, we are interested in determining whether trans-Planckian effects in the cosmic microwave background are detectable both through contemporary and simulated data. But why are detecting trans-Planckian effects interesting? First of all, any detection of these effects would indicate that *new* physics are at work; the trans-Planckian effects operate on the border of the validity of contemporary physics. If these effects were to be detected, it would revolutionize physics as we know it. *Something new* would actually be happening, something different than all known and well-tested physics, whether it be stringy theories or quantum gravity effects. But how are we to detect these effects?

The trans-Planckian effects are set up during the epoch of inflation, and co-evolve with the universe post inflation. We therefore need to engage the physical theory of cosmological inflation. But physical theories are written in the language of mathematics, so the mathematical language we must speak.

1.1.1 Physical theories

While mathematical structures are universally true, proved rigorously by theorems, lemmas and propositions, the truthness of a physical theory will forever stay uncertain. This is because all physical theories are approximations to reality, and are never a complete description of the system it mimics. If such a theory happens to neatly describe a physical phenomena, it does not rule out the possibility that there might exist other equally correct theories describing the same system, but with a different take on the interpretation.

A physical theory therefore has a space of validity. A complicated theory that has a large space of validity might for certain limits of observables converge to simpler subtheories with smaller spaces of validity. This can be compared to the natural mathematical division of sets into subsets (see figure 1.1). As an example, consider the theory of general relativity, which has a larger space of validity than the more static Newtonian gravity. Newton's theory isn't *incorrect*, but rather inaccurate when describing systems operating with velocities close to the speed of light. But for non-relativistic systems,

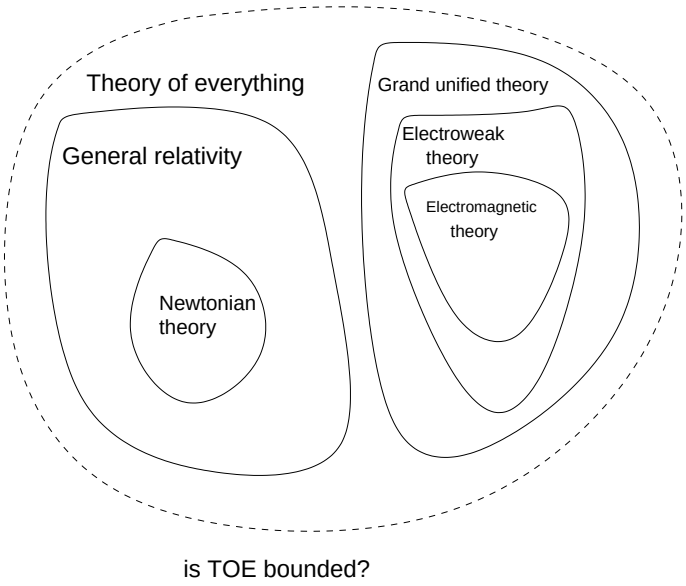

Figure 1.1: Unifying theories

Newton's theory of gravity is perfectly adequate. It can be shown that general relativity converges to the Newtonian limit for low-velocity systems. Eventually, general relativity breaks down for extremely small systems, which marks the boundary of its space of validity.

Another example is the theory of quantum fields and the standard model. This is a theory that describes subatomic systems, and each subsequent experiment performed during the past century has strengthened the theory. But quantum field theory is just a neat approximate description of subatomic systems, it can never incorporate the whole truth. And it can never be proved. As with Newtonian gravitational theory (and general relativity), QFT breaks down on energy scales larger than the Planck scale. From a few eV to a couple GeV, we know the standard model to be a correct, but not necessarily unique description of subatomic events. But what lies beyond is yet uncertain. It is possible that certain string theories that converge to QFT in low-energy limits might suggest an answer, but nothing is certain yet, string theories are still considered to be pure speculations.

1.1.2 Cosmology

Another successful physical theory is the concordance model of cosmology. The preferred model of today is the ΛCDM-model, a model where the universe is homogeneous and isotropic with dynamics determined by dark matter and vacuum energy (Λ). Again we press that ΛCDM is a physical model - it does *not* incorporate the whole truth of the real-world universe, but is the *simplest* theory that *most correctly* explains the effects we observe in the universe as today. And this does *not* mean that it is the only model that fits. The ΛCDM-model is a phenomenological model, designed *after*

observations, and is not based on any fundamental physical principle.

A successful model for explaining problems in standard cosmology is the model of **inflation**. During inflation, the universe is supposed to have undergone a rapid, extreme accelerated expansion of space. Whether inflation actually happened has not been decided, but it is the simplest model that solves several previously unresolved problems in a swift, effective and beautiful manner. But an even more important consequence from the theory of inflation is that it presents a mechanism that will eventually give rise to the observed anisotropies in the cosmic microwave background and matter densities observed today. In other words, it is a link that will enable us to compare observations with theory. We will investigate the properties of the inflaton field, its influence on structure formation and ultimately, how to compare theory with observations. The most important observational quantity will turn out to be the *angular power spectrum*, an object that will incorporate statistical information about the parameters used to describe the cosmic microwave background.

1.1.3 Trans-Planckian effects

The power spectrum mentioned in the previous subsection is set up during the epoch of inflation. The "standard" inflationary model sets up what is called a *flat* power spectrum (Harrison-Zel'dovich scaling), which translates into a near-constant primordial power spectrum. These are the assumed initial conditions for today's universe. But the epoch of inflation operates closely to orders of the Planck-scale - which suggests that there *might* exist additional effects initiated by unconfirmed theories, for instance stringy ones, that will modulate the scale-free primordial power spectrum. In this thesis, we assume that a string theory model known as the *Horava-Witten* model has modified the primordial power spectrum to include small oscillations. We will present the necessary tools for determining these modulations, and will modify and employ modern computational packages to determine whether these modulations are detectable with today's and tomorrow's technology.

1.2 Primary goals

We define *three* primary goals:

Primary goal 1.1 (PG1)**.** *Determine the the primordial spectrum of energy density fluctuations during the period of inflation and discuss the standard theoretical cosmological model of today.*

Primary goal 1.2 (PG2)**.** *Modify standard cosmological software to enable calculations of trans-Planckian models*

Primary goal 1.3 (PG3)**.** *Analyze and compare model results with current data and simulated "perfect" data*

1.3 Chapter partitioning

The thesis is partitioned into *three* parts with a total of *nine* chapters.

1.3.1 Part I: Introduction

Chapter 1 is an introduction to the workings of the thesis.
Chapter 2 contains a quick repetition of modern cosmology. The reader is expected to be familiar with the concepts, and most results will be stated without proof. This chapter does not affect any of the primary goals, and can be skipped by experienced readers.
Chapter 3 discusses the topics of symmetries, conservation laws, gauge theories, particle/vacuum concepts and the differences between flat and curved spaces. This chapter is intended to be more phenomenologically than analytical, as most derivations are omitted. This chapter contains crucial concepts concerning **PG1**.

1.3.2 Part II: Evolving the universe

Chapter 4 presents a thorough derivation of how the postulated inflaton field behaves in a curved space, especially in the Robertson-Walker background. The chapter culminates with the definition of the Bunch-Davies vacuum. This chapter ensures the detailed theoretical background for achieving **PG1**.
Chapter 5 concerns cosmological perturbation theory. An expression for the power spectrum in a RW background is established, and the mechanics of scalar perturbations are developed. The chapter ends with bridging theory with observations by investigating the properties of the co-moving curvature scalar and defining the spectral index. This chapter concludes **PG1**.
Chapter 6 gives a quick introduction to post-inflationary events in the universe. The most important effects from the radiation-dominated, matter-dominated and cosmological constant-dominated epochs are discussed. This chapter does not directly affect any of the primary goals.

1.3.3 Part III: Trans-Planckian effects

Chapter 7 gives an introduction to the anisotropies in the cosmic microwave background, tools for cosmological data analysis and a rough introduction to likelihood analysis. A method for generating data is presented, and the most common software packages are mentioned. This chapter does not directly affect any of the primary goals.
Chapter 8 reviews various papers concerning trans-Planckian effects in the cosmic microwave background. An argument for a modified power spectrum including a Planck-cutoff scale is discussed, and gives a basis for the numerical analysis in the following chapter. This chapter is a bridge between theory and observations, and is a build-up for **PG2**.
Chapter 9 Cosmological software is modified and comparisons between models are performed. The validity of the modulated power spectrum is considered, and WMAP data are ruled out for determining trans-Planckian effects. A perfect data set is generated, and CosmoMC is modified to employ this new data set. Simulations are performed in order to determine the original input parameters. We continue by investigating the properties of the exact likelihood functions for the modulating input parameters, and conclude the thesis with a summary and outlook. This chapter concludes **PG2** and **PG3**.

1.4 A note on notation

Each chapter begins with a short introduction to the subject in question. A chapter is partitioned into several sections, and each section is presented with a *section goal* (Except introduction/conclusion sections, which have trivial goals) . The section goal is intended to motivate the reason for including the section, will eventually lead to fulfilling the primary goals. The reader is advised to consider the section goals and determine whether to read or not. Each chapter ends with a concluding section where a series of conclusions and predictions will be presented.

Important parts of the thesis will be presented as *theorems*. Most theorems will have proofs omitted, and the reader is referred to another source. Examples are Noethers theorem or the fundamental theorem of vector calculus. Other theorems containing proofs will often be linked to a *lemma*. The lemma is a helping-theorem. Direct consequences of theorems give rise to *corollaries*, while smaller theorems are called *propositions*. Text that is *emphasized* is written in *italic* font lock. **New terminology** is introduced in **bold** font lock.

This thesis is written on a Thinkpad X41 model 2525 using Ubuntu 7.04 (Feisty Fawn). The latex package is pdfTeXk, version 3.141592-1.40.3 (Gutsy Gibbon alpha). All plots are created in Gnuplot or Matlab, except plot 9.5 from [7]. All figures are created in xfig and gimp.

Chapter 2

Cosmology

Cosmology is the theory that mathematically describes the evolution of the universe. In this chapter a quick review of the basics of modern cosmology is presented. No explicit derivations will be performed, and the reader is expected to be familiar with most aspects of this section.

Unless otherwise stated, the contents of this chapter is based on [8], [9] and [4].

2.1 The Robertson-Walker metric

Section goal 2.1.1. *Establish the Robertson-Walker (RW) line element*

The simplest background for the universe is the Robertson-Walker metric. Later, more general metric spaces will be considered. Inflation takes place in a RW universe called de Sitter space. This will be our starting point.

Definition 2.1. *A fluid is considered to be **homogeneous** if its mass density is uniform. **Isotropy** is the property of being independent of direction.*

On scales corresponding to large galaxy clusters, the universe is assumed to be spatially homogeneous and isotropic. We introduce an expanding frame of reference with the line element

$$ds^2 = -dt^2 + a(t)^2\big[d\chi^2 + r(\chi)^2 d\Omega^2\big]$$

where $d\Omega$ is the **solid angle**, $a(t)$ is the **scale factor** and t is the **cosmic time**. For standard clocks at rest with proper time τ in the expanding system, $d\chi = d\Omega = 0$ and $ds^2 = -d\tau^2 = -dt^2$, hence $dt = d\tau$. Using Cartan formalism[4] by introducing an orthonormal basis, we obtain:

Theorem 2.2. *The Robertson-Walker (RW) line element*

$$ds^2 = -dt^2 + a^2(t)\big[\frac{dr^2}{1-kr^2} + r^2 d\Omega^2\big] \tag{2.1}$$

is an exact solution of the Einstein field equations

$$E_{\mu\nu} = 8\pi G T_{\mu\nu} \tag{2.2}$$

for a homogeneous, isotropic and expanding/contracting universe provided $a(t)$ and k satisfy the Friedmann equations (see section 2.2). Here, $E_{\mu\nu}$ is the Einstein curvature tensor and $T_{\mu\nu}$ is the energy-momentum tensor. The Robertson-Walker line element is the unique line-element for a homogeneous and isotropic space.

For a detailed derivation of these equations, see [4]. Now

$$dr = \sqrt{1 - kr^2}d\chi$$

and $r = \{\sinh\chi, \chi, \sin\chi\}$ for open, flat or closed universes respectively. We will only consider a flat universe, as recent observational data confirms the near-flatness of our universe (if, and only if the Hubble constant is correctly measured to be around $h = 0.72 \pm 0.08$, where $H_0 = 100h^2(\mathrm{km/s})/\mathrm{Mpcs}$ [10]).

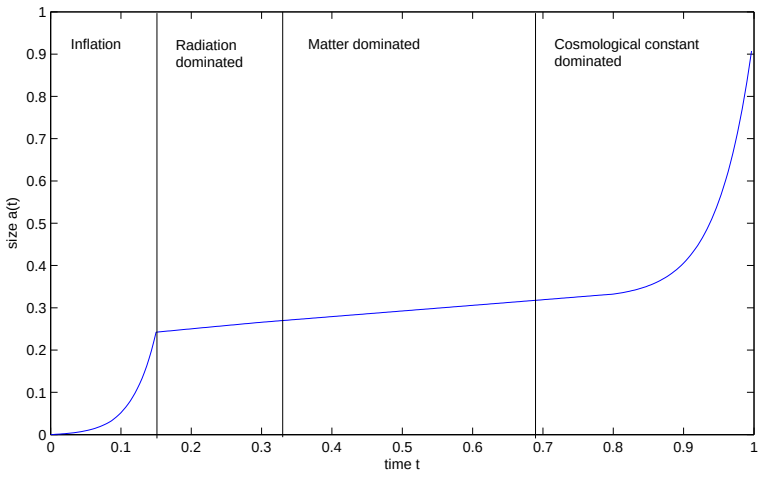

Figure 2.1: A schematic diagram of the scale factor $a(t)$ during different epochs of the ΛCDM model. $t = 0$ represents the beginning of the universe, while $t = 1$ represents today.

2.2 The Friedmann equations

Section goal 2.2.1. *Establish the Friedmann equations.*

We start by making an assumption:

Definition 2.3. *The equation of state of a perfect fluid is characterized by a dimensionless number w such that the pressure p and energy density ρ are proportional:*

$$p = w\rho$$

The Cartan formalism gives rise to two independent equations. These are summarized as the **Friedmann** equations with an equation of state $p_i = w_i \rho_i$:

$$\mathbf{F1}: H^2(t) = H_0^2\Big(\Omega_r(1+z)^4 + \Omega_m(1+z)^3 + \Omega_k(1+z)^2 + \Omega_\Lambda\Big)$$

$$\mathbf{F2}: \frac{\ddot{a}}{a} = -\frac{4}{3}\pi G \sum_i \rho_i(1+3w_i)$$

$$\mathbf{F3}: \dot{\rho}_i = -3H\rho_i(1+w_i)$$

where $\sum \Omega_i = 1$ for a flat universe. Note that any two of the equations can be combined to produce the third. The Friedmann equations **F1** and **F2** follows from the Einstein-equations assuming a homogeneous and isotropic universe, while **F3** follows from $D_\nu T^{\mu\nu} = 0$. A nice derivation of the Friedmann equations can be found at [11].

Definition 2.4. *The **critical density***

$$\rho_{c0} = \frac{3H_0^2}{8\pi G}$$

is the energy density of a spatially flat universe with no cosmological constant.

Definition 2.5. *The **Hubble parameter** is defined as*

$$H \equiv \frac{\dot{a}}{a}$$

and describes the rate of expansion of the universe.

Definition 2.6. *The **co-moving particle horizon** is the maximum co-moving distance from which particles can have travelled to the co-moving observer in a given time t since the beginning the the universe:*

$$d_{ph} = \int_0^t \frac{dt'}{a(t')}$$

*This definition assumes a **flat** universe.*

2.3 De Sitter space

Section goal 2.3.1. *Introduce de Sitter space and give a graphical illustration.*

2.3.1 Definition

Assume a universe dominated by a cosmological constant Λ. Then **F1** reads

$$H^2(t) = H_0^2\Omega_\Lambda$$

and the scale factor can trivially be found to be

$$a(t) = e^{H_0(t-t_0)}$$

This enables an exponential expansion of the universe, given by the expansion factor H_0. Note that this scale factor doesn't have a solution for $a(t) = 0$ unless $t \to -\infty$.

Definition 2.7. *The n-dimensional **de Sitter** space is the vacuum solution to Einstein's field equations with a cosmological constant. The de Sitter space has constant-curvature, and is the Lorentzian analog of an n-sphere.*

The isometry group of de Sitter space is the Lorentz group $O(1, n)$. The metric therefore has $n(n+1)/2$ independent Killing vectors and has constant positive curvature.

2.3.2 Embedding de Sitter space

Topologically, de Sitter space is homeomorphic to $\mathbb{R}\times\mathbb{S}^{n-1}$, or $\mathbb{R}\times\mathbb{S}^3$ in 4 dimensional space. One can think of the de Sitter space as a n-dimensional expanding sphere $\mathbb{S}^{n-1}$ propagating in a straight time-like dimension $\mathbb{R}$.

Example 2.8. *Assuming a de Sitter universe with only one spatial dimension, the shape of space can be embedded as a cylinder $\mathbb{S}^1 \times \mathbb{R}$ (See figure (2.3.2)).*

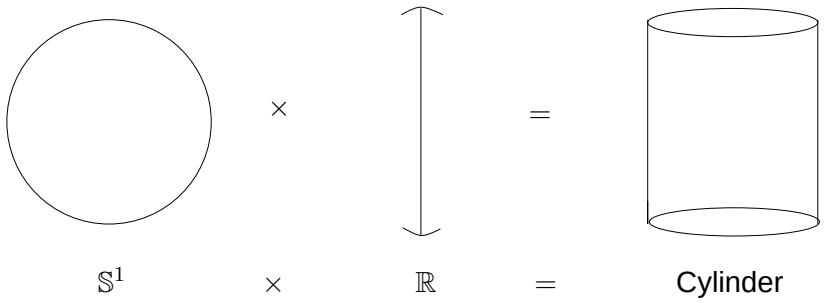

Figure 2.2: An illustrative example: The de Sitter space in 1 spatial dimension can be thought of as a cylinder, where the time-like dimension is $\mathbb{R}$

2.3.3 Real-life de Sitter

The accelerated expansion in the current stage of our universe is most likely due to a cosmological constant, which is believed to couple to the non-vanishing energy expectation value of the vacuum. A positive cosmological constant corresponds to negative pressure, causing the scale factor a to increase exponentially. When calculating the expectation value of the vacuum energy quantum mechanically, the expressions diverge. This is fixed by regularizing the equations, yielding a finite (but very large) vacuum expectation value. However, the observed cosmological constant is very small, giving a total of 120 orders of magnitude difference between theory and observations. This is still an unsolved problem in physics today [11].

The de Sitter space is also the background space in the theory of inflation. Postulating that the primordial universe was filled with a scalar field possessing the same properties as a cosmological constant enables an accelerated expansion of space. This is done by assuming that the scalar field must be invariant under any Lorentz transformation, or that the energy-momentum tensor is proportional to $g_{\mu\nu}$. For the energy-

momentum tensor for a perfect fluid

$$T_{\mu\nu} = (p + \rho)u_\mu u_\nu + p g_{\mu\nu}$$

to be proportional to $g_{\mu\nu}$, the first term must vanish. This gives rise to an equation of state with $w = -1$, and $p = -\rho$. When this equation of state is inserted into **F3**, we find that $\ddot{a} > 0$, which describes an accelerating scale factor.

2.4 Conformal time

Section goal 2.4.1. *Define the concept of the conformal time η.*

It is sometimes useful to introduce a different concept of time. Later, when we explicitly solve the equations of motion for a scalar field in the RW metric, we will see much use of this notion. We first state a formal definition:

Definition 2.9. *A **conformal transformation** of a metric $g_{\mu\nu}$ is a transformation that is invariant to the geometry of the space-time manifold*

$$g_{\mu\nu}(x) \to C^2(x) g_{\mu\nu}(x)$$

***Conformal symmetry** is a symmetry under dilatation (scale invariance), and conformal transformations especially preserve angles.*

Definition 2.10. *The **conformal time** η is defined to be the co-moving distance of the particle horizon at a given time t:*

$$\eta = \int_0^t \frac{dt'}{a(t')}$$

or $a^2(\eta)d\eta^2 = dt^2$. This gives rise to a line element on the form

$$ds^2 = a^2(\eta)\big(- d\eta^2 + dx^2)$$

which is manifest conformally flat.

Note that the definition assumes a *flat* universe.

2.4.1 Conformal time during inflation

Space-time is de Sitter during inflation, with scale factor $a \propto e^{H_0 t}$. We wish to define a model in where the universe begins when $\eta \to -\infty$. At this stage, $a(\eta) = 0$. When inflation ends ($\eta = 0$), the scale factor should have grown to a healthy size of $a(\eta = 0) = 1$. We therefore use a slightly modified version of the conformal time

$$\eta = \int_{t_e}^t \frac{dt'}{a(t')} = \frac{1}{H_0 a(t)}\Big(\frac{a(t)}{a(t_e)} - 1\Big)$$

where $a(t_e) = a(\eta_e) = a(0) = 1$ is when inflation ends. We solve for the scale factor $a(\eta)$ and find

$$a(\eta) = \frac{1}{1 - H_0\eta} \tag{2.3}$$

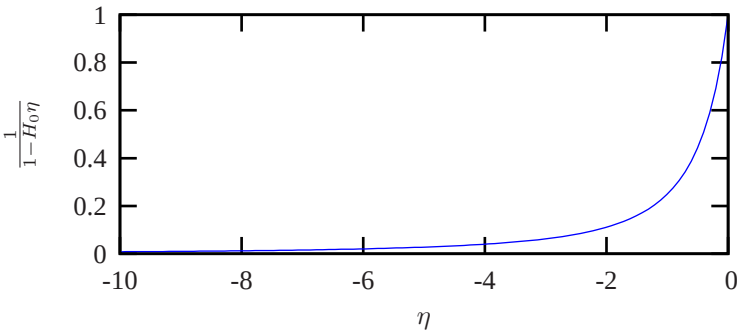

Figure 2.3: The modified scale factor $a(\eta)$ for the de Sitter space

This equation diverges for $\eta = 1/H_0$, but this happens *after* inflation, where space is no longer de Sitter. In the limit where $\eta \to -\infty$, we can approximate the scale factor to

$$a(\eta) \approx -\frac{1}{\eta H_0} \tag{2.4}$$

Later, we'll see that space-time is essentially Minkowski in this limit, so it is possible to define a suitable vacuum solution for the inflaton field.

2.4.2 Conformal Hubble parameter

It is also convenient to express the Hubble parameter in terms of conformal time. Recall from the definition of conformal time that $a = dt/d\eta$, so

$$H = \frac{da}{dt}\frac{1}{a} = \frac{da}{d\eta}\frac{d\eta}{dt}\frac{1}{a} = a'\frac{1}{a^2} = \frac{1}{a}\mathcal{H}$$

Definition 2.11. *The **conformal Hubble parameter** $\mathcal{H}$ is defined as*

$$H = \frac{1}{a}\mathcal{H}$$

We will see more use of the conformal time when investigating perturbations of the inflaton.

2.5 The inflation model

Section goal 2.5.1. *Motivate the theory of inflation.*

There are several good reasons for why the concept of inflation has seen much success. A few problems with the standard non-inflationary models are stated here, without detailed treatment:

2.5.1 The horizon problem

Inflation solves the **horizon problem**: the isotropy of the measured CMB temperature implies that large chunks of the observable universe must once have been in thermal equilibrium, and hence in casual contact. Inflation solves this problem by postulating that the observable universe today was once squeezed well within the particle horizon, enabling causal contact. During inflation, the co-moving particle horizon decreased rapidly, such that scales that once was in causal contact falls outside the horizon and freezes.

2.5.2 The flatness problem

Let $\Omega \equiv \sum_i \Omega_i$. Observations show that the present universe has $\rho_{tot} \approx \rho_{c0}$. **F1** then gives $\Omega(t) - 1 = \frac{k}{a^2 H^2}$. Assuming the universe is dominated by a fluid with $a \propto t^p$ for $p \in \mathbb{R}$, we find $aH \propto t^{p-1}$ and $\Omega(t) - 1 \propto t^{2-2p}$. We see that for $p \leq 1$ the deviation from the critical density increases with time. This is true for matter-dominated ($p = 2/3$) or radiation-dominated ($p = 1/3$) universes. Hence the density must have been even closer to the critical in earlier times. As we are already close to the critical density today, the universe must have started out extremely flat. This seems unlikely, and would require fine-tuning of initial parameters beyond any common sense.

2.5.3 The inhomogeneity problem

A universe model that is initially completely homogeneous will *remain* so throughout the evolution of the universe. However, the observed universe is not homogeneous on smaller scales. Can the theory of inflation give predictions on how these inhomogeneities came into existence?

2.5.4 Introductory inflation

Assume that the universe right after big bang went through a phase of rapid accelerated expansion, so rapid and so vast that it expanded more than 60 e-foldings. This way, all eventual geometric structures are smeared flat, solving the flatness problem. The horizon problem is also solved, by allowing observers before inflation to be in casual contact, but not after. But what are the mechanics of such a model?

To obtain inflation, we postulate a field that exhibits the effect of accelerated expansion. This means $\ddot{a}$ must be greater than zero, and condition **F2** require $w < -1/3$. We must also assume the field remains invariant in every Lorentz transformation, so we consider a **scalar field** ϕ. We saw previously in this chapter that this requirement results in a equation of state $w = -1$, such that $\rho = -p$. We say the field must possess the property of **negative pressure**. This field is promptly called the **inflaton**. Before inflation, the only field that existed in the universe was a homogeneous field of inflatons in a vacuum state. This field was fluctuating strongly, where some of these fluctuations created excited inflaton states (particles). Where this happened, the inflaton particles (or excitations in the inflaton field) began driving the accelerated expansion of space.

A space that is dominated by a scalar field with $w = -1$ is a de Sitter space. As the universe expanded, the energy density of the inflaton field decreased, until the inflaton

field reached its vacuum state. The friction energy released was dumped to baryonic matter and photon fields. In the end, the accelerated expansion stopped when the inflaton field returned to its vacuum state [9].

The universe following inflation was radiation dominated and homogeneous, and a crucial problem emerges: if the universe started off homogeneous and isotropic, what formed the eventual density perturbations? A gas that starts off homogeneous will *stay* so. In the following chapters we will see how quantum fluctuations in the inflaton field gave rise to perturbations in the metric *after* inflation. These perturbations in turn seeded the structure formation, resulting in the anisotropy observed in today's cosmic microwave background.

2.6 Chapter conclusions

In this Introductory chapter we have stated the basic workings of modern cosmology. We mention the most important conclusions

Conclusion 2.1. *The conformal time will be essential in chapter 4 and 5.*

Conclusion 2.2. *Inflation takes place in a de Sitter space, and is driven by a scalar field ϕ possessing negative pressure.*

Conclusion 2.3. *The particle concept in de Sitter space (see figure 2.4.1) will be established in chapter 3.*

Readers who aren't quite familiar with the topics in this chapter are advised to review [12].

Chapter 3

Curved spaces and Symmetries

3.1 Introduction

We proceed by explaining the major differences between a curved space-time and the Minkowski space-time. The topics will be mostly conceptual, but will find much practical use in the following chapters. Chapter 3 does not *directly* affect any of the primary goals, but is an important reference for the following chapters. The foundations for understanding **PG1** are defined. This chapter makes use of the *mathematical preliminaries* defined in chapter 0. Unless otherwise stated, the contents of this chapter is based on [13], [14] and [15].

3.2 Conserved currents

Section goal 3.2.1. *Explain the connection between symmetries and conserved physical quantities. Establish Noether's theorem and its analogue for curved spaces. Define the energy-momentum tensor and the covariant derivative.*

It seems our physical universe is governed by symmetries. This section will give an introduction to these physical concepts of symmetries, and explain how symmetry transformations give rise to conserved quantities in both flat and curved spaces. This will prove important when investigating the properties of the energy-momentum tensor for the inflaton field. Explicit derivations are omitted, and interested readers are advised to consult [13] and [15].

3.2.1 Symmetries

For a classical system to possess a **symmetry** we mean that it is *invariant* under a group of transformations on the system. Quantum mechanically, the *Hamiltonian* should commute with all the symmetry group transformations. Let G be a (symmetry) group. We say a system $\mathcal{S}$ is **invariant** under the symmetry transformation if for all $g \in G$ then $g[\mathcal{S}] = \mathcal{S}$.

Example 3.1. *Let $\mathcal{S} = G = S_3$, the group of permutations of 3 elements $\{a, b, c\}$. This group can be represented as a triangle with three edges a, b and c. The group elements $g \in S_3$ then act as rotations and mirroring of the triangle.*

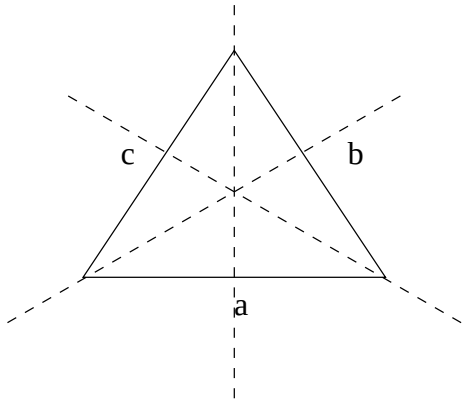

Figure 3.1: Triangle representations of S_3

Example 3.2. *Let $G = SO(n)$ and $\mathcal{S} = \mathbb{S}^n$, the n-sphere. This is our "most symmetric" example, as $\mathcal{S}$ is invariant under any rotation and mirroring, but not scaling.*

Example 3.3. *Let $\mathcal{S}$ be the QED-Lagrangian*

$$\mathcal{S} = \mathcal{L}_{qed} = \bar{\psi}(x)(i\not{D}_\mu - m)\psi - \frac{1}{4}F^2 \tag{3.1}$$

*and let G be the Poincaré group. The Poincaré group has two subgroups, the **Lorentz** group and the **translation** group. $\mathcal{L}_{qed}$ is known to be both Lorentz-invariant and translation-invariant, and therefore invariant under all the symmetry transformations from G.*

All conservation laws in special relativity can be derived from the following theorem:

Theorem 3.4 (Noethers theorem)**.** *Any differentiable continuous symmetry transformation that leaves the Lagrangian invariant corresponds to a conserved current.*

We state the formal definition of the **energy-momentum density**

Definition 3.5 (Energy-momentum)**.**

$$T_{\mu\nu} = \frac{2}{\sqrt{-g}}\frac{\partial(\sqrt{-g}\mathcal{L})}{\delta g^{\mu\nu}} = 2\frac{\partial\mathcal{L}}{\partial g^{\mu\nu}} - g_{\mu\nu}\mathcal{L}$$

Example 3.6. *Consider $\mathcal{L}_{qed}$ and let G be the Poincaré group. Translation in space results in conserved momentum ($\nabla \sim p$). Translation in time corresponds to conserved energy ($\partial_t \sim E$). Rotation corresponds to conserved angular momentum.*

Another way of writing Noethers theorem for the translation group is $\partial^\mu T_{\mu\nu} = 0$. The Poincaré transformations are all examples of **external** symmetries. The qed-Lagrangian is also invariant to **internal** symmetries:

Example 3.7. *Let $G = U(1)$ and $\mathcal{S} = \mathcal{L}_{qed}$ as in (3.1). The construction of the covariant derivative $D_\mu = \partial_\mu - ieA_\mu$ with connection $-ieA_\mu$ ensures the Lagrangian's invariance under local $U(1)$-transformations. Another way of interpreting this is saying that a free electron field under the condition that it is invariant under local $U(1)$ gauge-transformations* must *connect to a Maxwell-field. This is a purely geometric argument.*

3.2.2 Symmetries in curved spaces

The previous section concerned *flat* space-time only. We now consider more general curved spaces, and explain how the covariant derivative replaces the partial derivative.

Definition 3.8. *The **covariant derivative** D_μ is defined as*

$$D_\mu A^\nu = \frac{\partial A^\nu}{\partial x^\mu} + \Gamma^\nu_{\sigma\mu} A^\sigma$$

*where $\Gamma^\nu_{\sigma\mu}$ is the **connection***

The connection can be interpreted geometrically as *a measure of change of the basis coordinates*. (Recall from equation 0.1 that $D_\mu e_\nu = \Gamma^\sigma_{\mu\nu} e_\sigma$)

As we now consider curved space-time, translations are ill-defined. Instead we consider invariants due to local coordinate transformations. The conservation of the energy-momentum tensor (3.5) now yields

$$D^\mu T_{\mu\nu} = 0$$

We now state without proof (for a long derivation, see [11]):

Theorem 3.9 (Analogue to Noethers theorem for curved spaces)**.** *Conservation of physical quantities in **curved** spaces are due to invariance with respect to coordinate transformations, as conservation of physical quantities in a **flat** space-time are due to invariance with respect to translations.*

3.3 Gauge transformations

Section goal 3.3.1. *Explain how gauge transformations reduce to infinitesimal coordinate transformations.*

The theory of gauge transformations will be essential when investigating the perturbed RW metric in chapter 5. This section presents a short introduction to this theory.

3.3.1 Introduction

In cosmological perturbation theory two different space-time manifolds are dealt with: the unperturbed background space-time $\mathcal{M}$ and the perturbed physical space-time $\mathcal{M}'$. In order to relate quantities defined on these distinct space-times, we must first define a diffeomorphism $\mathcal{D} : \mathcal{M} \to \mathcal{M}'$.

Definition 3.10. *The chosen diffeomorphism*

$$\mathcal{D} : \mathcal{M} \to \mathcal{M}'$$

*corresponds to a **choice of gauge***

Let x be a set of coordinates defined on $\mathcal{M}$. Then any diffeomorphism $\mathcal{D} : \mathcal{M} \to \mathcal{M}'$ will induce a set of coordinates $x' = \mathcal{D}(x)$ on $\mathcal{M}'$. Let ϕ be a quantity defined in the perturbed $\mathcal{M}'$, and ϕ_0 be the unperturbed quantity in $\mathcal{M}$. Then the perturbation of ϕ is defined as

$$\delta\phi(x) = \phi(\mathcal{D}(x)) - \phi_0(x)$$

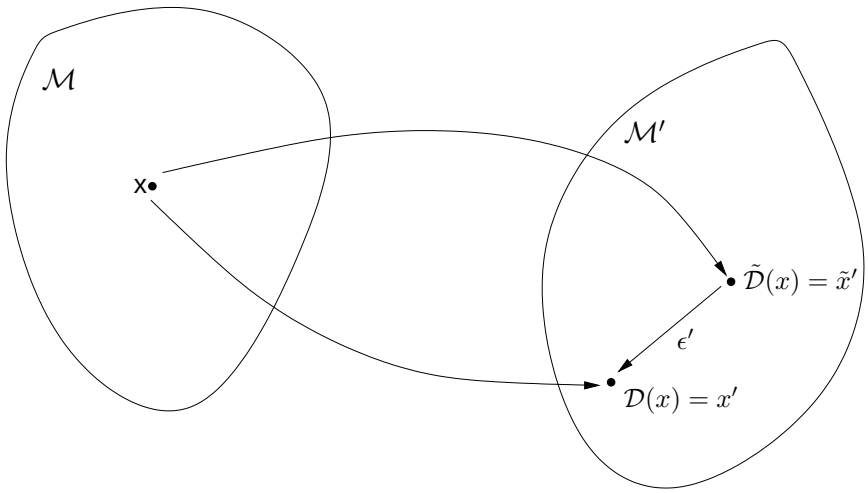

For a different choice of a diffeomorphism $\tilde{\mathcal{D}} : \mathcal{M} \to \mathcal{M}'$, the perturbation is different

$$\delta\tilde{\phi}(x) = \tilde{\phi}(\tilde{\mathcal{D}}(x)) - \phi_0(x)$$

This induces a coordinate transformation in $\mathcal{M}'$:

$$x' \to \tilde{x}' = x' + \epsilon'$$

which can be viewed as a coordinate transformation on $\mathcal{M}$:

$$x' \to x' + \epsilon' = \mathcal{D}(x + \epsilon) \approx x' + \epsilon\mathcal{D}(x)$$

for a fixed diffeomorphism. This shows that x' transforms to a coordinate that can be expressed as x' plus a term proportional to the infinitesimal transformations ϵ on $\mathcal{M}$. Hence the study of gauge transformations are reduced to the study of infinitesimal coordinate changes in the unperturbed $\mathcal{M}$. We will later engage gauge transformations when studying scalar perturbations (see chapter 5).

Definition 3.11. *We say that a quantity Q is **gauge invariant** if the corresponding coordinate transformation leaves Q invariant. That is, if*

$$Q(x) \to Q(x + \epsilon) = Q'(x) = Q(x) \tag{3.2}$$

3.3.2 An example from QED

In Quantum Electrodynamics, the electron field $\psi(x)$ can undergo a $U(1)$ gauge-transformation that is supposed to leave the Lagrangian invariant. But for a $V(x) \in U(1)$, the derivative of the transformed field $\partial_\mu V(x)\psi(x)$ is not well-defined:

$$\partial_\mu V(x)\psi(x) = \lim_{\epsilon\to 0} \frac{1}{\epsilon}\big(V(x+\epsilon)\psi(x+\epsilon) - V(x)\psi(x)\big)$$

because $V(x + \epsilon)$ and $V(x)$ are two different phases. The **covariant derivative** is defined to include a compensating term, the **comparator** $U(x, y)$ such that D_μ is invariant under the $U(1)$-transformation:

$$D_\mu V(x)\psi(x) = V(x)D_\mu\psi(x)$$

The comparator must then transform as $U(x,y) \to V(x)U(x,y)V^\dagger(y)$, such that the covariant derivative transforms as follows:

$$D_\mu V(x)\psi(x) = \lim_{\epsilon\to 0}\frac{1}{\epsilon}\big(V(x+\epsilon)\psi(x+\epsilon) - V(x+\epsilon)U(x+\epsilon,x)V^\dagger(x)V(x)\psi(x)\big)$$

$$= V(x)D_\mu\psi(x)$$

Hence the covariant derivative D_μ enables the QED-Lagrangian to become $U(1)$-*gauge-invariant.*

3.4 The particle concept

Section goal 3.4.1. *Establish the problems with the particle concept in curved spaces.*

We state a formal definition from a symmetry viewpoint:

Definition 3.12. *An **elementary particle** is an **energy-eigenstate** that transforms as an **irreducible representation** of the symmetry group of the universe.*

By irreducible, we mean that the representation is nontrivial with no nontrivial subrepresentations. See the notation chapter for information about representations.

3.4.1 Flat Minkowski space

The symmetry group of Minkowski space is the Poincaré group. Ignoring translations, we consider only the Lorentz group to be the symmetry group. The Lorentz group is isomorphic to $SL_2(\mathbb{C}) \oplus SL_2(\mathbb{C})$, and has different representations for different spin n-particles. In flat space there exists a natural set of modes

$$u_k = \frac{1}{\sqrt{2\omega(2\pi)^3}}e^{ikx-i\omega t} \tag{3.3}$$

with a normalized inner product:

$$(u_k, u_{k'}) = i\int d^3x\sqrt{g}(u_k^*\partial_\mu u_{k'} - (\partial_\mu u_k)u_{k'}^*) = (2\pi)^3\delta(k-k') = [\hat{a}_k, \hat{a}_{k'}^\dagger] \tag{3.4}$$

These modes are associated with the natural *rectangular* coordinate system, and are in turn associated with the Poincaré group. Recall that a symmetry transformation from the Poincaré group leaves the Minkowski line element invariant. Specifically, the vector ∂_t is a *Killing* vector of Minkowski space, orthogonal to the space-like hypersurfaces $t =$ constant. The special modes mentioned are the *eigenfunctions* of this killing vector, with eigenvalues $-i\omega$ for positive frequencies.

Example 3.13. *For a **Dirac field** of spin $1/2$, the irreducible representation (irrep) is $(\frac{1}{2},0)\oplus(0,\frac{1}{2})$. This is a direct sum of the left handed and right handed **Weyl-spinor**. This means an elementary spin $1/2$-particle can be interpreted of as two independent particle states, one left-handed and one right-handed that is **mixed** through the particle mass.*

However, our primary interest resides in the process of inflation, which is driven by the inflaton, a scalar field of zero spin. The common irrep for such a field in Minkowski space is $(0, 0)$ the Lorenz scalar representation, and is simpler to work with.

Note that nature is *not* invariant under all transformations of space-time: scaling (dilatation) is not a symmetry because *mass* is not a scale invariant attribute.

3.4.2 Curved spaces

In a curved space, the symmetry group is no longer given by the Poincaré group. It is therefore hard to decide what the concept of a particle really means. A generalization of the particle concept to curved spaces can be found in [15]. The construction of a Fock space (A Hilbert space made from several single-particle Hilbert spaces), vacuum states etc can proceed as described for the Minkowski space. The problem arises due to the ambiguity of the formalism, as the Poincaré group is no longer the symmetry group of the space-time. Then there are no Killing vectors at all with which to define positive frequency modes.

In *some* classes of space-time there may be symmetry under certain restricted transformations (like rotations), or the de Sitter group (see definition 0.17). But in general, no such privileged coordinates are available and *no natural mode decomposition of ϕ based on the separation of the wave equation will be possible*. This violates the principle of general covariance, that **coordinate systems are physically irrelevant**.

3.5 The troublesome vacuum

Section goal 3.5.1. *Defining the quantum mechanical vacuum in flat and curved spaces. Building the foundation for finding a suitable set of vacua in a de Sitter space-time.*

Definition 3.14. *For a field ϕ, the quantum mechanical **vacuum** $|0\rangle$ is defined to be the **lowest possible energy state** of the field. The **vacuum expectation value** of a field ϕ is*

$$\langle 0|\phi|0\rangle$$

For a field in a quadratic potential, the vacuum expectation value should equal zero. This corresponds to the average, expected value of the field in a state where there are *no particles*. Some fields are however described by a different potential, and may give rise to a non-zero vacuum expectation value. At temperatures below the electroweak scale, the Higgs-boson is such a particle. Above this scale, the potential regains its quadratic form.

We already know that the vacuum defined in the Minkowski space is invariant under the Poincaré group. The question arises as to which set of modes gives the 'best' description of a physical vacuum, i.e. corresponds most closely to the actual experience of "no particles". This is a troublesome question, as even in a Minkowski space, a free-falling detector will not always register the same particle density as a non-inertial accelerating detector (the Unruh-effect [11]). The vacuum in Minkowski space is **not** unique, but the conventional vacuum states defined in terms of the modes is the agreed vacuum for *all inertial* observers. This is because the vacuum defined by $a_k|0\rangle = 0$ is invariant under the Poincaré group.

Definition 3.15. *The state* $|0\rangle$ *such that* $a_k|0\rangle = 0$ *for all* k *is the* ***ground state of vacuum****.*

Part of the reason for these troubles is due to the *global* nature of the modes. They are defined on the whole of space-time, so that a particular observer's specification of the field mode decomposition will depend on the observer's entire past.

3.5.1 In and out mode-solutions

In many problems the space-time can be treated as asymptotically Minkowskian in the remote past and/or future. Here, the usual choice of the "natural" Minkowskian vacuum has a well-understood meaning: the absence of particles according *to all* observers in the asymptotic flat region.

Definition 3.16. *The remote past and future are referred to as the* ***in*** *and* ***out*** *modes respectively.*

Example 1: A universe with both in and out-modes

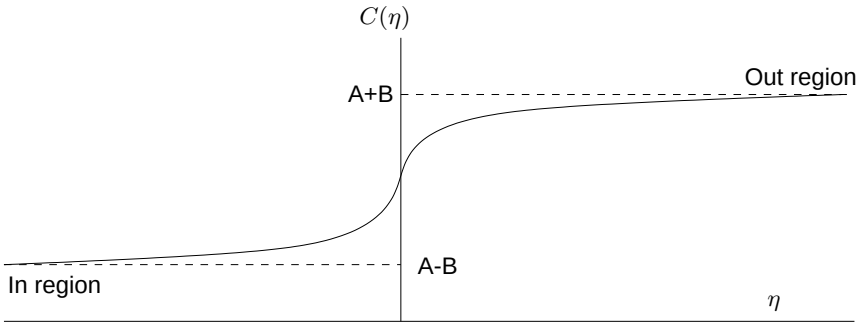

Figure 3.2: A universe with $C(\eta) = A + B\tanh(\eta)$ is essentially Minkowskian in the in/out regions

Assume a universe described with a line element

$$ds^2 = C(\eta)(-d\eta^2 + dx^2) \tag{3.5}$$

where $C(\eta)$ is a **conformal scale factor**. This form of line element is **manifestly conformal** to Minkowski space, as it is both diagonal and has the same signs as the Minkowski line element. Assume that $C(\eta) = A + B\tanh(\eta)$. We then see that in the far past and future

$$C(\eta) \to A \pm B \quad \text{for} \quad \eta \to \pm\infty$$

In this limit, A and B being only constants, the space-time essentially becomes Minkowskian.

Example 2: A de Sitter space

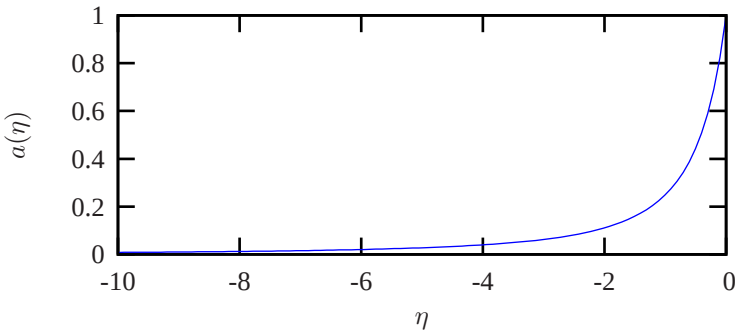

Figure 3.3: A de Sitter space expressed in conformal time is Minkowskian in the in region

Assume a de Sitter space described in equation (2.3). This space is very small when $\eta \to -\infty$, but is close to flat and essentially Minkowski in the in-region.

3.5.2 The effect of a curved space

Working in the Heisenberg picture (where states are static while operators are time-dependent), a vacuum state chosen in an in-mode region will remain so during its evolution. However, at later times, outside the region, freely falling observers may still register particles in this "vacuum" state. In particular, if there is also an out region, then the in-vacuum may **not** coincide with the out-vacuum. One might say that *particles have been created by the time-dependent external gravitational field, or curvature of space*.

We will later encounter a special vacuum for the RW metric:

Definition 3.17. *In a RW metric, the **adiabatic vacuum** is the vacuum that closest resembles the "common" vacuum in flat space-time, i.e where the probability of particle creation due to curvature effects is minimized.*

3.6 Scalar fields

Section goal 3.6.1. *Determining the equation of motion for a scalar field in a general metric*

The assumption that inflation is driven by a scalar field require us to investigate the properties of such fields. We first consider a general scalar field in a curved space, before working explicitly with the RW background. We proceed by determining the general equation of motion for a scalar field.

Definition 3.18. *A (real-valued) **scalar field** is a C^k map $\phi : X \to \mathbb{R}$, where X is a Riemannian manifold. The intrinsic spin of the scalar field is 0.*

3.6.1 Hamilton's principle and the equations of motion

Even though the reader is expected to be familiar with Hamilton's principle, an introduction is presented. Recall that the Lagrangian is a function of coordinates and their derivatives $\mathcal{L} = \mathcal{L}(\phi, \partial_\mu \phi)$, and the action is the space-time integral over the Lagrangian $S = \int \sqrt{-g} d^4x \mathcal{L}$. Here, g denotes the determinant of $g_{\mu\nu}$ and $\sqrt{-g}$ is the Jacobian.

Definition 3.19 (Hamilton's principle)**.** *The equations of motion for a field ϕ is determined by the condition that the action S is extremal for all infinitesimal variations of curves which keep $\phi_i \equiv \phi(\tau_i)$ and $\phi_e \equiv \phi(\tau_e)$ rigid,*

$$\delta S = \delta \int_{\tau_i}^{\tau_e} \sqrt{-g} \mathcal{L}(\phi, \partial_\mu \phi) d^4x = 0 \tag{3.6}$$

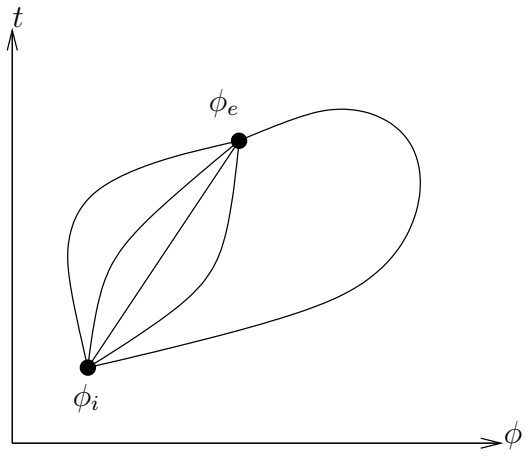

Equation (3.6) can also be expressed as

$$\delta \int \sqrt{-g} \mathcal{L} d^4x = \int d^4x \sqrt{-g} \Big(\frac{\partial \mathcal{L}}{\partial \phi} \delta\phi + \frac{\partial \mathcal{L}}{\partial(\partial_\mu \phi)} \partial_\mu \delta\phi \Big) = 0$$

where we have used that $\delta \partial_\mu \phi = \partial_\mu \delta\phi$. Partial integration of the last term gives

$$= \int d^4x \sqrt{-g} \Big(\frac{\partial \mathcal{L}}{\partial \phi} - \partial_\mu \frac{\partial \mathcal{L}}{\partial(\partial_\mu \phi)} \Big) \delta\phi + \frac{\partial \mathcal{L}}{\partial(\partial_\mu \phi)} \delta\phi \Big|_{\tau_i}^{\tau_e} = 0$$

The last term is zero due to the conditions that ϕ_i and ϕ_e remain rigid, so only the terms in the *integral must vanish*. The equation of motion for a general field ϕ is then:

$$\frac{\partial \mathcal{L}}{\partial \phi} - \partial_\mu \frac{\partial \mathcal{L}}{\partial(\partial_\mu \phi)} = 0$$

3.6.2 Equations of motion for a scalar field

A scalar field ϕ in a general space has the Lagrangian

$$\mathcal{L} = \frac{1}{2} g^{\mu\nu} \partial_\mu \phi \partial_\nu \phi - V(\phi) \tag{3.7}$$

with corresponding action

$$S = \int d^4x\sqrt{-g}\left[\frac{1}{2}g^{\mu\nu}\partial_\mu\phi\partial_\nu\phi - V(\phi)\right] \tag{3.8}$$

Using the Hilbert-action principle $\delta S = 0$ we obtain the equation of motion of the field

$$\delta S = \delta\int d^4x\mathcal{L} = \delta\int d^4x\sqrt{-g}\left[\frac{1}{2}g^{\mu\nu}\partial_\mu\phi\partial_\nu\phi - V'\phi\right] = 0$$

which equals

$$\delta S = \int d^4x\sqrt{-g}\left[\frac{1}{2}\frac{1}{\sqrt{-g}}\partial_\nu(\sqrt{-g}g^{\nu\mu}\phi\partial_\mu\phi) - V'\right]\delta\phi = 0$$

where $g = \det(g_{\mu\nu})$. The action principle states that the terms in brackets must equal zero, which is the equations of motion.

Definition 3.20. *The $d'Alembertian$ operator is defined as*

$$\Box = \frac{1}{\sqrt{-g}}\partial_\nu(\sqrt{-g}g^{\nu\mu}\phi\partial_\mu)$$

and can be viewed as the covariant version of the laplacian $D^\mu D_\mu\phi = \Box\phi$, where $D_\mu A^\mu = \partial_\mu A^\mu + A^\sigma\Gamma^\nu_{\sigma\mu}$

The equation of motion for a scalar field in a general space can now be written as

$$\boxed{\Box\phi + V' = 0} \tag{3.9}$$

3.7 Chapter conclusions

We conclude this Introductory chapter by stating the most important observations:

Conclusion 3.1. *The universe is governed by symmetries. Symmetry invariance results in conserved physical quantities such as energy, momentum or charge.*

Conclusion 3.2. *In curved spaces, global symmetries are reduced to local symmetries.*

Conclusion 3.3. *Gauge transformations can be reduced to infinitesimal coordinate transformations.*

Conclusion 3.4. *In curved spaces, particles have no well-defined meaning: two separated observers measuring the same event in curved space-time will observe different particle states.*

Conclusion 3.5. *The de Sitter space has a well-defined particle state in the in-mode region, the infinite past.*

Conclusion 3.6. *The equation of motion of a scalar field has been established.*

Part II

Evolving the universe

Chapter 4

Inflation in the Robertson-Walker universe

Until now, we've been concerned with purely theoretical aspects of our universe. We now proceed by investigating the physical properties of of our local universe in its infancy – emphasizing that it was indeed a local event. This chapter introduces the theory of inflation, and describes events that occurred between 10^{-35} and 10^{-32} seconds after $t = 0$. We will only consider inflationary models with *one* scalar field.

The basic differences between a curved and a flat space have been established. We will argue that the space during inflation is the constantly curved de Sitter space, and this will from now on be the standard background space for the theory of inflation. This chapter will pursue **PG1**, and culminates in the definition of a suitable vacuum in the de Sitter inflationary space.

Unless otherwise stated, the contents of this chapter is based on [11], [16], [9] and [8].

4.1 Giving birth to a universe

Assume that a universe is initiated at $t = 0$. The scale factor is close to zero, but the universe is still infinitely large. As an analogue, consider the map $f : \mathbb{R} \to \mathbb{R}$ that sends $x \mapsto \epsilon x$. f is still surjective, even though it scales the infinitely sized space $\mathbb{R}$ onto a "more compact" infinite space $\mathbb{R}$ (see figure 4.1). Similarly, our universe was infinitely large when it was initialized - it was just infinitely more compact than today.

4.1.1 The epoch of unified forces

Very little is known during this first period of the universe, which is called the **Planck epoch**. If super-symmetry is correct, then all four known forces were unified and so shared a coupling constant. Roughly 10^{-43} seconds after the birth, gravity is separated from the other three forces. The stage after gravity is separated out is called the **grand unified epoch**. Eventually, the grand unification is also broken when the strong nuclear force is separated from the electroweak force.

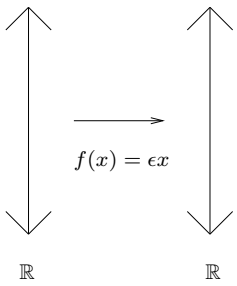

Figure 4.1: An analogue to the scale factor $a(t)$ at the beginning of the universe. The scale factor ($f(x) = \epsilon x$) maps an infinite space $(\mathbb{R})$ to an infinitely more compact space $(\epsilon\mathbb{R} \simeq \mathbb{R})$, which is still infinite.

4.1.2 The epoch of Inflation

10^{-35} seconds after the big bang, the strong nuclear force decoupled from the electroweak force. We now need to introduce a first assumption, namely that the universe is solely populated by a homogeneous heavy scalar field (the **inflaton**) in a vacuum state that fluctuated quantum mechanically (see figure 4.2).

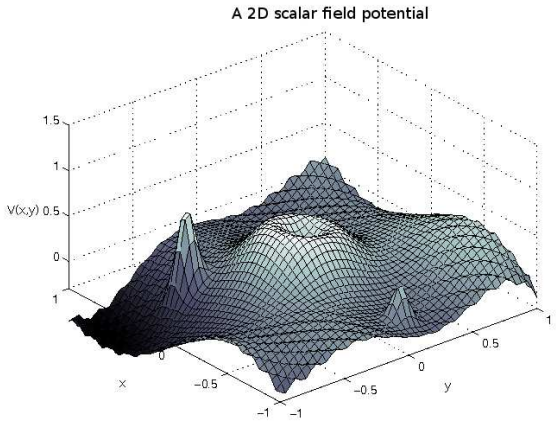

Figure 4.2: A two-dimensional schematic diagram of an inflaton potential $V(x, y)$. Notice the "false vacuum" state at the center of the image.

In areas where the potential is large, the process of inflation may start. Here, the inflaton field is located high up in an excited particle state, and proceeds by rolling slowly down (see figure 4.3). While (slow) rolling, the scalar field drives the inflation

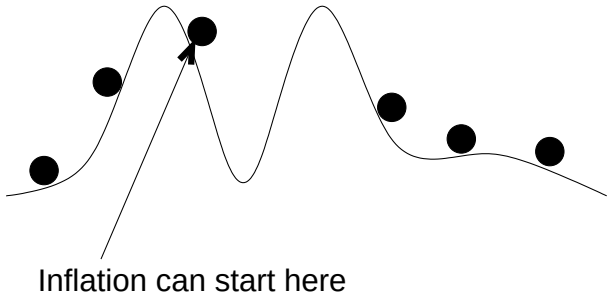

Figure 4.3: Areas in the universe where inflation might happen

and expands the the scale factor $a(t)$ by e^{60} until the minimum is reached and inflation stops. However, when the slow-roll conditions break down, the field rolls faster and doesn't initially settle in the minimum (or vacuum state). It will continue to roll back and forth while dumping friction energy into other particle fields. In the end, the inflaton field has settled in the minimum, meaning it has vaporized, leaving only baryons and photons in the newly created (local) universe (see figure 4.4).

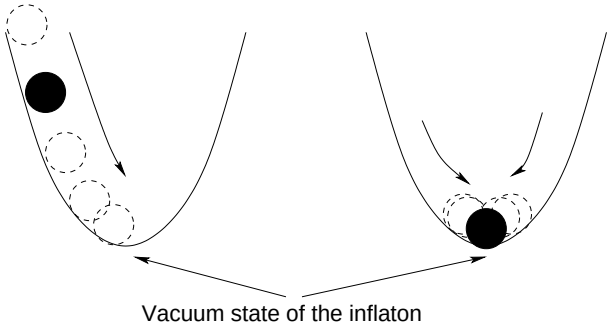

Figure 4.4: The field proceeds by slow-rolling down the potential, until settling in the safe vacuum state at the minimum. Baryons and photons are created from the friction energy leftovers.

4.1.3 Inflation consequences

The assumption that the universe before inflation was homogeneous and isotropic would classically mean that the universe *after* the period of inflation would remain so. We know today that the universe is definitely *not* homogeneous and isotropic on small scales, which means that there must have been a mechanism that produced anisotropies in the energy density early on. Luckily, the theory of inflation does not only solve a number of problems - it also predicts *why* and *how* these anisotropies came into existence.

Before inflation, more particles were in casual contact than after inflation, as the co-moving horizon decreased. The different modes, which were well within the horizon before inflation, ensured causal contact (and thus thermal equilibrium) between great portions of space at early times, see figure 4.5.

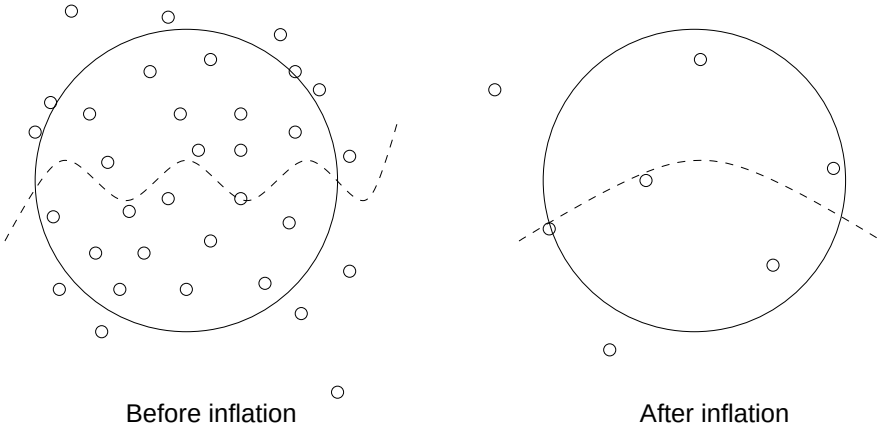

Figure 4.5: The decay of the co-moving horizon - before and after inflation.

During inflation, the inflaton field ϕ fluctuated, enabling creation of particles and anti-particles. But inflation was so rapid that some of these particle pairs were separated well outside the co-moving horizon, effectively breaking the homogeneity of the early universe.

We will in the following chapter explain how the quantum fluctuations $\delta\phi$ in the inflaton field gave rise to perturbations in the metric *after* inflation has ended. This could be problematic, as by now the inflaton had completely vaporized. Luckily, the perturbations $\delta\phi$ initiated perturbations in the metric during the end of inflation, leaving a fresh radiation dominated universe with small perturbations in the metric. Compare this with a stone hitting a still pond - the stone "disappears" to the bottom, while the water "metric" is perturbed. These perturbations would in turn seed the anisotropies in energy densities as observed today.

We proceed by a more quantitative treatment of the introduction presented here.

4.2 The equation of motion

Section goal 4.2.1. *Establish the equation of motion of a scalar field in a Robertson-Walker background.*

Recall from chapter 2 that a scalar field-driven accelerated expansion results in a de Sitter universe. We proceed by deriving the equations of motion in a de Sitter space, described by the RW line element.

Proposition 4.1. *The equation of motion for a scalar field in a RW background is*

$$\boxed{\ddot{\phi} + 3H\dot{\phi} - \frac{1}{a^2}(\nabla^2\phi) + V' = 0} \tag{4.1}$$

where $V' \equiv \frac{dV}{d\phi}$. Proof: The RW line element in Cartesian coordinates is

$$ds^2 = -dt^2 + a^2(t)d\mathbf{x}^2$$

where the metric is

$$g_{\mu\nu} = \begin{pmatrix} -1 & 0 & 0 & 0 \\ 0 & a^2 & 0 & 0 \\ 0 & 0 & a^2 & 0 \\ 0 & 0 & 0 & a^2 \end{pmatrix}$$

such that $g \equiv \det g_{\mu\nu} = -a^6$. Using (3.8), the action for a scalar field ϕ in a RW-background is

$$S = \int d^4x a^3 \left[+\frac{1}{2}\dot{\phi}^2 - \frac{1}{a^2}(\nabla\phi)^2 + V(\phi) \right] \tag{4.2}$$

Infinitesimal variations in the scalar field $\phi \to \phi + \delta\phi$ applied with Hilbert's principle of stationary action $\delta S = 0$ gives the equation of motion for ϕ:

$$\delta S = \int d^4x a^3 \left[\dot{\phi}\delta\dot{\phi} - \frac{1}{a^2}(\nabla\phi)\underbrace{\delta(\nabla\phi)}_{=\nabla\delta\phi} + V'\delta\phi \right]$$

Noting that $\delta\dot{\phi} = \frac{d}{dt}\delta\phi$, extract $\delta\phi$ and include the determinant a^3 to get

$$= \int d^4x \left[\frac{d}{dt}(a^3\dot{\phi}) - a\nabla^2\phi + a^3V' \right]\delta\phi$$

Perform the differentiation: $\frac{d}{dt}(a^3\dot{\phi}) = 3a^2\dot{a}\dot{\phi} + a^3\ddot{\phi} = a^3(3H\dot{\phi} + \ddot{\phi})$ where H is the Hubble parameter. Insertion yields

$$\delta S \stackrel{!}{=} 0 = \int d^4x a^{-3} \left[3H\dot{\phi} + \ddot{\phi} - \frac{1}{a^2}(\nabla^2\phi) + V' \right]\delta\phi$$

The action principle demands the expression in the brackets vanish, and the equation of motion is obtained:

$$\ddot{\phi} + 3H\dot{\phi} - \frac{1}{a^2}(\nabla^2\phi) + V' = 0$$

□

Alternate derivation

The equation of motion can also be obtained from (3.9):

$$\Box\phi + V' = 0 = \frac{1}{\sqrt{-g}}\partial_\nu(\sqrt{-g}g^{\mu\nu}\partial_\mu\phi) + V'$$

The kinetic part is

$$\frac{1}{\sqrt{-g}}\partial_\nu(\sqrt{-g}g^{\nu\mu}\partial_\mu\phi) \stackrel{RW}{=} \frac{1}{a^3}\partial_\nu(a^3g^{\nu\mu}\partial_\mu\phi) = \frac{1}{a^3}\partial_t(a^3(-1)\partial_t\phi) + \frac{1}{a^3}\nabla(a\nabla\phi)$$

such that

$$\Box\phi + V' = -\frac{1}{a^3}\frac{d}{dt}(a^3\dot{\phi}) + \frac{1}{a^2}\nabla^2\phi$$

This expression equals (4.2) when including the potential, and equation (4.1) has been retrieved.

4.3 The slow-roll approximation

Section goal 4.3.1. *Explain the basics of the slow-roll approximation. Define the slow-roll parameters.*

This section introduces the standard approximation method of inflation, the **slow-roll approximation**. The reader is expected to be familiar with this topic, so all derivations are omitted. A proper review of the slow-roll approximation can be found at [9].

4.3.1 Introduction

In the previous section, the general equation of motion for a scalar field (4.1) was derived. The field ϕ is in this section considered to be spatially homogeneous: $\phi(\mathbf{x}, t) \rightarrow \phi(t)$. We impose two constraints on the field and its potential in order to simplify the model.

1. The potential V exceeds the kinetic energy term, or $V \gg \dot{\phi}^2$.

2. The friction term $3H\dot{\phi}$ dominates over the curvature $\ddot{\phi}$.

Equation (4.1) can now be expressed as

$$\ddot{\phi} + 3H\dot{\phi} + V' = 0 \tag{4.3}$$

Constraint 2 means that

$$3H\dot{\phi} \approx -V' \tag{4.4}$$

and **F1** gives

$$H^2 \approx \frac{V}{3M_p^2}$$

4.3.2 The slow-roll parameters

The conditions of successful inflation can be expressed in a dimensionless form. The two criteria are reformulated as the slow-roll parameters:

$$\epsilon_{sr} \equiv \frac{M_p^2}{2}\Big(\frac{V'}{V}\Big)^2 \ll 1 \tag{4.5}$$

$$\eta_{sr} \equiv M_p^2\Big(\frac{V''}{V}\Big) \ll 1$$

The subscript on η_{sr} distinguishes the parameter from the *conformal time* η. As inflation demands the field ϕ to roll slowly in the potential, the potential's derivatives must be small. We therefore say that inflation is equivalent with having $\epsilon \ll 1$. Thus inflation *ends* when the derivative term exceed the potential itself, or when $\epsilon = 1$. When the era of inflation is complete, the inflaton field has settled in the vacuum state and the friction energy has been converted to other particles.

4.4 Quantizing a scalar field

Section goal 4.4.1. *To promote the inflaton field ϕ to a field operator $\hat{\phi}$.*

We now leave the world of classical mechanics and enter quantum field theory. Quantizing a theory is *always* a correct choice, as a classical theory has a smaller space of validity than a quantized. When quantizing the inflaton field, it will be decomposed into a set of Fourier **modes** k. Each mode corresponds to a plane wave with wavelength $\lambda = 2\pi/k$. These Fourier modes k of a density perturbation corresponds to a variation in the density of a length scale λ. In linear perturbation theory, the modes will evolve **independently** from each other, reducing a set of coupled partial differential equations to ordinary differential equations.

This will lead to, among others, *the primordial spectrum*. But first we give a reminder of how to perform a quantization of a scalar field in the Minkowski metric.

4.4.1 Fourier expansion

First, decompose the field into its time and space components by expanding into Fourier modes:

$$\phi(\mathbf{x}, t) = \frac{1}{\sqrt{V}} \sum_k \phi_k(t) e^{ikx}. \tag{4.6}$$

Then promote the Fourier-coefficients to operators. The field ϕ and the canonical conjugate $\pi = \frac{\partial L}{\partial \dot{\phi}}$ should now satisfy the commutator relation

$$[\phi(\mathbf{x}, t), \pi(\mathbf{x}', t)] = i\delta^{(3)}(\mathbf{x} - \mathbf{x}')$$

The Lagrangian density $\mathcal{L}$ for a scalar field in the Minkowski space is given as

$$\mathcal{L} = \frac{1}{2}\partial_\mu \phi \partial^\mu \phi = -\frac{1}{2}\dot{\phi}^2 + \frac{1}{2}(\nabla\phi)^2$$

The Lagrangian L is found by insertion:

$$L = \int d^3x \mathcal{L} = \frac{1}{2V} d^3x \sum \left(\dot{\phi}_k \dot{\phi}_{k'} e^{i(k+k')\cdot x} + k^2 \phi_k \phi_{k'} e^{i(k+k')\cdot x} \right)$$

Using that $\int d^3x \exp\left(i(k - k') \cdot x\right) = V\delta_{k,-k'}$ we find

$$L = \frac{1}{2} \sum_k \left(\dot{\phi}_k \dot{\phi}_{-k} - k^2 \phi_k \phi_{-k} \right)$$

The field satisfies $\phi_k^* = \phi_{-k}$, so

$$L = \frac{1}{2} \sum_k \left(|\dot{\phi}_k|^2 - \omega_k^2 |\phi_k|^2 \right)$$

where $\omega_k = \sqrt{k^2}$. The Hamiltonian $H = p\dot{q} - L$ is

$$H = \frac{1}{2} \sum_k \left(|\dot{\phi}_k|^2 + \omega_k^2 |\phi_k|^2 \right)$$

The Hamiltonian now describes a one-dimensional harmonic oscillator for each wavenumber k, while ω_k is the oscillation frequency. The quantization procedure of such a Hamiltonian is well-known.

4.4.2 Quantizing the harmonic oscillator

If one already knows the classical equations of motion for a field, it can be promoted to the equation for the time-dependent operator $\phi(t)$. This is done in the Heisenberg picture, where operators become time-dependent while states are not. It is in general always possible to introduce the raising and lowering operators in the following way:

$$\phi_k(t) = v_k(\omega, t)a_k + v_k^*(\omega, t)a_k^\dagger$$

where u, v satisfy the classical equation of motion. We now rewrite the canonical variables ϕ, π in terms of raising and lowering operators, using the special modes defined in eq (3.3) $v = u^* = (2\omega_k)^{-1/2}$:

$$\phi_k(t=0) = \sqrt{\frac{1}{2\omega_k}}\left(a_k + a_{-k}^\dagger\right)$$

$$\pi_k(t=0) = -i\sqrt{\frac{\omega_k}{2}}\left(a_k - a_{-k}^\dagger\right)$$

Cumbersome algebra will confirm that the new operators satisfy the commutator relation

$$[a_k, a_{k'}^\dagger] = \delta_{k,k'}$$

Including time dependence, ϕ is expressed as

$$\phi_k(t) = \sqrt{\frac{1}{2\omega_k}}\left(a_k e^{-i\omega_k t} + a_{-k}^\dagger a^{i\omega_k t}\right) \tag{4.7}$$

insert into (4.6) and find

$$\phi_k(\mathbf{x}, t) = \int \frac{d^3k}{(2\pi)^3}\sqrt{\frac{1}{2\omega_k}}\left(a_k e^{-ikx} - a_k^\dagger a^{ikx}\right)$$

having used the continuous shift $\sum_k \to V\int d^3k/(2\pi)^3$. A similar expression can be found for the canonical conjugate $\pi(\mathbf{x}, t)$.

4.5 Perturbing the inflaton

Section goal 4.5.1. *To perturb the inflaton and define a set of solutions for the perturbations in de Sitter space.*

4.5.1 Introduction

Assume our universe starts off completely homogeneous and isotropic. Its only component is the *inflaton field* ϕ, the postulated scalar field that drives inflation. The space is de Sitter, and all *perturbations in the metric are neglected*. This can be done as long as a mode stays well inside the horizon. [8]

Thus the only thing we consider are the **quantum fluctuations** of ϕ, expressed as a small perturbation in the field itself. These perturbations will obey the equations of motion for a scalar field with a *special* mass, a mass proportional to the curvature of the potential V. A rewriting to a more suitable expression using conformal time is then performed. This will tune the equations to follow the expansion of space and thus eliminating friction terms. In the end the solutions to the perturbed field will be scrutinized, and the **Bunch-Davies vacuum** is established.

4.5.2 Perturbing the inflaton

Assume the quantum fluctuations of the inflaton gives rise to perturbations of the form

$$\phi(\mathbf{x},t) = \underbrace{\phi_0(t)}_{\text{classical evolution}} + \underbrace{\delta\phi(\mathbf{x},t)}_{\text{fluctuations}} \tag{4.8}$$

Proposition 4.2. *The curvature of the potential V gives rise to an effective mass-term:*

$$V'' = m^2$$

This is in analogue with the Higgs-mechanism (See [13], page 351).

Proof: The potential V has a minimum for $\phi = 0$. Expanding V,

$$V(\phi) \approx V(0) + \frac{1}{2}V''\phi^2 = \frac{1}{2}V''\phi^2$$

The scalar Lagrangian now yields

$$\mathcal{L} = \frac{1}{2}g^{\mu\nu}\partial_\mu\phi\partial_\nu\phi - \frac{1}{2}V''\phi^2$$

where $\frac{1}{2}V''\phi^2$ is interpreted as an *effective mass term*. Hence $V'' \equiv m^2$. □

Lemma 4.3. *The perturbed field $\delta\phi$ will satisfy the equation of motion:*

$$\boxed{\ddot{\delta\phi} + 3H\dot{\delta\phi} - \frac{1}{a}(\nabla^2)\delta\phi + m^2\delta\phi = 0} \tag{4.9}$$

Proof:
Both ϕ and ϕ_0 will obey (4.1):

$$\ddot{\phi} + 3H\dot{\phi} - \frac{1}{a^2}(\nabla^2\phi) + V' = 0 \tag{4.10}$$

Insertion of (4.8) into (4.1) gives

$$\ddot{\phi_0} + \ddot{\delta\phi} + 3H(\dot{\phi_0} + \dot{\delta\phi}) - \frac{1}{a}(\nabla^2\delta\phi) + V'(\phi_0 + \delta\phi) = 0 \tag{4.11}$$

Returning to the perturbed potential in (4.11), we expand the potential as follows:

$$V'(\phi_0 + \delta\phi_0) \approx V'(\phi_0) + V''(\phi_0)\delta\phi = V'(\phi_0) + m^2\delta\phi$$

Insert this potential back into (4.11) and recall that the field ϕ_0 alone satisfies (4.1). Using proposition (4.2) to eliminate V'' for m^2, the perturbed field $\delta\phi$ then satisfies (4.9).□

4.5.3 Fourier expansion

Separating the spatial and time dependence, we perform a Fourier expansion of the perturbed field $\delta\phi$:

$$\delta\phi(\mathbf{x},t) = \frac{1}{V}\sum_k \varphi_k(t)e^{ik\cdot\mathbf{x}}$$

where k is the co-moving wave number. Using

$$\nabla^2\delta\phi(\mathbf{x},t) = -\frac{1}{V}\sum_k k^2\varphi_k e^{ikx}$$

we obtain

$$\ddot{\varphi} + 3H\dot{\varphi} + (\frac{k^2}{a^2} + m^2)\varphi = 0$$

The solutions are the classical mode-functions

$$u_k = \varphi_k(t)e^{ik\cdot x}$$

4.5.4 Rewriting to conformal time

We proceed by expressing the field equation with respect to conformal time.

$$\dot{\varphi} = \frac{d\varphi}{dt} = \frac{\partial\varphi}{\partial\eta}\frac{d\eta}{dt} = \varphi'\frac{1}{a}$$

such that (3.4) can be expressed as

$$\varphi_k'' + 2\mathcal{H}\varphi_k' + (k^2 + m^2a^2)\varphi_k = 0 \tag{4.12}$$

Lemma 4.4. *To first order, the mass-term $\propto m^2$ can be neglected during inflation.*

Proof: The slow-roll parameter η_{sr} in equation (4.3.2) gives

$$\eta_{sr} \equiv M_p^2\frac{V''}{V} \propto V'' = m^2$$

One of the slow-roll conditions for inflation to occur is that $|\eta_{sr}| \ll 1$. In this limit, the mass-term can henceforth be neglected. □

Proposition 4.5. *The friction term in (4.12) vanishes with a suitable choice of co-moving mode functions*

$$\varphi_k = \frac{u_k}{a}$$

From a physical viewpoint, the removal of the friction term can be explained by a co-moving observer that is stationary in a co-moving frame. In this frame, $\mathcal{H} = 0$ and the term is effectively removed. One can also interpret $\mathcal{H}$ as the friction experienced by the expansion of the universe, assuming a particle following a geodesic curve. A detailed "proof" follows:

$$\varphi_k' = \frac{1}{a}u_k' - \frac{1}{a}\mathcal{H}u_k$$

$$\varphi_k'' = -\frac{1}{a}\mathcal{H}u_k' + \frac{1}{a}u_k'' + \frac{1}{a}\mathcal{H}^2u_k - \frac{1}{a}\mathcal{H}'u_k - \frac{1}{a}\mathcal{H}u_k' = -2\frac{1}{a}\mathcal{H}u_k' + \frac{1}{a}u_k'' + \frac{1}{a}\mathcal{H}^2u_k - \frac{1}{a}\mathcal{H}'u_k$$

insert back into (4.12) to obtain

$$-\frac{2}{a}\mathcal{H}u_k' + \frac{1}{a}u_k'' + \frac{1}{a}\mathcal{H}^2u_k - \frac{1}{a}\mathcal{H}'u_k + \frac{2\mathcal{H}}{a}u_k' - \frac{2\mathcal{H}^2}{a}u_k + \frac{k^2}{a}u_k = 0$$

which is

$$\frac{1}{a}u_k'' - \frac{1}{a}\mathcal{H}^2u_k - \frac{1}{a}\mathcal{H}'u_k + \frac{k^2}{a}u_k = 0$$

Using that $\mathcal{H}' = \frac{a''}{a} - \mathcal{H}^2$:

$$\frac{1}{a}u_k'' - \frac{a''}{a^2}u_k + \frac{k^2}{a}u_k = 0$$

which equals

$$u_k'' + \Big(k^2 - \frac{a''}{a}\Big)u_k = 0 \tag{4.13}$$

From (2.4), $a = -1/(H\eta)$:

$$\frac{a''}{a} = \frac{-2H\eta}{-H\eta^3} = \frac{2}{\eta^2}$$

Inserting into (4.13):

$$u_k'' + \Big(k^2 - \frac{2}{\eta^2}\Big)u_k = 0 \tag{4.14}$$

and the u_k'-term has vanished. Note that at early times, $\eta \to -\infty$ and the $1/\eta$-term can be neglected. The classical equation then reduces to that of a harmonic oscillator, with solutions described in (4.7). □

Letting $v_k = \eta u_k$ and $x = k\eta$, equation (4.14) can be rewritten as

$$\frac{d^2 v_k}{dx^2} + \frac{2}{x}\frac{dv_k}{dx} + (1 - \frac{2}{x^2})v_k = 0$$

The solution for this equation is given by the Bessel-functions for $\ell = 1$, that is $j_1(k\eta)$ and $y_1(k\eta)$ and satisfy

$$\boxed{u_k(\eta) = A_k e^{-ik\eta}\Big(1 - \frac{i}{k\eta}\Big) + B_k e^{ik\eta}\Big(1 + \frac{i}{k\eta}\Big)} \tag{4.15}$$

where A_k, B_k are the yet unknown **Bogoliubov-coefficients**. We

4.5.5 Bogoliubov-coefficients

We perform a small detour to investigate the properties of the Bogoliubov-coefficients. The field needs to be decomposed into *positive and negative* frequency components before defining the creation and annihilation operators. This can only be done in space-times with a **timelike Killing vector field**. Luckily, the de Sitter space has this property. The Bogoliubov transformation relates the two different coordinate systems.

Consider the canonical commutator relation for bosonic creation/annihilation operators:

$$[\hat{a}, \hat{a}^\dagger] = 1$$

and define a new set of operators

$$\hat{b} = A^* \hat{a} - B\hat{a}^\dagger$$

$$\hat{b}^\dagger = A\hat{a}^\dagger - B^* \hat{a}^\dagger$$

Definition 4.6. *The **Bogoliubov-coefficients** are the complex coefficients A and B.*

The canonical transformation of these operators is called a **Bogoliubov transformation**. The commutator of the new operators must satisfy

$$[\hat{b}, \hat{b}^\dagger] = 1 = [A^*\hat{a} - B\hat{a}^\dagger, A\hat{a}^\dagger - B^*\hat{a}^\dagger] = (|A|^2 - |B|^2)[\hat{a}, \hat{a}^\dagger]$$

Hence the Bogoliubov-coefficients fulfill

$$|A|^2 - |B|^2 = 1$$

This identity closely resembles the hyperbolic identity. Thus, the Bogoliubov-coefficients can be parametrized as

$$A = e^{i\theta}\cosh r \quad \text{and} \quad B = e^{i\theta}\sinh r$$

4.5.6 Horizon crossing

We are especially interested in modes that *cross the particle horizon*. The modes that have left the horizon *cannot* be affected by casual processes. The co-moving wavelength is $\lambda \sim 1/k$, and the quantized fluctuations derived will now satisfy

$$\delta\phi(\mathbf{x}, t) = \frac{1}{a}\int \frac{d^3k}{(2\pi)^3}\Big[a_k u_k(\eta)e^{i k\mathbf{x}} + a_k^\dagger u_k^*(\eta)e^{-ik\mathbf{x}}\Big]$$

Definition 4.7. *A mode is **inside** a horizon provided the wavelength is smaller than the horizon.*

Note from (2.4) that the horizon during inflation equals the conformal time η. A mode is then inside the horizon provided

$$\lambda < |\eta| \qquad \rightarrow \qquad |k\eta| > 1$$

Similarly, a mode will cross the horizon when $|k\eta| = 1$ and be outside if $|k\eta| < 1$. During inflation $\eta < 0$, hence the absolute sign.

4.6 Bunch-Davies vacuum

Section goal 4.6.1. *Establish a suitable vacuum state for the perturbed inflaton field. Analyze how the modes of the field cross the inflation horizon.*

We consider the early stages of inflation, and investigate the properties of the inflaton. The general solution for the perturbed co-moving modes of ϕ were found to satisfy (4.15):

$$u_k(\eta) = A_k e^{-ik\eta}\Big(1 - \frac{i}{k\eta}\Big) + B_k e^{ik\eta}\Big(1 + \frac{i}{k\eta}\Big)$$

In the previous section we reasoned that $|k\eta| \gg 1$ during early stages of inflation. Equation (4.15) is then approximated to:

$$u_k(\eta) \approx A_k e^{-ik\eta} + B_k e^{ik\eta}$$

One of the solutions is chosen, and the default one is the *in-mode* (See chapter 3 for details). In the limit of the infinite past, the modes are infinitely small, and the effects of the inflationary horizon *can be ignored*. This means space-time is essentially Minkowski, and there exists a unique vacuum for the inflaton field. This vacuum is the *Bunch-Davies vacuum*:

Definition 4.8. *We define the **Bunch-Davies vacuum** to be the in-mode solution of (4.15) assuming early stages of inflation ($|k\eta| \gg 1$)*

$$u_k = \sqrt{\frac{1}{2k}} e^{-ik\eta}$$

where the Bogoliubov-coefficient $A_k = (2k)^{-1/2}$ is decided from the harmonical oscillator:

$$\phi_k = \sqrt{\frac{1}{2\omega_k}} (a_k + a^\dagger_{-k})$$

The perturbed inflaton field is then

$$\delta\phi_k = \varphi_k e^{ik\mathbf{x}} = \frac{1}{a} u_k(\eta) e^{ik\mathbf{x}}$$

We conclude this section by the following observation:

Lemma 4.9. *The perturbed u_k modes are (conformal) time-dependent within the horizon. The modes will freeze and stay constant when crossing outside the horizon. In other words, when a Fourier mode has left the horizon, the physics on the scale k is not causally connected, and thus the mode does not evolve.*

Proof: Inside the horizon, $|k\eta| \gg 1$, so

$$|\delta\phi_k| = |\frac{u_k}{a}| = \sqrt{\frac{1}{2k}} (H\eta)$$

which is dependent of the conformal time η. Outside, $|k\eta| \ll 1$ and we find $|u_k| \sim |\sqrt{\frac{1}{2k}} \frac{1}{k\eta}|$. The perturbed field is

$$|\delta\phi_k| = |\frac{u_k}{a}| = \sqrt{\frac{1}{2k^3}} H$$

which is (conformal) time-independent. □

4.7 Chapter conclusions

We conclude this Introductory chapter by stating the most important observations:

Conclusion 4.1. *The metric perturbations during inflation are negligible, only the quantum fluctuations of the inflaton field are important.*

Conclusion 4.2. *The de Sitter space has a well-defined particle vacuum state in the infinite past (Bunch-Davies)*

Conclusion 4.3. *The perturbed modes are time dependent within the horizon, but freeze when leaving. This is natural, as modes outside a horizon have no causal connection.*

Chapter 5

Cosmological perturbation theory

This chapter continues the investigation of inflationary perturbations. We will see that the quantum fluctuations in the inflaton field give rise to scalar perturbations in the metric, seeding the anisotropies in the early universe. In the end, **PG1** will be fulfilled.

Unless otherwise stated, the contents of this chapter is based on [11], [16], [17] and [8].

5.1 Introduction

We have seen that during early inflation, the quantum fluctuations in the inflaton field gave rise to conformal time-dependent modes inside the horizon, while the modes froze when leaving the horizon. This is natural, as causal effects only operates on scales smaller than a particle horizon. In order to simplify the equations, we also neglected the perturbations in the metric. This is a valid assumption during the early stages of inflation, but the metric perturbations become important when inflation ends. As the inflaton perturbations $\delta\phi$ slowly regain its vacuum state, the energy leftovers are dumped into these metric perturbations. We will in this chapter see that these metric perturbations can be divided in to *three* classes: *scalar, vector* and *tensor* perturbations, each which will evolve independently. When inflation ended, the universe was purely radiation-dominated, but with small tensor, scalar and vector perturbations in the metric. Eventually, as the co-moving particle horizon started growing, the scalar perturbations would seed the structure formation of the universe as observed in the cosmic microwave background today.

5.2 The primordial spectrum

Section goal 5.2.1. *Define the power spectrum. Determine the power spectrum for the perturbed inflaton field.*

The primordial spectrum describes the properties of the primordial fluctuations, or the density variations in the early universe. These fluctuations seeded the structure

formation, and the variations originated as quantum fluctuations expanded during the inflation period. We now turn our attention to the **power spectrum**.

Definition 5.1. *A **two-point correlation function** $\rho_{x,y}$ is the correlation between random variables x, y at two different points in space-time, and is defined as*

$$\rho_{xy} \equiv \frac{\langle xy\rangle - \langle x\rangle\langle y\rangle}{\sqrt{\mathrm{Var}(x)}\sqrt{\mathrm{Var}(y)}}$$

For a regular scalar field ϕ in a vacuum state, $\langle\phi(x)\rangle = \langle 0|\phi(x)|0\rangle = 0$. The two-point correlation function is then

$$\rho_{\phi(x)\phi(y)} = \frac{\langle\phi(x)\phi(y)\rangle - \langle\phi(x)\rangle\langle\phi(y)\rangle}{\sqrt{\mathrm{Var}(\phi(x))}\sqrt{\mathrm{Var}(\phi(y))}} = \frac{\langle\phi(x)\phi(y)\rangle}{\sqrt{\langle\phi(x)^2\rangle\langle\phi(y)^2\rangle}} \propto \langle 0|\phi(x)\phi(y)|0\rangle$$

Example 5.2. *For a scalar field, the two-point correlation function gives rise to the **Dirac propagator**: The probability amplitude for a particle to propagate from x to y:*

$$D(x-y) = \langle 0|\phi(x)\phi(y)|0\rangle = \int \frac{d^3p}{(2\pi)^3}\frac{1}{2E_p}e^{-ip(x-y)}$$

The **vacuum fluctuations** are similarly defined, and describes the probability of a virtual state to be created/annihilated within the uncertainty time: $\langle 0|\phi(x)\phi(x)|0\rangle$.

5.2.1 Gaussianity

We assume the fluctuations to follow a **Gaussian distribution**. This is a reasonable assumption, as it is possible to expand a perturbed potential:

$$V(\phi_0+\delta\phi) = \underbrace{V(\phi_0) + \frac{1}{2}V''(\phi_0)(\delta\phi)^2}_{\text{Gaussian}} + \underbrace{\frac{1}{6}V(\phi_0)(\delta\phi)^3 + \dots}_{\text{Non-Gaussian}}$$

In quantum field theory, the second order term gives rise to the two-point correlation function while the higher-order terms ≥ 3 gives rise to interactions, or **vertices**. These higher-order terms spoil Gaussianity, and are neglected.

5.2.2 The power spectrum

The power spectrum is a useful quantity when one is interested in classifying the properties of perturbations. Assume ϕ is a free field in Minkowski space. The field can be expanded in Fourier space as

$$\phi(x) = \frac{1}{\sqrt{V}}\sum_k \left(a_k\varphi_k(t)e^{ik\mathbf{x}} + a_k^\dagger\varphi_k^*(t)e^{-ik\mathbf{x}}\right)$$

where $\varphi_k = (2k)^{-1/2}e^{ikt}$ and $\omega_k = \sqrt{k^2+m^2} = k$ (if the field is assumed massless). The field fluctuates in a vacuum described by a Minkowski-metric, and is a two-point correlation function given by

$$\langle\phi^2\rangle = \langle 0|\phi^2|0\rangle = \frac{1}{V}\langle 0|\sum_{k,'k}\left(a_k\varphi_k(t)e^{ik\mathbf{x}}+a_k^\dagger\varphi_k^*(t)e^{-ik\mathbf{x}}\right)\left(a_{k'}\varphi_{k'}(t)e^{ik'\mathbf{x}}+a_{k'}^\dagger\varphi_{k'}^*(t)e^{-ik'\mathbf{x}}\right)|0\rangle$$

The lowering operator (and the adjoint rising operator) destroys the vacuum $a_k|0\rangle = 0$, so the vacuum expectation value is reduced to

$$\langle\phi^2\rangle = \frac{1}{V}\langle 0|\sum_{k,k'} a_k a^\dagger_{k'}|0\rangle\varphi_k(t)\varphi^*_{k'}(t)e^{i(k-k')\mathbf{x}}$$

The double sum is removed by the commutativity of $[a_k, a^\dagger_{k'}] = \delta_{k,k'}$ for $k \neq k'$, as the operators are free to "commute" their way out and annihilate the vacuum. The double sum is only non-vanishing when diagonal (or $k = k'$), and the expression is

$$\langle\phi^2\rangle = \frac{1}{V}\sum_k |\varphi_k^2| \to \int \frac{d^3k}{(2\pi)^3}|\varphi_k|^2 = \int \frac{dk}{k}\frac{k^3}{2\pi^2}|\varphi_k|^2 = \int \frac{dk}{k}\Delta^2_\phi(k)$$

The final step was done rewriting the expression using spherical coordinates. Assuming isotropy, $\int d^3k = \int d\Omega_3 k^2 dk = \int 4\pi k^2 dk$, where k^2 is the Jacobi-determinant.

Definition 5.3. *The **power spectrum** $\Delta^2_\phi(k)$ is defined as*

$$\boxed{\Delta^2_\phi(k) = \frac{k^3}{2\pi^2}|\varphi_k^2|} \tag{5.1}$$

*and describes the **amplitude** of the fluctuations as a function of the **scale** k.*

Definition 5.4. *We say that a power spectrum is **scale invariant** if it is independent of k.*

Recall that the vacuum expectation value $\langle\phi\rangle = \langle 0|\phi|0\rangle$ for the inflaton is zero. The **variance** of a variable is defined as $\langle\phi^2\rangle - \langle\phi\rangle^2$ and is here reduced to $\langle\phi^2\rangle$. The power spectrum of a field ϕ therefore describes the *variance* of fluctuations.

Example 5.5. *In Minkowski space, $\varphi_k = (2k)^{-1/2}$ so the power spectrum of the inflaton fluctuations is*

$$\Delta^2_\phi(k) = \frac{k^2}{4\pi^2}$$

5.2.3 Harrison-Zel'dovich scaling

We are interested in describing the power-spectrum in a de Sitter space. Recall from (4.5) that a set of new modes in terms of the co-moving coordinates was expressed as

$$\varphi_k = \frac{1}{a}u_k$$

We concluded that fluctuations *outside* the (co-moving) horizon will be constant and the scale of the mode will be

$$|\delta\phi_k| = |\frac{u_k}{a}| = \sqrt{\frac{1}{2k^3}}H \tag{5.2}$$

Proposition 5.6. *The power spectrum during inflation for scalar fluctuations outside the horizon is given by*

$$\Delta^2_\phi(k) = \left(\frac{H}{2\pi}\right)^2 \tag{5.3}$$

Proof: By direct insertion of (5.2) into the expression for the power spectrum (5.1). □

This shows the power spectrum outside the horizon is *scale invariant* when H is constant. This is called the **Harrison-Zel'dovich (HZ)** scaling, and is correct in the limit of infinitely slow rolling of ϕ. Modes with different wave-numbers k will leave the (co-moving) horizon at different times, which makes the HZ scaling inexact without the slow-roll approximation. This means the scalar potential $V \sim \sqrt{H}$ will have different values when the modes cross the horizon. It is at the horizon crossing that the power spectrum is to be evaluated.

5.3 Cosmological perturbation theory

Section goal 5.3.1. *Define cosmological perturbation theory. Pursue scalar field perturbations, and explain why tensor and vector perturbations are neglected.*

We present a short introduction to the theory of cosmological perturbations before venturing deeper into the theory of scalar perturbations. For a comprehensive introduction to cosmological perturbation theory, see [14].

5.3.1 The decomposition theorem

The Lagrangian describing the inflaton is naturally dependent on the inflaton field itself. The energy-momentum tensor's dependence of the Lagrangian $\mathcal{L}(\phi, \partial_\mu \phi)$ is clear from equation (3.5). Then the Einstein field equations (2.2) establish a connection between the energy-momentum tensor and the curvature of space, and the curvature is described by the metric tensor $g_{\mu\nu}$. Hence scalar perturbations of the form

$$\phi \to \phi + \delta\phi$$

will give rise to perturbations in the metric tensor $g_{\mu\nu}$

$$g_{\mu\nu} \to g_{\mu\nu} + \delta g_{\mu\nu}$$

Theorem 5.7 (Decomposition theorem)**.** *Any arbitrary perturbation in the metric can be expressed as the sum of **scalar**, **vector** and **tensor** fluctuations.*

$$\delta g_{\mu\nu} = \delta g_{\mu\nu}^{tensor} + \delta g_{\mu\nu}^{vector} + \delta g_{\mu\nu}^{scalar}$$

These three components can be expanded in terms of spherical coordinates, and will be orthogonal to each other. They are solved separately, and evolve independently in linear perturbation theory. This means that initial tensor perturbations will never affect scalar or vector perturbations at later times, and vice versa.

The **scalar perturbations** will give rise to density fluctuations, while the **tensor perturbations** initiate gravity wave production. The gravity waves have a negligible effect on physics except for the B-modes of the cosmic microwave background polarization. The tensor perturbations are anyways gauge invariant, and evolve identically with any choice of gauge. The **vector perturbations** decays rapidly as the universe expands exponentially, and are ignored [11].

5.3.2 Perturbing the RW metric

A general first-order perturbation of the RW metric is given by

$$g_{\mu\nu} = g^{(0)}_{\mu\nu} + \delta g_{\mu\nu} = a^2(\eta_{\mu\nu} + h_{\mu\nu})$$

where $\eta_{\mu\nu}$ is the Minkowski metric, and

$$h_{\mu\nu} = \begin{pmatrix} 2A & B_i \\ B_i & -C_{ij} \end{pmatrix}$$

where $h_{\mu\nu}$ has 10 degrees of freedom. We rewrite the line element in terms of the perturbations:

$$ds^2 = a^2\Big[-(1+2A)d\eta^2 - 2B_i dx^i d\eta + (\delta_{ij} + C_{ij})dx^i dx^j\Big]$$

We state a well-known theorem without proof:

Theorem 5.8 (Fundamental theorem of vector calculus)**.** *A smooth vector field can be decomposed into irrotational (**curl-free**) and solenoidal (**divergence-free**) component vector fields. This implies that any vector field B_i can be considered to be generated by a pair of potentials: a scalar potential B and a vector potential V_i such that*

$$B_i = -\partial_i B + V_i$$

The C_{ij}-term can similarly be decomposed as

$$C_{ij} = -2D\delta_{ij} + 2\partial_i\partial_j E + \partial_i E_j + \partial_j E_i + h_{ij}$$

where E and D are scalar potentials and E_i a divergence free vector potential. Both sides of the equation has 6 degrees of freedom. Note that the term $\partial_j E_i + \partial_i E_j$ normally has three degrees of freedom, but the divergence relation $\partial_i E_i = 0$ reduces the expression to two degrees of freedom. We characterize the three constituents of the metric perturbations:

- Contributions to the **tensor perturbations** are given by

$$ds^2 = a^2\Big[-d\eta^2 + (\delta_{ij} + \mathcal{H}_{ij})dx^i dx^j\Big]$$

- Contributions to the **vector perturbations** are given by the terms V_i and $\partial_i E_j + \partial_j E_i$, but will decay rapidly as the universe expands during inflation. These perturbations will give little or no effects.

- Contributions to the **scalar perturbations** are given by

$$ds^2 = a^2\Big[-(1+2A)d\eta^2 - 2\partial_i B dx^i d\eta + \big((1-2D)\delta_{ij} + 2\partial_i\partial_j E\big)dx^i dx^j\Big] \quad (5.4)$$

The scalar perturbations will be studied in more detail in the following sections. They will eventually give rise to the density perturbations and seed the structure formation in the early universe.

5.4 Tensor perturbations

Section goal 5.4.1. *Describe the tensor perturbations. Reason for why they are neglected.*

Tensor perturbations do not directly affect **PG1**, but will be treated anyway. This is because they are both interesting and will give aid to the investigation of scalar perturbations. In the previous section, the perturbed metric was defined as

$$g_{ij} = a^2(\delta_{ij} + \mathcal{H}_{ij})$$

where we have chosen to investigate a gravitational wave propagating along the z-axis:

$$\mathcal{H}_{ij} = \begin{pmatrix} h_+ & h_\times & 0 \\ h_\times & -h_+ & 0 \\ 0 & 0 & 0 \end{pmatrix}$$

$\mathcal{H}_{ij}$ has the property that it is *divergenceless, traceless and symmetric*, as $k^i\mathcal{H}_{ij} = 0$ and $\mathrm{tr}(\mathcal{H}) = 0$. What needs to be done is to derive the Christoffel symbols (connection coefficients), then the Ricci tensor followed by the Ricci scalar. A thorough derivation of these quantities can be found in [8] or [11]. We state a recipe for finding an equation of motion for the perturbations.

5.4.1 Golden recipe

1. Calculate the connection coefficients $\Gamma^\mu_{\alpha\beta}$. They are defined from the metric

$$\Gamma^\mu_{\alpha\beta} = \frac{1}{2}g^{\mu\nu}\left(g_{\alpha\nu,\beta} + g_{\beta\nu,\alpha} - g_{\alpha\beta,\nu}\right)$$

2. Find the Ricci tensor using the connection coefficients. The Ricci tensor is defined as

$$R_{\mu\nu} = \Gamma^\alpha_{\mu\nu,\alpha} - \Gamma^\alpha_{\mu\alpha,\nu} + \Gamma^\alpha_{\beta\alpha}\Gamma^\beta_{\mu\nu} - \Gamma^\alpha_{\beta\nu}\Gamma^\beta_{\mu\alpha}$$

3. Calculations show that tensor perturbations *do not affect the Ricci scalar* (to first order).

4. Determine the (spatial) perturbed Einstein tensor from the Ricci-tensor to first order:

$$\delta E_{ij} = \delta(R_{ij} - \frac{1}{2}g_{ij}R) = \delta R_{ij}$$

5. Use the Einstein equation $\delta E_{\mu\nu} = \kappa\delta T_{\mu\nu} = 0$ for tensor perturbations to first order.

After performing these steps (see [8]) it follows from the Einstein equation that $h_\times$ and h_+ obey the equation of motion:

$$\ddot{h} + 2H\dot{h} + k^2 h = 0 \tag{5.5}$$

5.4.2 Solutions to the wave equation

Recall from chapter 4 that the equation of motion for the perturbed scalar field (4.12) satisfies

$$\varphi_k'' + 2\mathcal{H}\varphi_k' + (k^2 + m^2a^2)\varphi_k = 0 \tag{5.6}$$

Equation (5.5) equals (4.12) for a massless field, and was solved rigorously in chapter 4. Still, we mention a basic recipe of obtaining the equation of motion.

First, introduce a new co-moving variable such that the friction terms disappear (see proposition 4.5). The equation of motion should now be that of an harmonical oscillator. Quantize the new solution, that is, promote h to an operator and expand in Fourier space. Let

$$h(k,\eta) = v(k,\eta)a_k + v^*(k,\eta)a_k^\dagger$$

where v are solutions to the classical equation of motion (5.5) and a and $a^\dagger$ are creation/annihilation operators. In the end, the general solution to the equation is given by the Bessel-functions for $\ell = 1$, see equation (4.15). Choose the default in-mode solution such that $B_k = 0$ and the vacuum solution is given by

$$v(k,\eta) = \frac{e^{ik\eta}}{\sqrt{2k}}\Big(1 - \frac{i}{k\eta}\Big)$$

5.4.3 Conclusion

The tensor perturbations behave in much the same way as the fluctuations in the inflaton field. With the same solutions, their power spectra are proportional. But the tensor perturbations evolve independently of scalar and vector perturbations, and are untouched by the same physical effects that modify the scalar perturbations. Detecting these gravity waves would prove very interesting, as they would give a screen shot of the early universe with more information than the cosmic microwave background. There have been several proposed experiments that might measure the existence of gravitational waves, such as LISA [18].

5.5 The freedom of gauge

Section goal 5.5.1. *Define different choices of gauge. Reason why the conformal Newtonian gauge is selected.*

We now turn our attention to scalar perturbations. The tensor perturbations are all gauge-invariant, so there was no need for choosing any specific gauge. This is not the case for scalar perturbations. The scalar metric (5.4) has four perturbing functions: A, B, D and E. We need to determine whether these functions are **gauge invariant**. In chapter 3, we saw that the general gauge transformation is given by the infinitesimal coordinate transformation

$$x^\mu \to x^\mu + \epsilon^\mu$$

By theorem (5.8), this equation can be separated into scalar part (gradient) and a (transverse) vector part:

$$\epsilon^\mu = \partial^\mu\epsilon + \epsilon^\mu_{tr}$$

such that the metric now transforms as

$$\delta g_{\mu\nu} \to \delta g_{\mu\nu} - D_\mu \epsilon_\nu - D_\nu \epsilon_\mu$$

where the covariant derivative is defined in (3.8). For the perturbing functions A, B, D, E to remain gauge invariant, they need to transform as (3.2). If the scalar part of the variation of the metric perturbations is extracted, they will transform as [11]

$$A \to A - \epsilon'^0 - \mathcal{H}\epsilon^0 \tag{5.7}$$
$$B \to B + \epsilon^0 + \epsilon' \tag{5.8}$$
$$D \to D + \mathcal{H}\epsilon^0 \tag{5.9}$$
$$E \to E + \epsilon \tag{5.10}$$
$$\tag{5.11}$$

The physical quantity in question may therefore obtain different values depending on the chosen gauge. This problem needs to be eliminated, and is done by creating a gauge-invariant set of potentials from the metric perturbations.

5.5.1 The Bardeen potentials

From the transformations in (5.7) we can create a set of potentials that transform as gauge-invariant functions.

Definition 5.9. *The **Bardeen potentials** are defined as*

$$\Phi = A + \mathcal{H}(B - E') + (B - E)' \tag{5.12}$$
$$\Psi = D - \mathcal{H}(B - E')$$

Proposition 5.10. *The Bardeen potentials are gauge-invariant with respect to the transformations of the metric perturbations defined in (5.7)*

Proof: By direct insertion. For Φ,

$$\Phi \to A - \epsilon'^0 - \mathcal{H}\epsilon^0 + \mathcal{H}(B + \epsilon^0 + \epsilon' - E' - \epsilon') + (B' + \epsilon'^0 + \epsilon' - E' - \epsilon')$$

Summarizing terms,

$$= A + \mathcal{H}(B - E') + (B' - E') - \epsilon'^0 - \mathcal{H}\epsilon^0 + \mathcal{H}(\epsilon^0 + \epsilon' - \epsilon') + \epsilon'^0 + \epsilon' - \epsilon'$$
$$= A + \mathcal{H}(B - E') + (B' - E') = \Phi$$

A similar calculation shows that $\Psi \to \Psi' = \Psi$. □

5.5.2 The Newtonian gauge

We now employ the freedom of the choice of gauge to eliminate two of the scalar potentials. This is done by choosing ϵ and ϵ^0 such that E and B vanish during transformations. Note that E transforms as

$$E \to E + \epsilon$$

So if $\epsilon = -E$, this potential will vanish. Similarly,

$$B \to B + \epsilon^0 + \epsilon'$$

will vanish if $\epsilon^0 = -B$ for $\epsilon = -E$. Note that the potentials are not *removed*, but a gauge is chosen such that they will always vanish during coordinate transformations. The Bardeen potentials (5.12) now reduce to

$$\Psi = A$$

$$\Phi = D$$

such that the perturbed (scalar) line element (5.4) in turn is

$$ds^2 = a^2\Big[-(1+2\Psi)d\eta^2 + (1-2\Phi)\delta_{ij}dx^i dx^j\Big] \tag{5.13}$$

Definition 5.11. *The choice of gauge resulting in this line element (5.13) is named the* ***conformal Newtonian gauge***

The name "Newtonian" reflects the similarity of the weak-field limit of the line element in the Schwarzschild metric. It is clear from the definition of the line element that it is conformal.

5.5.3 Synchronous gauge

This choice of gauge is preferred for numerical calculations because it leads to better-behaved equations. In the synchronous gauge, ϵ and ϵ^0 is chosen such that A and B vanish. The line element is then

$$ds^2 = a^2\Big[-d\eta^2 + \Big((1-2D)\delta_{ij} + E_{,ij}\Big)dx^i dx^j\Big]$$

5.6 The co-moving curvature

Section goal 5.6.1. *Establish the co-moving curvature $\mathcal{R}$. Determine the power spectrum of $\mathcal{R}$, and define the spectral index. Couple theory to possible observations.*

We are interested in defining a gauge-invariant co-moving quantity that is a linear combination of the fluctuating inflaton $\delta\phi$ and the perturbation potential Ψ. This quantity will continue to exist even though the inflaton field has vanished - and give rise to the initial conditions of the metric perturbations after inflation.

5.6.1 Introduction

Consider the scalar curvature of a hyper-surface defined by a constant conformal time $d\eta = 0$. From its definition, the Ricci scalar (0.2) depends on the connection coefficients, which in turn are based on the metric. Working with scalar perturbations, choose the conformal Newtonian gauge (5.13) such that the scalar curvature of the 3-space hyper-surfaces is expressed as

$$R^{(3)} = \frac{4}{a^2}\nabla^2 D$$

Where D is the perturbed potential from the metric. We denote D as the **curvature perturbation** of the curvature scalar. Recall from the transformation law (5.7)

$$D \to D + \mathcal{H}\epsilon^0$$

that D is *not* a gauge-invariant variable. We proceed by the construction of a gauge-invariant curvature scalar.

Lemma 5.12. *Scalar field fluctuations $\delta\phi$ transform as*

$$\delta\phi \to \delta\tilde{\phi} = \delta\phi - \epsilon^{\mu}\partial_{\mu}\phi_0 \tag{5.14}$$

where ϕ_0 is the non-perturbed background field.

Proof: Recall that a general perturbation of a field ϕ is defined as

$$\delta\phi(x) \equiv \phi(x) - \phi_0(x) \tag{5.15}$$

where ϕ_0 is the unperturbed background field. The fluctuations transform as

$$\delta\tilde{\phi}(\tilde{x}) = \tilde{\phi}(\tilde{x}) - \phi_0(\tilde{x})$$

The scalar field is as always invariant ($\tilde{\phi}(\tilde{x}) = \phi(x)$), while $x \to x + \epsilon$. Hence

$$\delta\tilde{\phi}(\tilde{x}) = \phi(x) - \phi_0(x+\epsilon) = \underbrace{\phi(x) - \phi_0(x)}_{\delta\phi(x)} - \epsilon^{\mu}\partial_{\mu}\phi_0$$

Were we used that ϵ is infinitesimal and expanded ϕ_0. □

Definition 5.13. *The **co-moving curvature scalar** is defined as*

$$\boxed{\mathcal{R} \equiv D + \mathcal{H}\frac{\delta\phi}{\partial_{\mu}\phi_0}} \tag{5.16}$$

Theorem 5.14. *The co-moving curvature scalar is gauge-invariant*

Proof:

$$\mathcal{R} \to \tilde{\mathcal{R}} = \tilde{D} + \mathcal{H}\frac{\delta\tilde{\phi}}{\partial_{\mu}\phi_0}$$

using (5.15) and (5.7) we find

$$\tilde{\mathcal{R}} = D + \mathcal{H}\epsilon^0 + \frac{\mathcal{H}}{\partial_{\mu}\phi_0}(\delta\phi - \epsilon^0\partial_{\mu}\phi_0) = \mathcal{R}$$

□

5.6.2 The power spectrum of $\mathcal{R}$

We proceed by deriving the expression for the spectrum of the primordial curvature perturbations $P_{\mathcal{R}}(k)$. With the definition of the spectral index, it is possible to perform comparisons between theory and observations.

The co-moving curvature scalar can be expressed in terms of the slow-roll parameter ϵ_{sr}:

$$\mathcal{R} = (1 + \epsilon_{sr})\frac{H}{\dot{\phi}}\delta\phi_k$$

where $\dot{\phi}$ and H are now "normal" time dependent quantities. See [11] for a detailed derivation of this expression. In the SRA, ϵ is considered to be very small, so we approximate

$$\mathcal{R} \approx \frac{H}{\dot{\phi}}\delta\phi_k$$

The definition of the power spectrum (5.1) yields

$$\Delta^2_{\mathcal{R}}(k) = \frac{k^3}{2\pi^2}|\mathcal{R}_k|^2 = \frac{k^3}{2\pi^2}\Big(\frac{H}{\dot{\phi}}\Big)^2|\delta\phi_k|^2$$

This expression is to be evaluated at an initial time usually chosen a few Hubble times after horizon crossing. See [9] for further details. The power spectrum of the perturbed scalar field was derived in (5.3):

$$\Delta^2_{\phi}(k) = \Big(\frac{H}{2\pi}\Big)^2$$

The power spectrum is then

$$\Delta^2_{\mathcal{R}}(k) = \Big[\Big(\frac{H}{\dot{\phi}}\Big)^2\Big(\frac{H}{2\pi}\Big)^2\Big]_{k=aH} \tag{5.17}$$

where $\Delta^2_{\mathcal{R}}$ is now evaluated at the horizon crossing $k = aH$. Using the conditions that $H^2 \sim V$ and $\dot{\phi}^2 \simeq \epsilon$, the power spectrum is expressed in terms of the potential and slow-roll parameters:

$$\Delta^2_{\mathcal{R}}(k) \sim \frac{V^2}{\epsilon_{sr}} \tag{5.18}$$

5.6.3 From $\mathcal{R}$ to Ψ

We did not explicitly show that the perturbing potentials Ψ and Φ are negligible during inflation, but mentioned that the co-moving curvature scalar can be expressed as

$$\mathcal{R} \approx \frac{H}{\dot{\phi}}\delta\phi_k$$

In other words: During the time a mode with wave number k crosses the horizon, $\mathcal{R}$ is determined entirely by the inflaton ϕ. But what happens to $\mathcal{R}$ when inflation ends, and ϕ vanishes?

It can be shown [8] that after horizon crossing,

$$\mathcal{R} = -\frac{3}{2}\Psi$$

$\mathcal{R}$ is a *conserved quantity* ($\partial_t\mathcal{R} = 0$, see [8]) when the perturbations leaves the horizon. This means that it is possible to relate Ψ coming out of inflation to $\delta\phi$ at horizon crossing. Thus, fluctuations in the inflaton field during inflation gives rise to metric perturbations after inflation, see figure (5.6.3).

5.7 The Spectral Index

Section goal 5.7.1. *Define the spectral index and estimate its value.*

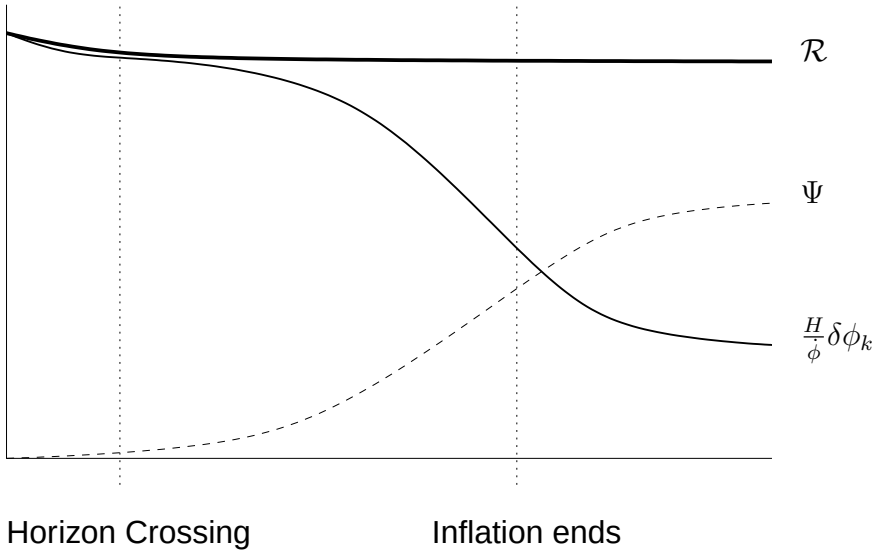

Figure 5.1: The co-moving curvature scalar $\mathcal{R}$ is a conserved linear combination of Ψ and $\delta\phi$

5.7.1 Introduction

We are now naturally interested in trying to *test* the theory of inflation, and this is performed by comparing theory with experimental data. Inflation gives two general predictions:

- The fluctuations in the inflaton field gives rise to scalar perturbations in the metric after inflation, which seed the large scale structures and the observed CMB temperature anisotropies.
- The tensor perturbations give rise to (yet undetected) gravitational waves.

So, did inflation occur or not? The only way to decide is by measuring the properties of the perturbations that inflation generates, that is, we need to decide the power spectrum $\Delta^2_{\mathcal{R}}(k)$ experimentally.

5.7.2 The spectral index

In the regime of the slow-roll approximation, the field $\dot{\phi}$ and the Hubble parameter $H \sim V$ vary little. This implies that the power spectrum of the curvature perturbation is almost *scale invariant* of k, and all the scales of cosmological interest will cross the horizon rapidly during inflation. This gives the physical conditions little time to modify the perturbations, so it is viable to assume a spectrum that follows a power-law behaviour

$$\Delta^2_{\mathcal{R}}(k) \propto k^{n_s - 1} \tag{5.19}$$

where n_s is the **spectral index**. General inflation models predict that $n_s < 1$, while complete scale-invariance would imply $n_s = 1$. A spectrum is **flat** if $n_s = 1$. Taking

the logarithm on both sides results in:

$$\frac{d\ln\Delta^2_{\mathcal{R}}}{d\ln k} \propto n_s - 1$$

motivated by this, we introduce:

Definition 5.15. *The **effective spectral index** $n_s(k)$ is defined as*

$$n_s(k) - 1 \equiv \frac{d\ln\Delta^2_{\mathcal{R}}}{d\ln k}$$

For an interval k with $n(k)$ constant, this definition equals our assumption (5.19). $n_s(k)$ can be described by the slow-roll conditions alone.

$$n_s = 1 - 6\epsilon_{sr} + 2\eta_{sr} \tag{5.20}$$

A nice and exact derivation of this expression can be found at [16]. The spectral index is an important quantity to measure; an observed $n_s < 1$ but close to 1 would strengthen the theory of inflation. We quote a statement from [9]:

Inflation predicts that the variation of the spectrum is small in an interval $\Delta\ln k \sim 1$

5.8 Conclusion and predictions

We conclude the theoretical part of the thesis with a set of predictions. These will be pursued in the following chapters.

Conclusion 5.1. *The fluctuations of the inflaton field ϕ are nearly Gaussian and isotropic.*

Conclusion 5.2. *The power spectrum is near scale-invariant: $n_s \sim 1$, and the fluctuations are equally strong on all scales.*

Conclusion 5.3. *The conserved co-moving curvature scalar $\mathcal{R}$ enables the quantum fluctuations in the inflaton field to give rise to scalar metric perturbations after inflation.*

Conclusion 5.4. *In effect, inflation predicts that n_s will be close to but less than one ($n_s = 1 - 6\epsilon_{sr} + 2\eta_{sr}$).*

Conclusion 5.5. *Only one variable is needed to describe the initial conditions from inflation: The spectral index n_s.*

In the end, we have come to understand the primordial spectrum of the energy density fluctuations during inflation, and **primary goal 1** has been completed.

Chapter 6

Evolving the universe

In the previous chapters we've been preoccupied with the theoretical aspects of inflationary physics. **PG1** was completed during chapter 5, and observational predictions from inflation such as the *spectral index* n_s was established. The intermediate steps between inflation and the universe today are important to comprehend, as different physical effects will shape the main observable in cosmology, the **cosmic microwave background**. This chapter is more phenomenological than the previous and following chapter, and is intended to give a brief introduction to the most important post-inflationary cosmological events. Interested readers are advised to look up chapter 4-8 in [8].

Unless otherwise stated, the contents of this chapter is based on [8].

6.1 Introduction

Section goal 6.1.1. *Establish the Boltzmann equation and initial conditions for the perturbed metric.*

In the previous chapter, the epoch of inflation was treated. Now, after inflation, the inflaton field ϕ has regained its vacuum state, and left a perturbed metric (Φ, Ψ) in a radiation-dominated universe. The evolution of the perturbed metric decoupled into three independent components, the *vector* component that rapidly decayed, the *tensor* component that resulted in gravity wave production and the *scalar* component that eventually seeds the perturbations in matter density. It is therefore the scalar perturbations that are of our primary interest.

6.1.1 The Boltzmann equation

In order to understand the anisotropies in the cosmic distribution of photons and the inhomogeneities in matter distribution, we need to decide on the equations that govern the evolutions of these energy components. The correct way to deduce these equations is through the unintegrated **Boltzmann equation**

$$\frac{df(t, x, p, \hat{p})}{dt} = C[f] \tag{6.1}$$

The Boltzmann equations describes the evolution of the probability distribution f, of a specific particle type around position x at time t with momentum p. Equation (6.1) then says that the number of particles in this phase space doesn't change unless there are collisions $C[f]$. In chapter 5, the scalar perturbations in the metric were defined as Ψ and Φ, where Φ was the spatial and Ψ the time-like perturbation. The Boltzmann equation needs to be solved in this perturbed RW metric for all particle types: *photons, neutrinos, baryons (including leptons)* and *dark matter*. A proper derivation of the Boltzmann equations can be found in [8].

The Boltzmann equation for photons

An important step when deriving the Boltzmann equation for photons is the assumption that the photon distribution is perturbed. This small perturbation is named Θ, such that the perturbed photon distribution can be expressed as

$$f(x,t,p,\hat{p}) = \exp\Big\{\frac{p}{T(t)\big(1+\Theta(x,p,t)\big)}\Big\}$$

This perturbation can be expanded in a series of spherical harmonics $\Theta \sim \sum_{\ell m} \Theta_i Y_{\ell m}$ named **multipoles**. These multipoles (and the photon perturbation) will in turn be identified with the anisotropies in the cosmic microwave background, that is, $\Theta \sim \Delta T$, where ΔT is the deviation of the observed average temperature map T. Photons collide via Compton scattering, which when energy densities are high "smooths" the anisotropies, resulting in negligible multipoles higher than 2 as long as photons are coupled to matter. The complete equations can be found in [8].

The Boltzmann equation for matter

The Boltzmann equations for matter are derived in the same manner as the Boltzmann equations for photons. When deciding the partial differentials, this time higher-order terms of velocities like p^2/c^2 are neglected. This means that free streaming is suppressed in massive fluids, and higher multipoles can be neglected. Cold dark matter is collision-less, which results in collision-less Boltzmann equations. Ordinary baryons do however collide via Thompson scattering, which will give rise to extra terms in the equations. The complete equations can be found in [8].

6.1.2 Evolving the primordial power spectrum

Recall that the primordial power spectrum of the metric perturbation Φ is assumed near-scale invariant (see chapter 5). These perturbations will eventually give rise to energy density anisotropies, and in the end define the anisotropies in the observed power spectrum of the cosmic microwave background. The late-time power spectrum of Φ can then be expressed as

$$P_\Phi(k,a) = P_\Phi^{\text{prim}}(k)\frac{9}{10}T(k)\frac{D_1(a)}{a}$$

where $T(k)$ is the **Transfer function** and $D_1(a)$ is the **Growth function**. The $9/10$-term arises from when the universe goes from radiation to matter domination, as derived in [8]. The transfer function describes the effects induced by evolving from a radiation to a matter dominated universe, while the growth function describes how the matter perturbations grow during late times.

Gravitational and radiation pressure

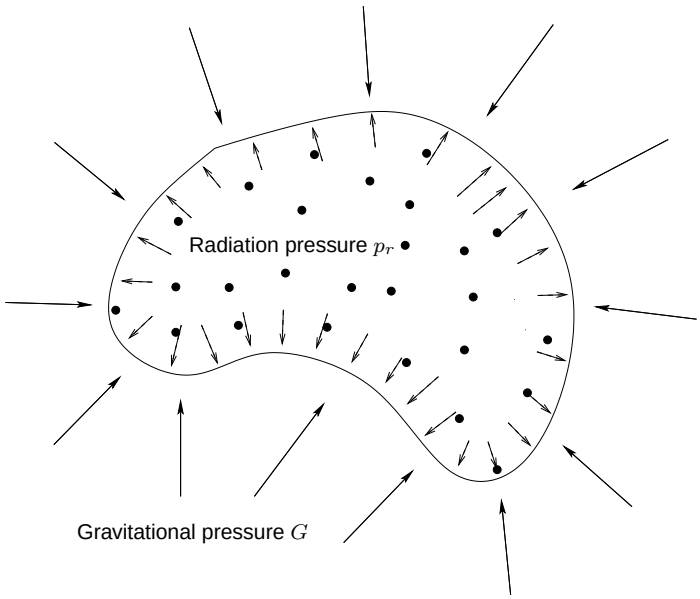

Figure 6.1: Radiation versus gravitational pressure

Two physical effects that impact the power spectrum are **gravitational attraction** and **radiation pressure** (see figure 6.1). For a near-homogeneous fluid of photons, an over-dense area will experience photons streaming away from the overdensities while and under-dense area will experience photons streaming into the area (see figure 6.2). The equations that govern this effect is that of a harmonical oscillator. This will induce sinusoidal oscillations in the power spectrum, first on small scales (first to cross the

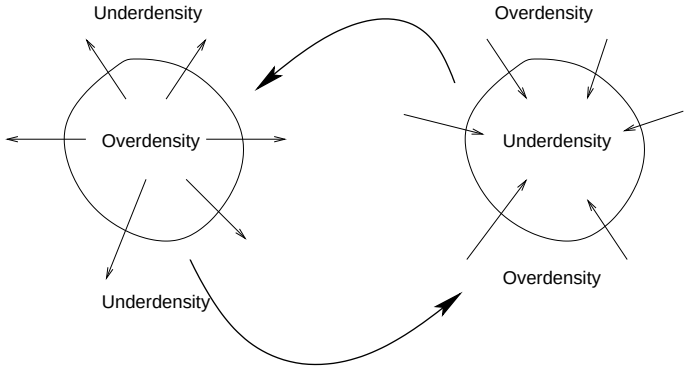

Figure 6.2: When a mode enters the horizon, causal effects begin operating on the corresponding scale. Energy will flow from overdensities to under-dense areas, until the under-dense area has become over-dense. The cycle continues.

horizon) and later on larger scales. However, including gravity, the effect is altered

significantly. Gravitation is attractive, making the streaming from overdensities less effective (see figure 6.1). In addition, photons has a tendency to escape (free-stream) on smaller scales. This will in turn damp the power spectrum on small scales. The harmonical oscillator thus becomes driven and damped. The effect on the angular power spectrum of the CMB will be investigated in the following chapter (see figure 7.5).

6.2 Post-inflationary events

Section goal 6.2.1. *Introduce the different epochs of the universe. State the most important effects.*

6.2.1 The radiation-dominated epoch

When inflation ended, the universe was radiation dominated. Solving the Friedmann equations for a radiation dominated universe, the scale factor becomes proportional to $\sqrt{t}$. As the universe expanded, the radiation dominated epoch lasted until the energy density of matter equaled the energy density of radiation a_{eq}. This epoch had notable effects on the observed power spectrum. Most notably, the shrunk co-moving horizon began to grow, and small-scale Fourier modes of perturbations fell within the horizon, enabling causal contact. This in turn gave rise to acoustic oscillations as mentioned in the previous section.

The Meszaros effect

The Meszaros effect describes the decaying gravitational perturbation Φ during the radiation dominated epoch, and states that the growth of matter overdensities were logarithmic($D_1(a) \sim \ln a$) . This was due to the high radiation pressure, which effectively prevented clumping of matter. In the following chapter, we will explicitly show how these effects modify the angular power spectrum of the cosmic microwave background.

6.2.2 The matter-dominated period

As the universe expanded, the energy density of radiation ($\rho_r \propto a^{-4}$) eventually was surpassed by the energy density of matter ($\rho_m \propto a^{-3}$). The epoch this occurred is called **equality**. Now, the universe became matter-dominated, and the growth of the scale factor became proportional to $t^{2/3}$. This happened about $70\,000$ years after $t = 0$, where the radiation pressure now dropped significantly enough to prevent further decay in Φ. Thus, matter density perturbations began growing steadily proportional to the scale factor ($D_1(a) \sim a$), enabling clumping of matter.

The Sachs-Wolfe effect

A notable event during this epoch was when the energy density of photons became less than the binding energies of electrons and protons, enabling the creation of neutral atoms. At this stage, photons stopped interacting with the electron-proton plasma, enabling free-streaming. This is known as **decoupling**, and happened around $t = 380\,000$ years. The free-streaming photons defines the cosmic microwave background we ob-

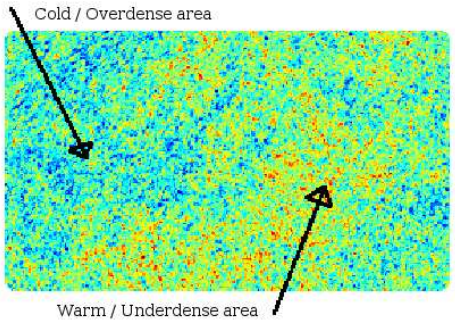

Figure 6.3: Warm and cold spots in the CMB map corresponds to under-densities and over-densities, respectively. This is due to the **Sachs-Wolfe** effect; that photons travelling from an over-dense area needs to escape the gravitational potential well, losing energy.

serve today. When these photons left an over-density, they had to climb a potential well Ψ and therefore lost energy. If these photons were in an under-density, they correspondingly gained energy. This effect is called the **Sachs-Wolfe** effect (see figure 6.4). The observed CMB today is therefore a combination of $\Theta + \Psi$, where cold areas correspond to overdensities and warm spots to under-densities (see figure 6.3).

6.2.3 The cosmological constant-dominated period

The universe today is believed to be dominated by a cosmological constant Λ. The energy density of Λ is constant, and is coupled to the divergent energy density of vacuum (see chapter 2). As the universe expands, there is increasingly more vacuum and hence more vacuum energy. We've seen that vacuum energy exerts negative pressure, which makes the universe expand exponentially. The scale factor today is therefore nearing $a \sim e^{H_0 t}$.

A notable effect in the cosmological constant dominated universe is the integrated Sachs-Wolfe effect. When photons free-stream through a universe, they enter and leave gravitational wells. The overall shift in energy from entering and leaving these wells are cancelled as long as the wells are constant, which is the case with a matter-dominated universe. This is however not the case for a cosmological constant-dominated universe, where the gravitational potential will decay as the universe expands exponentially. This means that photons might enter the gravitational potential well (and gain energy), but then the potential decays as the universe becomes dominated by a cosmological constant. The photon thus gains extra energy, which defines the integrated Sachs-Wolfe effect (ISW) (see figure 6.4). The (late-time) ISW-effect is an important observable when determining whether a universe is in a cosmological constant dominated epoch.

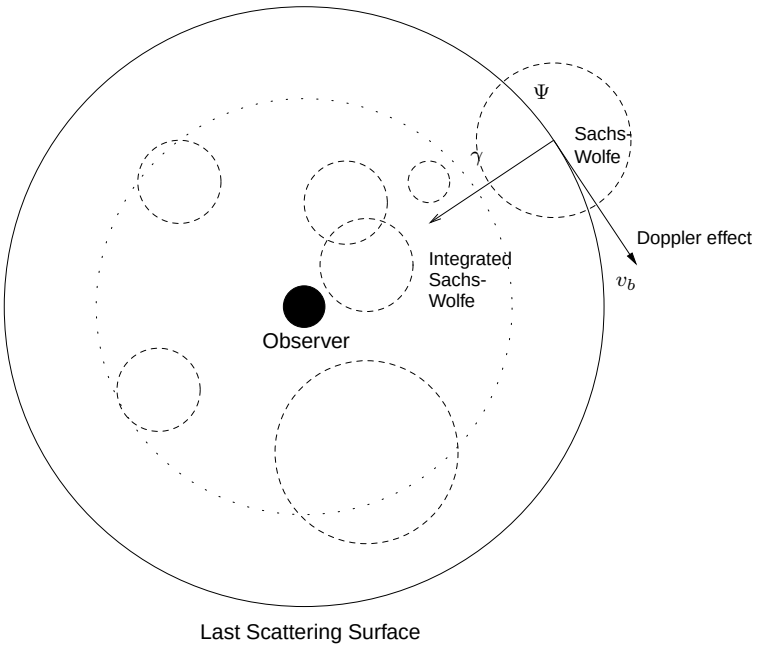

Figure 6.4: Three observable effects: The Sachs-Wolfe effect, the Integrated Sachs-Wolfe effect and Doppler shift.

6.3 The geometry of space

Section goal 6.3.1. *Explain how different geometries affect observables*

We know from general relativity that freely falling particles follow geodesic curves: paths that locally minimize lengths. The equations of motion can be obtained from the geodesic equation

$$(u^{\mu}_{,\nu} + \Gamma^{\mu}_{\alpha\beta} u^{\alpha}) u^{\nu} = 0$$

where u is the geodesic curve. Using $\frac{d}{d\tau} = \frac{dx^{\mu}}{d\tau}\frac{d}{dx^{\mu}}$ one obtains the equation of motion for a particle

$$\ddot{x}^{\mu} + \Gamma^{\mu}_{\alpha\nu} \dot{x}^{\alpha} \dot{x}^{\nu} = 0$$

Flat, spherical and hyperbolic space

If the space-time metric is flat, then the connection coefficients vanish and a particle will follow a straight line: $\ddot{x}^{\mu} = 0$. In a curved space, a free particle will follow the curves of the space. When observing two free propagating particles in flat space, their world lines will stay parallel. If the space is spherical, their paths will eventually converge before oscillating back and forth. In a hyperbolic space, the particles diverge. From equations (2.1), this corresponds to a RW line element with $k = 0$, $k = 1$ and $k = -1$, respectively.

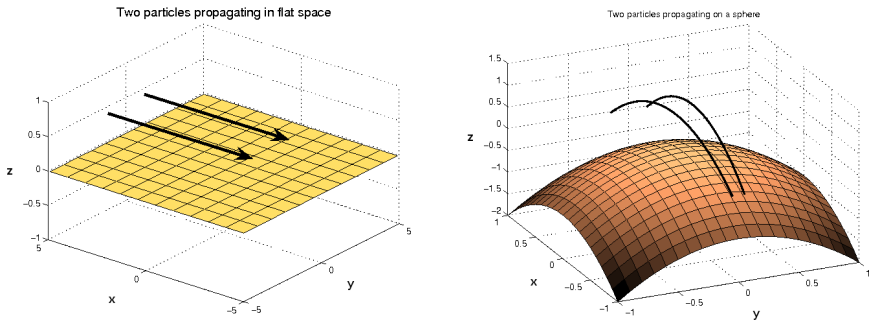

Figure 6.5: Two particles propagating in flat space and spherical space

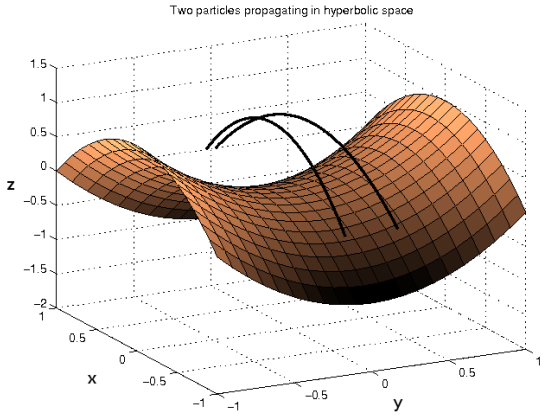

Figure 6.6: Two particles propagating in hyperbolic space will diverge

Measuring the geometry of space

Assume the size of the particle horizon at recombination and the distance to the last scattering surface is known. It is then possible to determine the geometry of space from the angular size of the horizon. The observed power spectrum will be scaled to larger or smaller scales, regarding whether space is open or closed. This will affect the angular power spectrum, shifting the graph left or right.

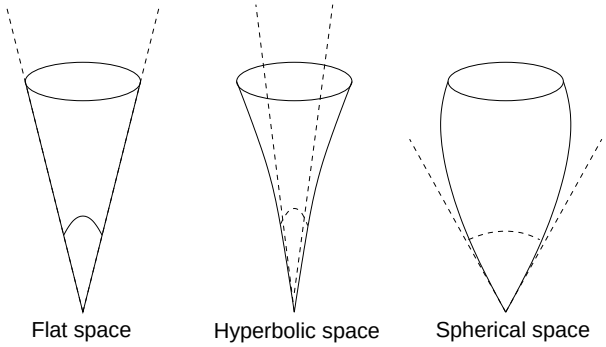

Figure 6.7: Areas observed in a hyperbolic space will appear smaller than reality, and areas observed in a spherical spaced will appear larger.

Current observations indicate that the universe is near flat, but this is only valid if the Hubble parameter is accurately determined to be $h = 0.72 \pm 0.08$, where $H_0 = 100h^2(\mathrm{km/s})/\mathrm{Mpcs}$ [10].

6.4 Chapter conclusions

Conclusion 6.1. *Inflation sets up the initial conditions for the perturbations in the metric (Φ, Ψ).*

Conclusion 6.2. *The universe after inflation has gone through three major epochs: Radiation dominated, matter dominated and cosmological constant dominated. Each epoch affects the growth of matter perturbations in different ways.*

Conclusion 6.3. *The cosmic microwave background was created when the photons decoupled from baryons at a_{dec}. The CMB anisotropies observed today is a combination of $\Theta + \Psi$, where Θ is the perturbation in the Boltzmann equation for photons.*

Part III

Model testing

Chapter 7

The angular power spectrum

7.1 Introduction

While the previous part was concerned with theoretical aspects of the evolution of the universe, we now shift focus to more observational matters. The cosmic microwave background (CMB) anisotropies was established in chapter 6 to be a screen shot of the anisotropies in the photon distribution Θ at a_{eq}. In addition, the Sachs-Wolf effect explained how the photon's wavelength was shifted as they travelled out of dense/underdense areas. In this chapter, we define the tools needed for working with the CMB, and present the standard method of projecting the anisotropies from the sphere onto a 1-dimensional representation, the **angular power spectrum**.

We begin by defining the cosmic microwave background (CMB), being the most important experimental data for testing cosmological models. We then relate the CMB power spectrum to different observables described in the previous chapter, and end with a short introduction to the numerical software needed for data analysis.

Unless otherwise stated, the contents of this chapter is based on [8] and [17].

7.1.1 The cosmic microwave background

Section goal 7.1.1. *Define the cosmic microwave background (CMB).*

We have explained how the quantum fluctuations in the inflaton field gave rise to the initial conditions of the metric perturbations after inflation. This was a radiation-dominated period, and the (scalar) metric perturbations gave rise to the density inhomogeneities observed today.

Definition 7.1. *The **cosmic microwave background** (CMB) is an observable near-isotropic gas of photons resulting from the time when photons and baryons decoupled ($T \approx \Theta + \Psi \sim 3000K$). This period is called the **recombination** era.*

The current average temperature in the CMB today is $2.73K$, and is steadily decreasing due to the expansion of the universe ($\lambda \sim 1/a$). The anisotropies are due to the density inhomogeneities initialized by the scalar perturbations, as seen in the previous part.

7.1.2 The Mollweide projection

The CMB map is defined on the surface of a 2-sphere $\mathbb{S}^2$. In order to be able to visualize a spherical map in flat two dimensions, we need to decide on a suitable projection from $\mathbb{S}^2$ onto $\mathbb{R}^2$ that minimizes loss of data. One such projection is defined in the following way:

Definition 7.2. *The **Mollweide projection** $M(\lambda, \phi) : \mathbb{S}^2 \to \mathbb{R}^2$ is defined as*

$$M(\lambda, \phi) = \Big(\sin^{-1}(\frac{2\theta + \sin(2\theta)}{\pi}), \frac{\pi x}{2\sqrt{2}\cos\theta} \Big)$$

where $\theta = \sin^{-1}(y/\sqrt{2})$, (λ, ϕ) are the spherical coordinates on the sphere $\mathbb{S}^2$ and (x, y) are the Cartesian coordinates in the plane $\mathbb{R}^2$. The Mollweide projection sacrifices fidelity to angle and shape in favor of accurate depiction of area.

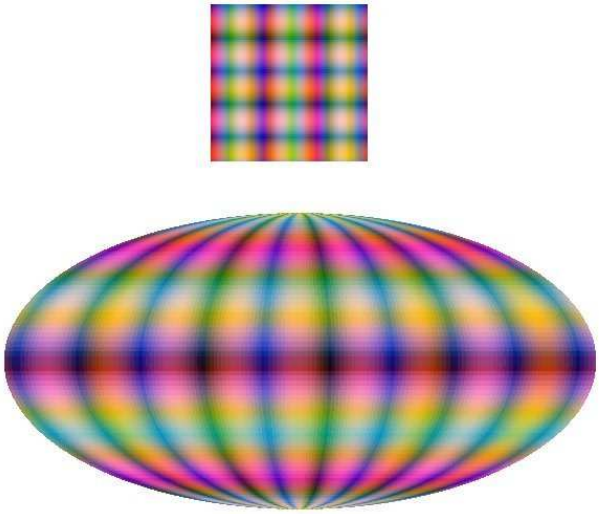

Figure 7.1: An example of a Mollweide projection, created in C++ by the author. The topmost image is *not* a map on the sphere, and shows the effect of how a map $\mathbb{R}^2 \to \mathbb{R}^2$ would transform.

7.2 CMB analysis

Section goal 7.2.1. *Define the standard methods for CMB analysis.*

7.2.1 Spherical harmonics

As in the case with the perturbed inflaton field $\delta\phi$ and the Boltzmann equations, it is useful to decompose the CMB map into Fourier waves with wave-modes. The mathematically inclined reader will recognize the following theorem's importance

Theorem 7.3 (Stone-Weierstrass)**.** *An algebra A of continuous real-valued functions on a compact metric space X that separates points and does not vanish on any points is **dense** in $C(X)$. By dense, we mean that any arbitrary open interval in $C(X)$ can be described by the algebra A.*

Applications of the Stone-Weierstrass-theorem includes the **Fourier** transformations: Any real-valued function $f : \mathbb{R} \to \mathbb{R}$ can be expanded as a set of wave functions, the wave functions are *dense* in $C(\mathbb{R})$. We are interested in decomposing a function defined on the 2-sphere $f : \mathbb{S}^2 \to \mathbb{R}$. The wave-equations on the sphere are defined from Laplace's equation

$$\nabla^2 \psi = 0$$

and its solutions $Y_{\ell m}$ are the well-known **spherical harmonics** functions. They are the analogue to the complex exponential e^{ikx} defined on $\mathbb{R}$, and are described by two quantum numbers: the modes $\ell \in \mathbb{Z}^+$ and $m \in \{-\ell, -\ell+1, \ldots, 0, \ldots, \ell-1, \ell\}$.

Definition 7.4. *The **spherical harmonics** are defined as*

$$Y_\ell^m(\theta, \phi) = \sqrt{\frac{(2\ell+1)}{4\pi}\frac{(l-m)!}{(l+m)!}} P_\ell^m(\cos\theta) e^{im\phi}$$

*where P_ℓ^m are the **associated Legendre polynomials**.*

We state a corollary from Stone-Weierstrass:

Corollary 7.5. *Let $n = (\theta, \phi) \in \mathbb{S}^2$. Then any bandwidth limited map $T : \mathbb{S}^2 \to \mathbb{R}$ can be expanded in spherical harmonics*

$$T(n) = \sum_{\ell=0}^{\ell_{max}} \sum_{m=-\ell}^{\ell} a_{\ell m} Y_{\ell m}(n) \tag{7.1}$$

where the expansion coefficients are given by

$$a_{\ell m} = \int_{\mathbb{S}^2} T(n) Y^*_{\ell m}(n) d\Omega \tag{7.2}$$

Definition 7.6. *The "mode numbers" ℓ and m are the analogue of the wave mode k. We denote different $\ell \in \mathbb{Z}^+$ as **multipoles**. $\ell = 0$ is called the **monopole** moment, $\ell = 1$ the **dipole**, $\ell = 2$ the **quadrupole** etc.*

A useful formula for deciding the relation between the observed *angle* of the sky θ and the multipole ℓ in degrees is

$$\ell \sim \frac{180^\circ}{\theta} \tag{7.3}$$

7.2.2 The angular power spectrum

In chapter 5, the *power spectrum* was defined (see equation (5.1)). It describes the *amplitude* of the fluctuations as a function of the *scale*. There exist several kinds of power spectra:

- $P_{\delta\phi}(k)$: The power spectrum of the fluctuations in the inflaton field.

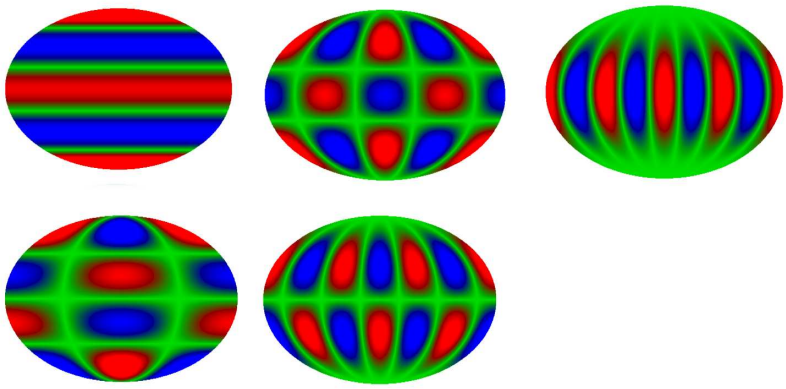

Figure 7.2: The spherical harmonics for $\ell = 4$ and $m = \{0, 1, 2, 3, 4\}$, from top-down left-right respectively. The images are created with a C++ program written by the author.

- $P_\Phi(k)$: The power spectrum of the fluctuation in the metric, induced by the fluctuations in the inflaton field. $P_\Phi(k)$ is assumed to be initially scale-free (near-constant), see chapter 5.
- P_δ: The power spectrum of the fluctuations in the matter density, which also evolves with the universe.

The angular power spectrum is similarly defined:

Definition 7.7. *The **angular power spectrum** measures amplitude as a function of wavelength, and is defined as an average over m for each ℓ:*

$$C_\ell = \frac{1}{2\ell + 1} \sum_{m=-\ell}^{\ell} |a_{\ell m}|^2 \tag{7.4}$$

Note that the averaging is only well-motivated if the map fulfills *isotropy*. This means the spherical harmonics coefficients $a_{\ell m}$ must be independent.

7.2.3 Gaussianity

Assuming that the spherical harmonics coefficients follows a Gaussian distribution, then *all statistical information* will be encoded in the coefficients. This requires the assumption that the isotropies in the CMB are due to quantum fluctuations in the inflaton field during inflation (see page 43).

Definition 7.8. *The Gaussian distribution for $a_{\ell m}$ is given by*

$$P(a_{\ell m}) = \frac{1}{\sqrt{2\pi C_\ell}} e^{-\frac{|a_{\ell m}|^2}{2C_\ell}}$$

In this case, the angular power spectrum is the *variance* of the expansion coefficients $a_{\ell m}$. See section 7.5 for an introduction to Gaussian distributions and likelihood analysis.

7.2.4 Theoretical and observed spectrum

When measuring the cosmic microwave background, we are performing an experiment at one specific point in space-time. Theoretically, an ensemble of data measured from several points in space-time should be gathered before averaging. Practically, the measurements would have to be performed either in other galaxies and/or over an interval of a few hundred hundred years. Needless to say, this isn't possible right now. We are therefore stuck with only *one* observed CMB map, the one measured from Earth.

Definition 7.9. *Given a specific CMB map, the angular power spectrum*

$$\hat{C}_\ell = \frac{1}{2\ell+1}\sum_{m=-\ell}^{\ell} |a_{\ell m}|^2$$

*is the **observed** power spectrum of a specific **realization**.*

Definition 7.10. *Given an ensemble of CMB maps, we define the **ensemble-average** to be*

$$C_\ell = \left\langle \frac{1}{2\ell+1}\sum_{m=-\ell}^{\ell} |a_{\ell m}|^2 \right\rangle$$

From a given set of parameters, the cosmological software package CAMB generates an ensemble-average angular power spectrum C_ℓ as output.

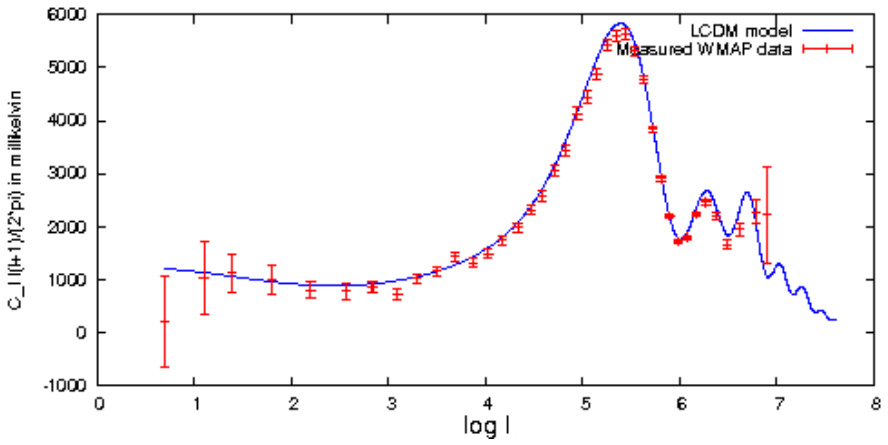

Figure 7.3: A logarithmic plot of the angular power spectrum of a simulated ΛCDM model (creating an ensemble of maps) compared with observed WMAP data (error bars for both noise and C_ℓ)

Notice how the error bars in figure 7.3 grow in size when nearing $\ell = 0$. This effect is due to the *cosmic variance*.

7.2.5 Cosmic variance

The CMB observations measure the different values of C_ℓ for a given multipole ℓ. When small, ℓ describes large angles across the observed CMB sphere (See 7.3). Correlations between such large angles are hard to determine, as there is only one sky to measure - therefore the *uncertainty* (or variance) in the measurements for small ℓ is large.

Example 7.11. *When interested in measuring the quadrupole moment $\ell = 2$, equation (7.3) shows that $90°$ of the sky is required for determining one realization. Thus, there are $360°/90° = 4$ different areas in which to extract data from, resulting in a high cosmic variance.*

The dipole moment is usually omitted, because our galaxy is moving through the local universe. This will red-and blue-shift half of the CMB map, resulting in a signal that is identical with the dipole. The dipole moment was first measured by George Smoot [19] in 1977. For larger ℓ, there are more correlations from smaller angles on the map to average over, and the variance is reduced. Notice how the error bars in figure (7.3) are reduced as ℓ increases. When the observed angle is smaller than the measuring devices can handle, the error increases again.

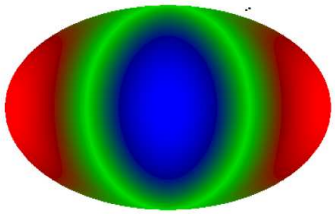

Figure 7.4: The "evil eye" dipole moment $(\ell = 1, m = 1)$ is hard to measure

Proposition 7.12. *The **cosmic variance** is given as*

$$\sqrt{\mathrm{Var}(C_\ell)} = \sqrt{\frac{2}{2\ell+1}} C_\ell$$

Proof: We have not yet developed the tools for performing this proof. Se section 7.4.2 for completion.

7.3 Interpreting the angular power spectrum

Section goal 7.3.1. *Explain how different physical effects modify the angular power spectrum*

In chapter 6, we described how physical effects during the radiation and matter-dominated phases of the universe would modify a power spectrum. We now give explicit graphical examples.

7.3.1 Acoustic oscillations

In the previous chapter, we discussed how density perturbations gave rise to acoustic oscillations (see figure 6.2). These oscillations were given by a damped, driven harmonical oscillator. The driving was a result from gravity preventing de-clumping of matter, while the damping was caused by diffusion of photons on small scales. During the radiation dominated epoch, the small scales were the first to cross the growing co-moving horizon, so the acoustic oscillations started out on small scales. As the horizon grew, increasingly larger scales fell within the horizon, and started oscillating. The acoustic oscillations should be the *most notable* effects in the angular CMB power spectrum.

Figure 7.5 is a descriptive schematic graph of a simulated damped, driven harmonical oscillator. This is what we should expect the angular power spectrum to look like. Compare with the theoretical power spectrum from the ΛCDM-model in figure 7.3.

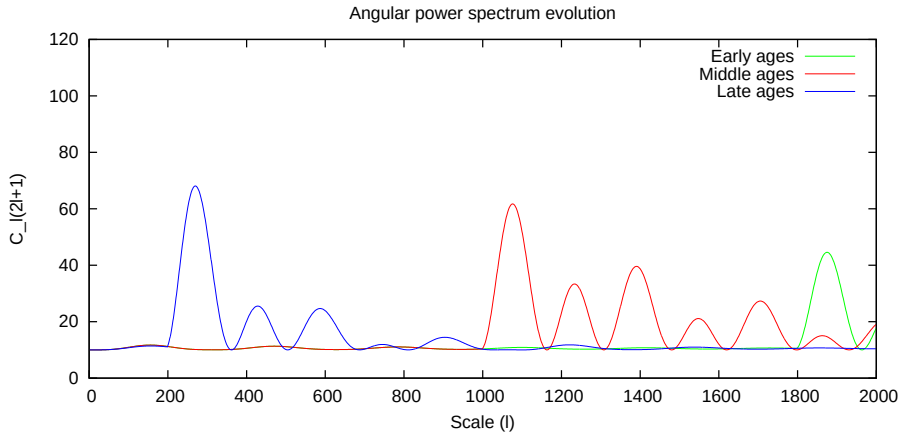

Figure 7.5: A driven, damped, harmonical oscillator in three stages. Notice the similarity with the observed CMB angular power spectrum. Created in C++ by the author.

7.3.2 The geometry of space

In section 6.3, it was explained how the geometry of space affects the measurements (see figure 6.7). In a closed universe, an observed area is smaller than the actual area - shifting the angular power spectrum to larger scales (left). In an open universe, an observed area is larger than the actual area - shifting the angular power spectrum to smaller scales (right). See figure 7.6.

7.3.3 The spectral index

As seen in chapter 5, inflation sets up a near scale-free primordial power spectrum with $n_s = 1 - 6\epsilon_{sr} + 2\eta_{sr}$, such that $P_\Phi(k) \propto k^{n_s - 1} \sim$ constant. But if n_s deviates significantly from 1, then the tilt of the power spectrum will change. This can be observed in figure 7.6.

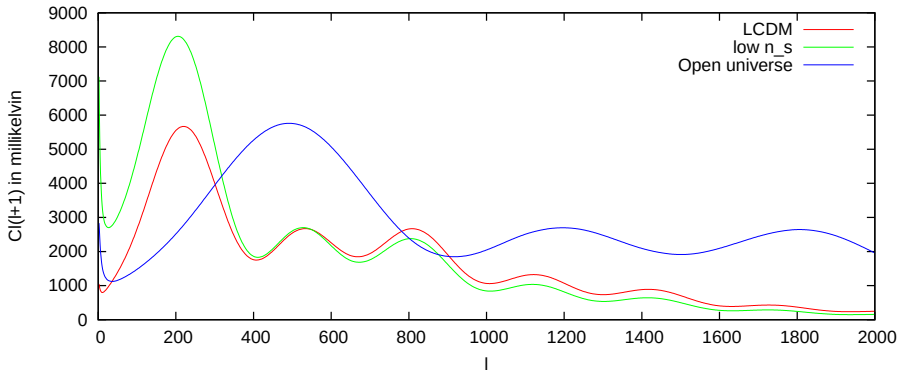

Figure 7.6: Three universe models: the ΛCDM (red line), a low-n_s universe (green line), an open universe (blue line)

7.3.4 The baryon density

The baryon density has a significant effect on the angular power spectrum. The baryons are responsible for setting up the pressure forces, driving the oscillations. Increasing the baryon density will decrease the frequency of the acoustic oscillations, because massive particles are slower than relativistic particles. The massive baryons decrease the acoustic sound waves. In addition, an increase in baryon density will increase the effect of gravity, boosting the "drive" in the harmonical oscillator. This will make the odd acoustic tops taller, and decrease the even tops. See figure 7.7.

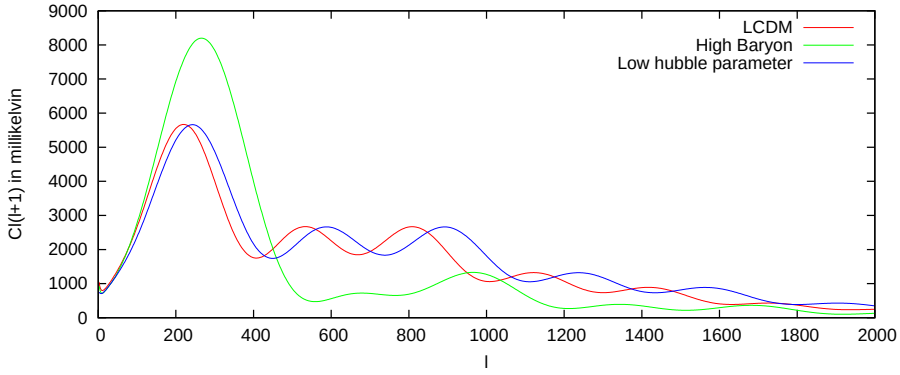

Figure 7.7: Three universe models: the ΛCDM (red line), a low-Hubble parameter universe (blue line), a high baryon universe (green line)

7.3.5 The ISW-effect

The integrated Sachs-Wolfe effect is notable in a cosmological constant-dominated universe. As seen in the previous chapter, a photon emitted from the last scattering surface will travel through a landscape of gravitational potential wells. If these wells

are constant, the overall shift in energy will cancel. This is not the case in a universe dominated by a cosmological constant where space expands exponentially, decaying the potentials. This happened during the *late* stages of a universe, therefore on *large* scales. The plateau before the first acoustic top in the angular power spectrum is most affected by the ISW effect, see figure 7.3. In a matter-dominated universe, this top is much lower than in a late-stage ΛCDM-universe.

7.4 Simulating data

Section goal 7.4.1. *Describe a method for simulating data. Present results from simulations.*

7.4.1 Introduction

It is sometimes interesting to *simulate* a data set based on a theoretical model. This data set can then be used in a parameter estimating process to determine whether parameters are detectable with more accurate data. We now wish to describe a method for generating data based on an assumed cosmological model. First, the parameters that describe the cosmological model must be decided. This is followed by feeding the parameters into CAMB, creating a theoretical power spectrum.

The next step is deciding which probability distribution the data follows. The simulated data will be calculated by drawing stochastic variables from this probability distribution. In section 7.2.3, the expectation value of the temperature fluctuations was mentioned to be zero, and that the fluctuations (or expansion coefficients $a_{\ell m}$) follow a Gaussian distribution. This enabled the definition of the *angular power spectrum* C_ℓ of the temperature fluctuations (eq 7.4).

7.4.2 The χ^2 distribution

In order to decide how C_ℓ is distributed, we need to determine how $\sum_{m=-\ell}^{\ell} |a_{\ell m}|^2$ is distributed. As the $a_{\ell m}$ follows a Gaussian distribution, C_ℓ will follow the distribution of the *sum* of the *square* of Gaussian distributed variables.

Proposition 7.13. *If a_i are n independent, Gaussian distributed random variables with mean 0 and variance 1, then the random variable*

$$C = \sum_{i=1}^{n} a_i^2$$

*is distributed according to the χ^2 **distribution** with n degrees of freedom.*

Definition 7.14. *The χ^2 **distribution** for a continuous, stochastic variable $x \in \mathbb{R}^+$ is defined as*

$$f(x; n) = \frac{1}{2^{n/2}\Gamma(n/2)} x^{n/2-1} e^{-x/2}$$

*where n is the **degrees of freedom**. The χ^2 distribution has expectation value $\langle x \rangle = n$ and variance $\mathrm{Var}(x) = 2n$.*

Summing from $-\ell, \ldots, \ell$, the angular power spectrum has $2\ell + 1$ degrees of freedom. But $a_{\ell m}$ is a complex number containing a real and an imaginary part, both following a Gaussian distribution. This results in $2(2\ell + 1)$ degrees of freedom. But the temperature map T is a real map, imposing constraints on the coefficients $a_{\ell m}$ such that the net results is $2\ell + 1$ degrees of freedom. Summarized,

- The expectation value of the angular power spectrum is the theoretical power spectrum: $\langle \hat{C}_\ell \rangle = C_\ell$
- The expectation value $\langle x \rangle$ of the χ^2 distribution with $(2\ell+1)$ degrees of freedom is $\langle x \rangle = (2\ell + 1)$
- The variance $\mathrm{Var}(x)$ of the χ^2 distribution with $(2\ell + 1)$ degrees of freedom is $\mathrm{Var}(x) = 2(2\ell + 1)$

Proof of the cosmic variance

In section 7.2.5, the proof of the cosmic variance was omitted. We proceed by presenting a small proof. For stochastic variables x and y where $y = bx$, it is true that $\mathrm{Var}(y) = \mathrm{Var}(bx) = b^2\mathrm{Var}(x)$. We find

$$\mathrm{Var}(C_\ell) = \mathrm{Var}\Big(\frac{1}{2\ell+1}\sum_{m=-\ell}^{\ell}|a_{\ell m}|^2\Big) = \Big(\frac{1}{2\ell+1}\Big)^2\mathrm{Var}\Big(\sum_{m=-\ell}^{\ell}|a_{\ell m}|^2\Big)$$

Assuming that $a_{\ell m}$ are Gaussian distributed

$$\mathrm{Var}(\sum|a_{\ell m}|^2) = \frac{1}{4}C_\ell^2 4(2\ell+1)$$

where the Gaussian distribution has been normalized. Inserting, we obtain

$$\mathrm{Var}(C_\ell) = 2\Big(\frac{1}{2\ell+1}\Big)^2\frac{1}{4}C_\ell^2 4(2\ell+1) = \frac{2}{2\ell+1}C_\ell^2$$

and proposition 7.12 has been proved. □

7.4.3 Method

Using the knowledge presented in the previous section, we present a method for simulating a theoretical model.

- Calculate a theoretical power spectrum C_ℓ^{theory} using CAMB
- For each ℓ in the power spectrum:
  - Draw a χ^2 random variable x with $(2l + 1)$ degrees of freedom
  - We observed that $\langle x \rangle = (2l + 1)$, such that $\langle x \rangle/(2l + 1) = 1$. Let the simulated data point be calculated as

$$C_\ell^{sim} = x \cdot C_\ell^{theory}\frac{1}{2l+1}$$

  - Calculate the error in C_ℓ^{sim} via the cosmic variance: $\sqrt{Var(C_\ell^{sim})} = \sqrt{2/(2l+1)}C_\ell$
  - Output $Var(C_\ell^{sim})$, ℓ and C_ℓ^{sim} to file

Implementation

We present a selection of a program **"GenerateData"** developed by the author that implements this method. ps contains the theoretical powers spectrum, xi contains the simulated data, $sigma$ calculates the cosmic variance and $genchi$ generates a χ^2 distributed random number with $2(2l+1)$ degrees of freedom.

```
for (int l=1;l<2000; l++) {
  double s = abs(sigma(l))*(ps[l]); // Cosmic variance
  double chi = genchi(2.0*l +1);
  xi[l]= chi*(ps[l])/(2*l+1.0);
  fs << l << " " << xi[l] << " " << s << endl;
}
```

7.4.4 Results

An example of a simulated data set with 41 data points is shown in figure 7.8.

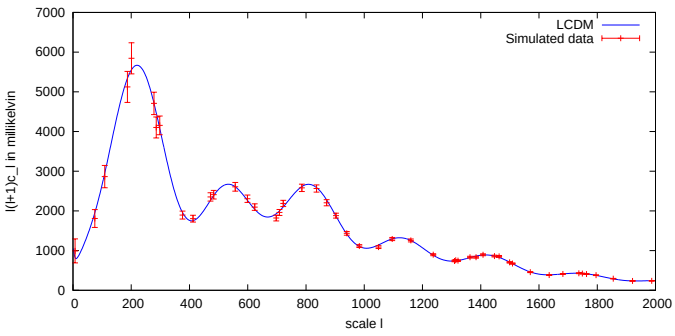

Figure 7.8: A simulated data set (red) compared with the theoretical power spectrum (blue)

7.4.5 Simulating a map from a power spectrum

Having calculated the power spectrum from a simulated ensemble of maps, it is quite a straight-forward technique to convert the spectrum to a visual spherical map. A program which does this is HEALPix. If the coefficients $a_{\ell m}$ is known, one can easily find a simulated CMB realization by

$$T(n) = \sum_{\ell=0}^{\ell_{max}} \sum_{m=-\ell}^{\ell} a_{\ell m} Y_{\ell m}(n)$$

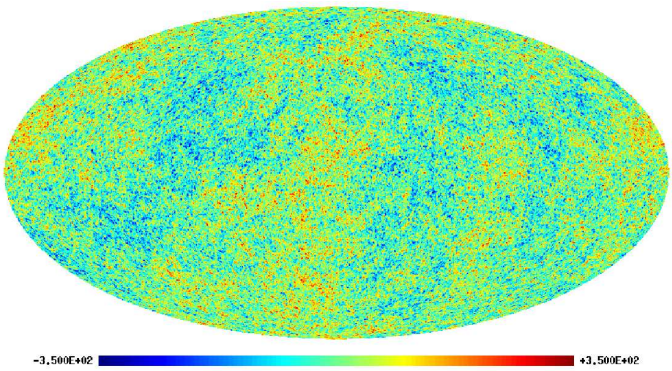

Figure 7.9: An example of a simulated map, created from a theoretical ΛCDM power spectrum generated by CAMB

7.5 Likelihood analysis

Section goal 7.5.1. *Give an introduction to likelihood analysis.*

It is important to test theoretical models given a sample configuration, as in the case with cosmology. For instance, CosmoMC walks a Monte Carlo walk through the parameter space that is used for creating a power spectrum. This theoretical power spectrum (generated from the CAMB modules included in CosmoMC) is tested against various data - WMAP, Supernovae data, etc. This "testing" a model against a sample configuration of data is called *likelihood analysis*, in which the likelihood describes the *probability* that a certain set of data is created from a given model. The likelihood function is spawned from *Bayes' theorem*:

Theorem 7.15 (Bayes' theorem)**.** *Let A and B be stochastic events. Then*

$$\underbrace{P(A|B)}_{\text{posterior}}\underbrace{P(B)}_{\text{evidence}} = \underbrace{P(B|A)}_{\text{likelihood}}\underbrace{P(A)}_{\text{prior}}$$

Definition 7.16. *The likelihood function is the probability for the occurrence of a sample configuration $d = \{x_1, ..., x_n\}$ given a probability density $f(x_i; p_i)$ with theoretical model parameters p_i, or*

$$P(d|p_i) = \mathcal{L}(p_i)$$

Corollary 7.17. *Given a constant or **flat prior**, then the likelihood function is proportional to the posterior:*

$$P(p_i|x_i) \propto \mathcal{L}(p_i)$$

When estimating parameters, we are interesting in maximizing the posterior probability. Corollary 7.17 says that in order to maximize the posterior, we need to *maximize the likelihood*.

7.5.1 Gaussian likelihood analysis

We begin by defining the normal (Gaussian) distribution:

Definition 7.18. *The probability distribution*

$$f(x,\mu,\sigma) = \frac{1}{\sqrt{2\pi\sigma^2}} e^{-\frac{(x-\mu)^2}{2\sigma^2}}$$

*is called the **normal** distribution $N(\mu,\sigma)$ with mean μ and standard deviation σ.*

An important theorem in statistics follows:

Theorem 7.19 (Central limit theorem)**.** *Given a set of stochastic variables $\{X_i\}$ following a probability density with mean μ and variance σ^2, the sum of the stochastic variables*

$$\overline{X} = \sum_{i=1}^{n} X_i$$

is $N(\mu,\sigma\sqrt{n})$-distributed.

Assuming that f is Gaussian,

$$f(x_i;p_i) = \frac{1}{\sqrt{2\pi\sigma_{p_i}^2}} e^{-\frac{(x_i-p_i)^2}{2\sigma_{p_i}^2}}$$

such that the likelihood function can be expressed as

$$\mathcal{L}(x_i;p_i) = \prod_i f(x_i;p_i) = \prod_i \frac{1}{\sqrt{2\pi\sigma_{p_i}^2}} e^{-\frac{(x_i-p_i)^2}{2\sigma_{p_i}^2}}$$

A way to interpret the likelihood function is as follows: Assume the model parameter p_i equals the sample configuration x_i. Then the likelihood probability gets a value of $e^0 = 1$, which means that the data fits *perfectly* with the model. The worse a model fits the sample configuration, the closer to 0 the likelihood probability gets.

7.5.2 Maximizing a Gaussian likelihood

It is often simpler to work with the natural logarithm of the likelihood, or the **log-likelihood**. We find

$$-2\log\mathcal{L}(x_i;p_i) = \sum_i \Big[\frac{(x_i-p_i)^2}{\sigma_{p_i}^2} + \ln\sigma_{p_i}^2\Big]$$

For what model data p_0 is the probability maximized? We differentiate to find

$$-2\frac{d}{dp_0}\log\mathcal{L} = 0 = \sum_i 2\frac{(x_i-p_0)}{\sigma^2}$$

which means

$$-2\frac{d}{dp_0}\log\mathcal{L} = 0 = \sum_i 2\frac{(x_i-p_0)}{\sigma^2}$$

$$0 = \sum_i (x_i-p_0) = \sum_i x_i - N\cdot p_0$$

$$p_0 = \frac{1}{N}\sum_i x_i$$

In other words, the most probable model value for a Gaussian distribution is the average over the data.

7.5.3 Cosmological model testing

We are interested in comparing CAMB-generated theoretical models against our "perfect" simulated data. As seen, a perfect data set (like the generated HW universe model) follows a χ^2 distribution. Thus, the assumption from the previous section shows that given a theoretical model with power spectrum C_ℓ^{theory} and a "perfect" simulated sample configuration C_ℓ^{sim}, the likelihood function is given as (see [20])

$$\mathcal{L} \propto \prod_{\ell m} \frac{e^{-|a_{\ell m}|^2/(2C_\ell^{theory})}}{\sqrt{C_\ell^{theory}}}$$

When summing over the m, the log-likelihood can be rewritten as [20]

$$-2\log\mathcal{L}(x_i;p_i) = \sum_\ell (2\ell+1)\Big[\ln\big(\frac{C_\ell^{theory}}{C_\ell^{sim}}\big) + \frac{C_\ell^{sim}}{C_\ell^{theory}} - 1\Big] \tag{7.5}$$

which is the log-likelihood we will use when modifying CosmoMC to include a set of "perfect" data.

7.6 Software packages

Section goal 7.6.1. *Give an introduction to the most common cosmological software packages*

7.6.1 CAMB

CAMB is an original acronym for "Code for Anisotropies in the Microwave Background". It is a software bundle created by *Antony Lewis* and *Anthony Challinor* [21] and can be downloaded freely *from http://camb.info/*. It is written in FORTRAN, and calculates a theoretical power spectrum from an ensemble of CMB maps generated by a few cosmological parameters. The main numerical methods used in CAMB are based on the original paper by Uros Seljak and Matias Zaldarriaga, who developed an improved method for calculating CMB power spectra [22]. CAMB is originally based on CMBFAST developed by Uros Seljak and Matias Zaldarriaga.

7.6.2 CosmoMC

CosmoMC (Cosmological Monte Carlo) is a software bundle written in FORTRAN by *Antony Lewis* and *Sarah Bridle* that explores the cosmological parameter space using a Markov chain Monte Carlo method. The software employs CAMB modules to calculate the theoretical angular power spectra, and uses the likelihood function to compare data with theoretical models. The time spent estimating d parameters by brute force grid integration scales exponentially with d, while the MCMC method scales linearly in d. Markov chains have the property that they always converge to a stationary distribution. Markov chains are forgetful, they do not remember their past, and the next position is only dependent on the current position. Random walkers are a typical example of Markov chains.

The Metropolis-Hastings algorithm

The core of CosmoMC is based on the Metropolis-Hastings algorithm. When releasing n random walkers from a common initial point in a d-dimensional flat space, the histogram of the walkers will for $n \to \infty$ converge to a d-dimensional Gaussian distribution with increasing variance. In other words; unrestricted "drunk" random walkers will generate a Gaussian distribution. Adding the Metropolis-Hastings algorithm ensures that the random walkers will *follow* a specified distribution, they no longer are "drunk". In CosmoMC, the "random walkers" ambulate through a cosmological parameter space, guided by the *likelihood function*. Hence the walkers are *forced* to converge to a distribution specified by the likelihood function. The Metropolis-Hastings algorithm can be summarized as follows:

- Initialize walkers at random positions in d-dimensional parameter space. A single walker is denoted $p = \{p_0, p_1, \ldots, p_d\}$.
- For a given walker's parameter p_i, decide whether it should consider going left or right in parameter space: $p_i = p_i + s$ were s is ΔP_i or $-\Delta p_i$ by 50% probability.
- Calculate the likelihood function $\mathcal{L}_{old}$ at p_i and $\mathcal{L}_{new}$ at $p_i + s$.
- If $\mathcal{L}_{old} < \mathcal{L}_{new}$ then accept p_i immediately.
- Else calculate a probability for accepting the new step by using $\mathcal{L}_{old}/\mathcal{L}_{new}$.
- Repeat for all parameters for all walkers until walkers converge to a distribution.

Mechanics of CosmoMC

Let P_n denote the parameter space after n steps. The algorithm CosmoMC employs is summarised as follows:

1. Initialize P_0 at random positions in the parameter space.
2. Call CAMB modules for determining a theoretical power spectrum C_l with P_0.
3. Calculate the likelihood function $\mathcal{L}(P_0)$ between C_l and different data sets.
4. Decide a new set of random parameters P_1 using the assumed input parameter distribution and P_0.
5. Call CAMB modules for generating a new power spectrum C_l' using P_1, and calculate a new likelihood $\mathcal{L}(P_1)$ by comparing C_l' with data.
6. Use the Metropolis-Hastings algorithm to decide whether to accept this new point P_1 in the chain or not using $\mathcal{L}(P_0)$ and $\mathcal{L}(P_1)$.
7. If step is accepted, update parameter distributions. Also update failure status if not accepted.
8. Go to step 2 until the distributions converge.

The first samples are affected by random initial parameters, and are usually omitted. This is named **burn-in** time, and CosmoMC usually needs to omit 1000 of its first samples. The chains eventually converges to their stationary distribution.

Likelihood contours

If two parameters are successfully estimated and correlated, their confidence contours should resemble those of figure 7.10.

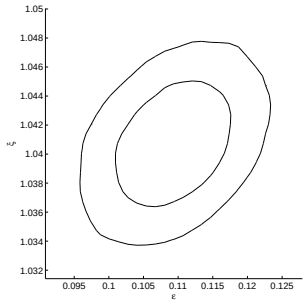

Figure 7.10: Parameter estimation for θ, Ω_b with 68% and 95% confidence contours.

7.7 Chapter conclusions

Conclusion 7.1. *The CMB anisotropies are decomposed into spherical harmonics. Assuming that the fluctuations are Gaussian, one sums over m and obtains the angular power spectrum.*

Conclusion 7.2. *Following a χ^2 distribution, the angular power spectrum encodes all statistical information about the distribution of anisotropies if the coefficients $a_{\ell m}$ are Gaussian.*

Conclusion 7.3. *The shape of the angular power spectrum is determined by different physical effects: Whether the universe is open/closed, the baryon density, the cold dark matter density, the cosmological constant, energy component dominance, etc.*

Conclusion 7.4. *The χ^2 distribution is used to create simulated data from a given theoretical model.*

Conclusion 7.5. *Likelihood analysis is used to to test a theoretical model against data. We have established a log-likelihood in equation 7.5 for using "perfect" data.*

Chapter 8

Paper review

This chapter is devoted to investigating papers concerning trans-Planckian effects in the primordial power spectrum. With *trans-Planckian*, we mean effects that occur when gravity becomes non-negligible and Minkowskian quantum field theory breaks down. Even though the underlying physics at the Planck scale is yet unknown, it is still possible to determine a generic *alteration* on some observables from the trans-Planckian effects. In our case, the intense curvature of space at the Planck-scale renders the inflaton vacuum non-trivial. This results in a postulated *modified* primordial power spectrum, no longer scale-free but dependent on two new parameters: the slow roll parameter ϵ_{sr} and a Planck-cutoff ξ. This modulation represents a *generic* form for how trans-Planckian effects modify the primordial power spectrum, and will be used in the following chapters.

8.1 Introduction

During the inflationary phase in the very early universe, quantum gravitational effects are expected to modify the primordial power spectrum. As seen in the previous chapters, the primordial fluctuations are the seeds for the anisotropies in the CMB and the large scale structures we observed in the universe today. It is therefore possible for cosmological observations to shed light on Planck-scale physics [7]. The difficult part is separating the primordial density fluctuations from the present-day observable power spectrum, which will be shown in the following chapter.

The idea from [23] and [24] is that the primordial power spectrum becomes modulated at Planckian scales. We do not know exactly *what* kind of new physics appear, whether it be stringy ones or unknown, but it will follow a generic pattern: the inflaton vacuum becomes nontrivial. The standard calculation of the perturbations produced during inflation is based on *flat-space* quantum field theory, and initial conditions on ϕ are imposed in the infinite past (see chapter 4 and 5). In chapter 3, we saw how the vacuum of a scalar field become nontrivial in a curved space, when gravity no longer can be neglected, as is the case during early inflation. This will alter the primordial power spectrum with a factor dependent on three parameters, k, ξ and ϵ_{sr} such that

$$P_0 \rightarrow P_0 \cdot f(k, \xi, \epsilon_{sr})$$

8.2 Note on inflation and trans-Planckian physics

Section goal 8.2.1. *To establish a modified power spectrum of the inflaton fluctuations that includes trans-Planckian oscillations.*

This paper [23] by *Ulf H. Danielsson* considers the influence trans-Planckian physics has on the primordial power spectrum. A practical "toy"-model is considered, such that analytical solutions are possible. In the end, the ambiguities in the choice of the vacuum will give rise to effects with a magnitude of the order H/Λ, where Λ is the cutoff scale for new physics.

8.2.1 Introduction

This section is devoted to the study of the adiabatic vacuum. We start off with a scalar field ϕ in an inflating RW metric. From (4.1) we found that the field evolves as

$$\ddot{\phi} + 3H\dot{\phi} - \frac{1}{a^2}(\nabla^2\phi) = 0 \tag{8.1}$$

for a zero potential. In terms of co-moving modes and conformal time in Fourier space, we found this to equal (4.13)

$$\mu_k'' + \Big(k^2 - \frac{a''}{a}\Big)\mu_k = 0$$

with the conjugate momentum

$$\pi_k \equiv \frac{\partial \mathcal{L}}{\partial \dot{\phi}} = u' - \mathcal{H}\mu_k$$

The author argues that the Heisenberg picture is the most convenient to use when quantizing the system. The field is then quantized:

$$\mu_k(\eta) = \sqrt{\frac{1}{2k}}\Big(a_k(\eta) + a_{-k}^\dagger(\eta)\Big)$$

with the conjugate

$$\pi_k(\eta) = -i\sqrt{\frac{k}{2}}\Big(a_k(\eta) - a_{-k}^\dagger(\eta)\Big)$$

8.2.2 Bogoliubov transformation

The author then proceeds by performing a Bogoliubov-transformation of the raising and lowering operators $\big($see definition (4.6)$\big)$. The purpose of this transformation is to *fix the oscillators at* $a_k(\eta_0) \equiv a_{k0}$ while the Bogoliubov-coefficients remain time-dependent. As stated earlier, we need to decompose the field into *positive and negative* frequency components before defining the creation and annihilation operators. Hence

$$a_k(\eta) = u_k(\eta)a_{k0} + v(\eta)a_{-k0}^\dagger$$

and

$$a_{-k}^\dagger(\eta) = u_k^*(\eta)a_{-k0}^\dagger + v^*(\eta)a_{k0}$$

The modes μ_k and its conjugate π_k are now expressed in terms of the B. coefficients. Define

$$f_k(\eta) \equiv \sqrt{\frac{1}{2k}}\Big(u_k(\eta) + v_k^*(\eta)\Big) \tag{8.2}$$

and

$$g_k(\eta) \equiv \sqrt{\frac{k}{2}}\Big(u_k(\eta) - v_k^*(\eta)\Big)$$

such that

$$\mu_k(\eta) = f_k(\eta)a_{k0} + f_k^*(\eta)a_{-k0}^\dagger$$

and

$$\pi_k(\eta) = -i\big(g_k(\eta)a_{k0} - g_k^*(\eta)a_{-k0}^\dagger\big)$$

We check by insertion that this is true for μ_k:

$$\mu_k(\eta) = f_k(\eta)a_{k0} + f_k^*(\eta)a_{-k0}^\dagger = \sqrt{\frac{1}{2k}}\Big(u_k(\eta) + v_k^*(\eta)\Big)a_{k0} + \sqrt{\frac{1}{2k}}\Big(u_k^*(\eta) + v_k(\eta)\Big)a_{-k0}^\dagger$$

which equals

$$\mu_k(\eta) = \sqrt{\frac{1}{2k}}\Big(u_k(\eta)a_{k0} + v_k(\eta)a_{-k0}^\dagger\Big) + \sqrt{\frac{1}{2k}}\Big(u_k^*(\eta)a_{-k0}^\dagger + v_k^*(\eta)a_{k0}\Big) = \sqrt{\frac{1}{2k}}\Big(a_k(\eta) + a_{-k}^\dagger(\eta)\Big)$$

8.2.3 The adiabatic vacuum

The author continues by discussing the choice of vacuum. The vacuum in the Minkowski-metric is quite different from a vacuum in a curved space-time. As we saw in chapter 2, symmetry transformations in the flat Minkowski-metric corresponds to conserved currents. A transformation of a vacuum in curved space doesn't necessarily result in a vacuum. In curved space-time, particles might be created/annihilated by the effect of curvature.

It is stated that a reasonable vacuum candidate is the **adiabatic vacuum:**

$$a(k, \eta_0)|0, \eta_0\rangle = |0, \eta_0\rangle = 0$$

where this corresponds to a class of vacua depending on η_0. For this particular choice,

$$a(k, \eta_0)|0, \eta_0\rangle = \Big(u_k(\eta_0)a(k, \eta_0) + v(\eta_0)a^\dagger(k, \eta_0)\Big)|0, \eta_0\rangle = 0$$

The first term is zero by definition, but the second term does not automatically vanish; hence

$$v_k(\eta_0) = 0$$

With this condition, we see that

$$g_k(\eta_0) = kf_k(\eta_0)$$

The conjugate momentum is then simplified as

$$\pi_k(\eta_0) = ik\mu_k(\eta_0)$$

8.2.4 Interpretation of the adiabatic vacuum

In the ideal situation, there would only exist a unique definition of the vacuum in the infinite past and the infinite future. The time evolution of the initial vacuum will not necessary generate the final vacuum, and will give rise to creation of particles (see chapter 3). The author argues for the adiabatic vacuum, even though it is not a solution of the exact field equation, it does correspond to *some* choice of vacuum. The adiabatic vacuum is *not* unique but depends on η. However, in de Sitter space, it happens that the finite order adiabatic vacuum obtained in the infinite past corresponds to an exact solution of the field equations, and is therefore distinguished [15]. When the modes are small enough, they are not affected by the (slow) expansion of the universe.

There are however also other vacuum choices, like the minimum uncertainty discussed in the paper. The author then argues that these vacua only agrees to zeroth order, and it is only in zeroth order that the expansion of the universe can be ignored, and the ambiguities are removed.

Note that *the distinction of various vacua only becomes important since we insist on imposing the choice of vacuum at a finite time corresponding to a energy on the Planck scale*. Any claim about the structure of the vacuum above the Planck-scale requires knowledge of physics on this scale. Since this knowledge is not yet available, one can only list various alternatives.

The author continues by deriving a general expression for a zeroth order adiabatic approximation, and the solution of a mode equation coincides with the choice in the previous section. Hence the vacuum used will be the zeroth order adiabatic vacuum.

8.2.5 The modified primordial power spectrum

The author proceeds by deriving a modified primordial power spectrum

$$P_\phi = \Big(\frac{H}{2\pi}\Big)^2 \Big(1 - \frac{H}{\Lambda}\sin\big(\frac{2\Lambda}{H}\big)\Big) \tag{8.3}$$

For a proper derivation of this expression, see appendix B. Note the following facts:

- Λ signifies the energy scale of where new physics occur (the Planck scale, stringy scale etc)
- When Λ increases, the oscillations fluctuate with higher frequencies as the amplitude decreases.
- The original primordial power spectrum (5.3) is regained when $\Lambda \to \infty$

8.3 Can MAP and Planck map Planck physics?

Section goal 8.3.1. *To enable the modified power spectrum to possess more familiar parameters*

This article [24] by *Lars Bergström* and *Ulf H. Danielsson* is a follow-up article of [23]. It explains how to modify the postulated power spectrum given in equation (8.3) to possess more familiar parameters. The paper starts off giving a review of the setup

of the modified power spectrum and the physics behind. The introduction discusses a class a vacua depending on η_0, and when $\eta_0 \to -\infty$, the Bunch-Davies vacuum (see page 46) is restored. This means it is done at a fixed scale, not a fixed time, and the physics will *be independent of time*.

8.3.1 What to look for

In this paper, *Danielsson* and *Bergström* develop a series of relations between the Hubble parameter H, the cutoff scale Λ and the slow roll parameter ϵ_{sr}, using two auxiliary parameters ξ and γ. For a thorough derivation of these relations, see appendix C. We now *define* the Planck-scale cutoff Λ:

Definition 8.1. *The Planck-scale cut-off Λ is defined to be proportional to the reduced Planck-mass:*

$$\Lambda \equiv \gamma M_p$$

*where $\gamma \approx 0.01$ and $M_p = 1/\sqrt{8\pi G}$ is the **reduced Planck mass**.*

Definition 8.2. *Let ξ be*

$$\xi \equiv \frac{H}{\Lambda} = \frac{H}{\gamma M_p} \sim 4.0 \cdot 10^{-4} \frac{\sqrt{\epsilon_{sr}}}{\gamma} \tag{8.4}$$

Example: the Horava-Witten model

The authors refer to [25] for an introduction to the **Horava-Witten** (HW) model. Here, unification occurs roughly at the same time a fifth dimension becomes visible. As a rough estimate, the author sets $\Lambda \sim 2 \cdot 10^{16} GeV$, and corresponds to $\gamma = 0.01$. The Hubble constant during inflation is restricted to $H \sim 7 \cdot 10^{13}$ GeV, corresponding to $\epsilon_{sr} \sim 0.01$. Using (8.4), we find

$$\xi \sim 0.0004$$

$$\frac{\Delta k}{k} \sim \xi \frac{1}{\epsilon_{sr}} \sim 1 = \Delta \ln k \tag{8.5}$$

which means one oscillation pr *logarithmic* interval in k. The authors claim this should be visible in high-precision CMB observation experiments.

8.3.2 Predictions for CMB measurements

The authors continue to parametrize the primordial power spectrum using ϵ_{sr} and $\xi = H_n/\Lambda$, where H_n is evaluated at some particular scale where k_n leaves the horizon. This results in a modified ξ:

$$\frac{H}{\Lambda} = \xi \Big(\frac{k}{k_n}\Big)^{-\epsilon_{sr}}$$

and enable the authors to *parametrize* the power spectrum (8.3):

$$\boxed{P(\epsilon_{sr}, \xi, k) = P_0(k)\Big(1 - \xi\Big(\frac{k}{k_n}\Big)^{-\epsilon_{sr}} \sin\Big[\frac{2}{\xi}\Big(\frac{k}{k_n}\Big)^{\epsilon_{sr}}\Big]\Big)} \tag{8.6}$$

where $P_0(k)$ is a scale-invariant spectrum. The authors argue that using ξ instead of γ is advantageous because it is a small parameter that can be extrapolated to zero

($\xi \sim 0.0004$ in the HW case). The trans-Planckian effects will have an unobservable small amplitude in this limit.

The possible variation of ϵ_{sr} is limited by the normalization of the observed temperature fluctuations, so effectively one can choose to regard the effects as being a *one*-parameter family of modulating functions, with amplitudes determined by ξ.

8.4 Chapter conclusions

We have seen that trans-Planckian effects in the power spectrum can be expressed as in equation (8.6), where

Conclusion 8.1. *The oscillations in the primordial power spectrum are caused by a nontrivial vacuum for the inflaton field [23, 26]. The oscillations modify the primordial power spectrum as given in equation 8.6.*

Conclusion 8.2. *ξ is the ratio of the Hubble parameter to the scale where trans-Planckian effects start, and is chosen to be $\xi =\sim 4 \cdot 10^{-4}\sqrt{\epsilon_{sr}}/\gamma$. γ is the scale of the Planck-mass where trans-Planckian effects occur, and is chosen to be $\gamma = 0.01$. ϵ_{sr} is the slow-roll parameter, restricted to 0.01 in our model.*

Chapter 9

Trans-Planckian effects

9.1 Introduction

In the previous chapter, we saw how trans-Planckian effects are supposed to give rise to a *generic* modulated primordial power spectrum. In this chapter, we begin by summarizing the most important work done on this field, before performing independent investigations. We will argue that some of the claims from the community might be overly optimistic.

9.1.1 Generic effects

In [23], *Ulf H. Danielsson* concludes with the following statement: " ... effects of trans-Planckian physics are possibly within the reach of cosmological observations even though much more detailed calculations are require to make a definite statement". Equation 8.6 describes a a *generic* expression for how trans-Planckian effects would modify the primordial power spectrum. As seen in the previous chapter, these oscillations are supposed to be caused by a nontrivial vacuum for the inflaton field [23, 26]. As the oscillations are expected to contribute to the energy density, this could change the way the universe expands. In a worst-case scenario, the inflationary phase could be destroyed. In [26], *Danielsson* investigates this possibility, and concludes that the "back reaction is under control and fully consistent with inflation, with a slow roll found to be completely dominated by the vacuum energy given the parameters suggested in [2]".

9.1.2 WMAP data and trans-Planckian effects

Earlier data analysis [27] concludes that no significant signals from trans-Planckian effects were found in the CMB. Another analysis [2] claims that there are some weak hints in the current data, and these indications have become slightly stronger with the WMAP3 data compared to earlier claims by the same authors [1, 2, 28, 29]. The parameters implied by the data suggests oscillations in amplitude that are periodic in the logarithm of the scale of the CMB fluctuations, just as predicted from trans-Planckian physics.

Another paper [7] is less optimistic, and concludes that "... it is unlikely that a trans-Planckian signature of this type can be detected in CMB and large-scale structure data". We will follow this line, and show that the current WMAP3 data does **not** give

valuable constraints on the slow-roll parameter and Planck-cutoff scale using MCMC methods.

9.1.3 Simulated data and trans-Planckian effects

In [1], *Jerome Martin* and *Christophe Ringeval* discuss the so-called **cosmic variance outliers**, i.e. points which lie outside the 1σ cosmic variance error. These outliers are considered interesting as the probability of their presence is very small [30]. The authors mention that it has been envisaged that the outliers could be a signature of new physics, even though the cosmic variance could be responsible for their presence. The conclusion of [1] is that there exist statistical justification for a presence of oscillations in the power spectrum.

Opposing this claim, the conclusion of [7] is that trans-Planckian effects in CMB and LSS data are in principle sensitive to modulations in the primordial power spectrum, but that is practically impossible to make a positive detection *even in future high-precision data*. This has to do with the *nature* of the oscillations, " ... the value of the likelihood function is extremely sensitive to ϵ and ξ". But what is meant by "extremely sensitive" is not mentioned in [7]. We will later show explicit examples of *why* and *how* this sensitive likelihood function means trouble, and why this renders the underlying MCMC method in CosmoMC useless.

9.2 The nature of the oscillations

Section goal 9.2.1. *Investigate the properties of the oscillations. Verify the validity of the modified code.*

From now on, we let ϵ denote ϵ_{sr}.

9.2.1 Introduction

We continue by investigating the properties of the oscillations in the primordial power spectrum. CAMB was modified to include two new parameters, the slow-roll ϵ and the Planck-cutoff ξ. See appendix A for details on these modifications. We present a first run of CAMB with the modulated power spectrum as given in the previous section. Recall from section 8.3.1 that the modulating parameters in the Horava-Witten model are $\xi = 0.0004$, $\gamma = 0.01$ and $\epsilon = 0.01$. This results in a slightly modified power spectrum, see figure 9.1. A table with the remaining parameters used for this model is given in table 9.1. These values will be used throughout the thesis.

Definition 9.1. *Let ΔC_ℓ denote the difference between a modulated and a non-modulated power spectrum.*

Notice how little the modulated power spectrum deviates from the original. Figure 9.3 is more clear on this.

Parameter	Value	Description
$\Omega_b h^2$	0.022	Baryon density
$\Omega_{cdm} h^2$	0.12	Cold Dark Matter density
τ	0.04	The optical depth
n_s	0.99	The spectral index
$log[10^{10} A_s]$	2.3	The amplitude of the primordial power spectrum
Ω_Λ	0.71020	Cosmological constant energy density
Age/GYr	13.592	Age of the universe in this model
H_0	70	The Hubble constant today in this model
w	-1	The equation of state $p = w\rho$

Table 9.1: Parameter values used for the simulated model.

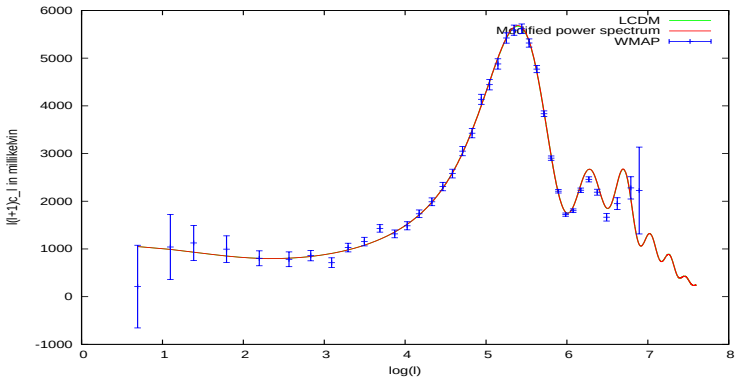

Figure 9.1: Logarithmic plot, $\xi = 0.0004$, $\gamma = 0.01$ and $\epsilon = 0.01$

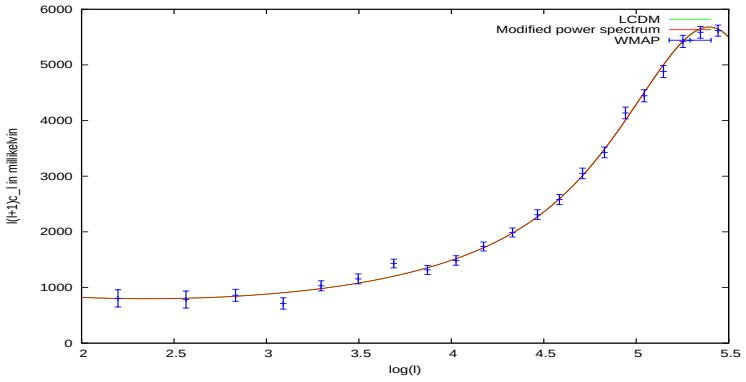

Figure 9.2: Logarithmic plot, $\xi = 0.0004$, $\gamma = 0.01$ and $\epsilon = 0.01$

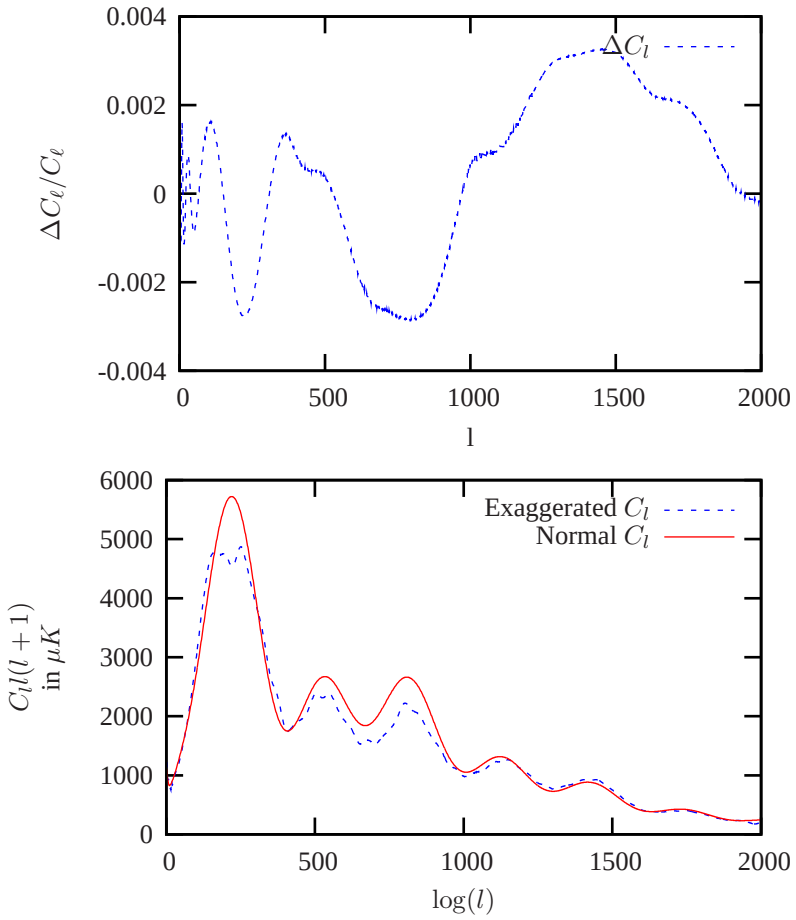

Figure 9.3: Ratio of modulated to unmodulated power spectrum for $\xi = 0.0004$, $\gamma = 0.01$ and $\epsilon = 0.01$.

9.2.2 Verifying the code

The next thing we do is verifying that the modifications are correct, and this is done by reproducing data from [7]. Compare with figure 9.5 from [7], and note that the modified code generates results in correspondence with [7].

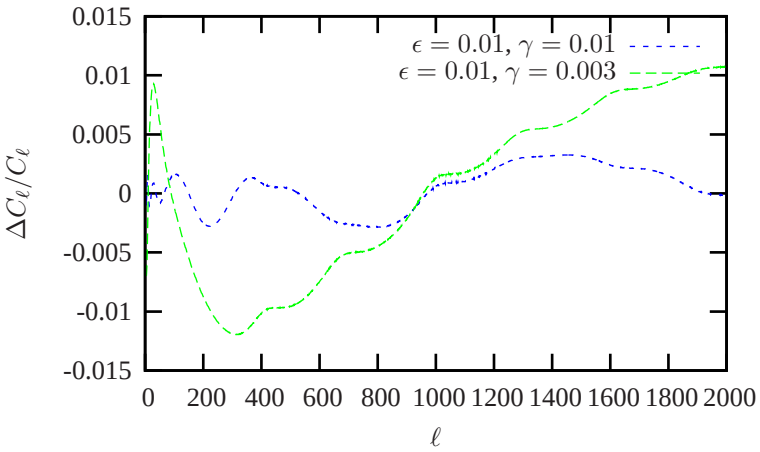

Figure 9.4: Ratio of modulated to unmodulated power spectrum for $\xi = 0.0004$, $\gamma = \{0.01, 0.003\}$ and $\epsilon = 0.01$. Compare with figure 9.5 from [7].

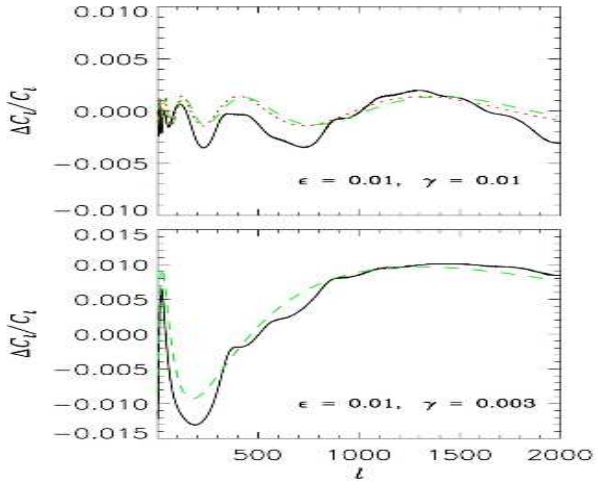

Figure 9.5: Modulated power spectra for $\epsilon = 0.01$, $\gamma = \{0.01, 0.003\}$ from [7].

9.2.3 Verifying logarithmic oscillations

In chapter 8, it was predicted that the modulated power spectrum would exhibit small oscillations, about one for each logarithmic k. When plotting figure 9.3 logarithmic, it is clear this is the case (see figure 9.6). In [1], *Jerome Martin* argues that these oscillations could statistically be accounted for by the cosmic variance outliers.

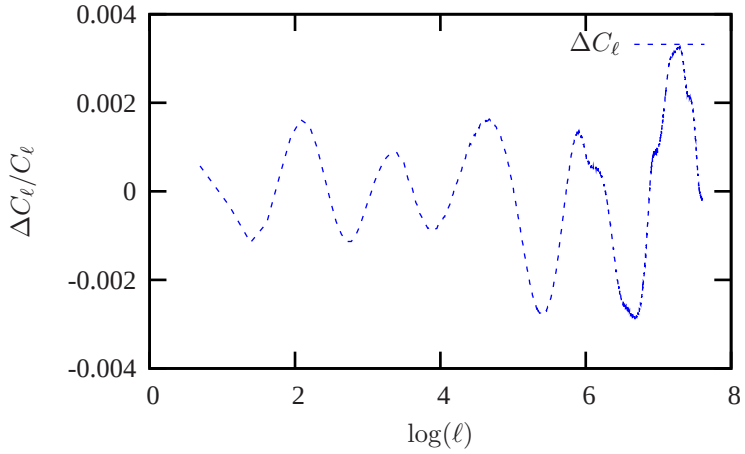

Figure 9.6: Ratio of modulated to unmodulated logarithmic power spectrum for $\xi = 0.0004$, $\gamma = 0.01$ and $\epsilon = 0.01$. Notice that there is approximately 1 oscillation pr logarithmic k, as predicted in chapter 8.

9.3 Behaviour of ΔC_l for ϵ and ξ

Section goal 9.3.1. *Determine how various ξ and ϵ modulate the angular power spectrum. Explain how the modulations are ill-tempered, and will give rise to problems when estimating parameters.*

We have seen how the nontrivial vacuum gives rise to small oscillations in the power spectrum, but we have not yet analyzed the behaviour of these oscillations. The solution to understanding the problem with the oscillations lie in their behaviour. By varying ϵ and ξ, two movies were created in order to visualize the erratic oscillations.

ϵ : *http://irio.co.uk/projects/thesis/epsilon.avi* where $\epsilon \in [0.001, 0.03]$.

ξ : *http://irio.co.uk/projects/thesis/xi.avi* where $\xi \in [0.0001, 0.0006]$.

At the first impression, the oscillations are frantic and "cross" the stationary power spectrum several times at chaotic intervals. This is the first sign that the parameter estimation will not be a simple process, as there seems to be several values for ξ and ϵ that fit well with the original input values. As mentioned in [7], this will have severe impacts on the likelihood function. The exact likelihood function will be investigated and presented later.

9.3.1 The behaviour of ΔC_l for varying ξ

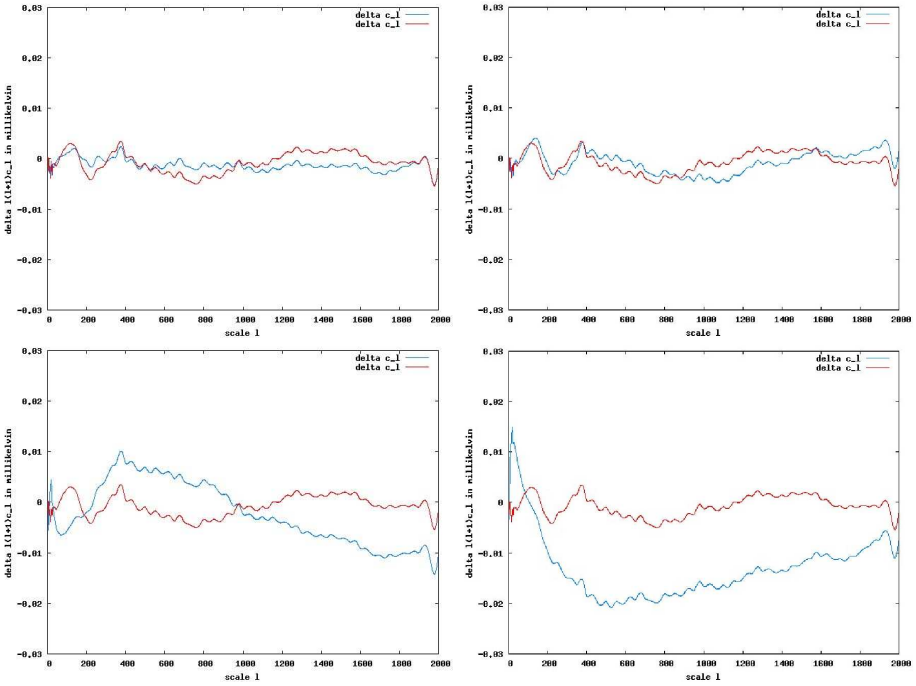

Figure 9.7: Modulated power spectra for $\epsilon = 0.01$, $\xi = \{0.0001, 0.000406, 0.000985, 0.0019\}$ (blue line) versus the HW-model (red line).

The cutoff parameter ξ has two impacts on the modulations in the angular power spectrum, as seen from the movie (see figure 9.7). First, as ξ increases, the frequency of the oscillations in the waves decrease. This means the graph "slows down" when ξ increases, making it simpler to determine an upper cutoff. Secondly, the *amplitude* of the modulations increase with ξ, all up to $\xi = 1$ Hence for a small value of ξ, the amplitude in the modulations are small, but as ξ grows, *the amplitude grows as the frequency decrease*. The convergence for large ξ is discussed in the following subsection.

Convergence of ΔC_l for large ξ

From figure 9.8, we see that a very low ξ will result in almost no modulations. The amplitude of the oscillations continue to grow, until a maximum amplitude difference of 1. As ξ continue to increases, the amplitude of the modulations is again lowered to a steady zero. This can also be seen from equation A.1, as

$$\lim_{B\to\infty} B\sin(2/B) = 1$$

Hence for constant ϵ, the primordial power spectrum becomes scale-free for large B as $\xi \propto B$. Physically, this means that the Harrison-Zel'dovich primordial power spectrum is restored when the cutoff ξ goes to infinity.

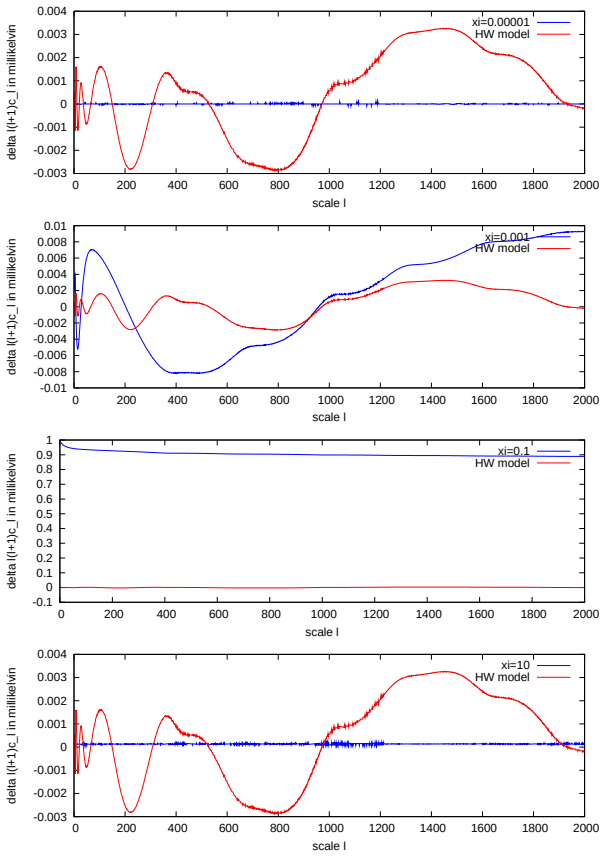

Figure 9.8: Difference between ΛCDM and the modulated HW model: ϵ is fixed at 0.01 while $\xi \in \{0.00001, 0.001, 0.1, 10\}$.

9.3.2 The behaviour of ΔC_l for varying ϵ

ΔC_ℓ varies with ϵ in much the same way as with ξ, but in a more chaotic manner. The likelihood should hence be even more non-systematic, as will be shown in the end of this chapter.

Convergence from ϵ

The ϵ parameter's impact on the power spectrum behaviour is not quite as nice as that of ξ. While ξ for large values makes the power spectrum modulations converge to zero, we see from figure 9.10 that this is not the case for ϵ. It seems that for large values of ϵ, a single peak is prominent. We will later see how this affects the parameter estimation success for ϵ.

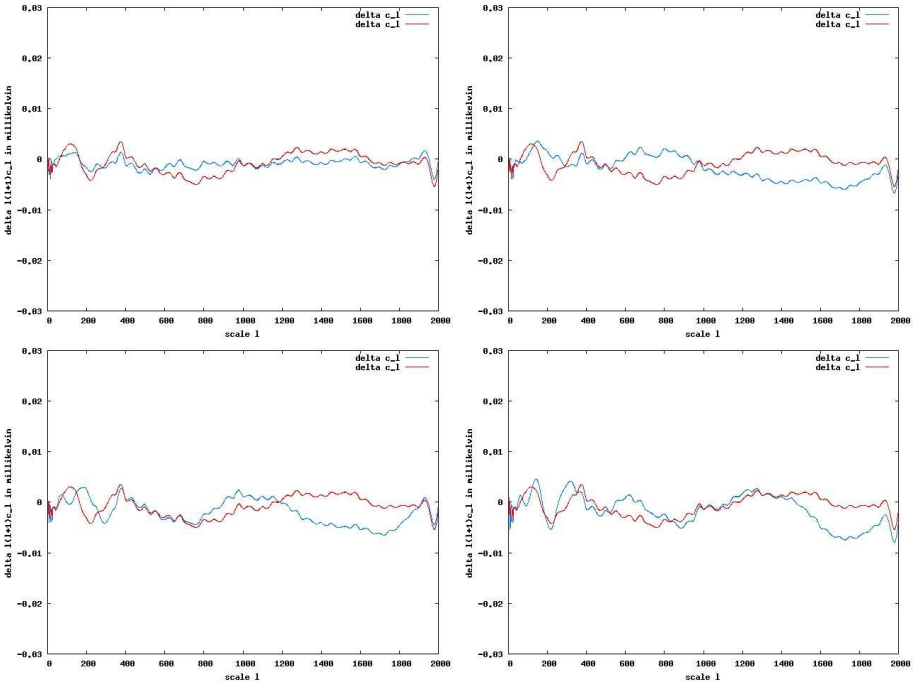

Figure 9.9: Modulated power spectra for $\xi = 0.0004$, $\epsilon = \{0.001, 0.007, 0.016, 0.03\}$ (blue line) versus the HW-model (red line).

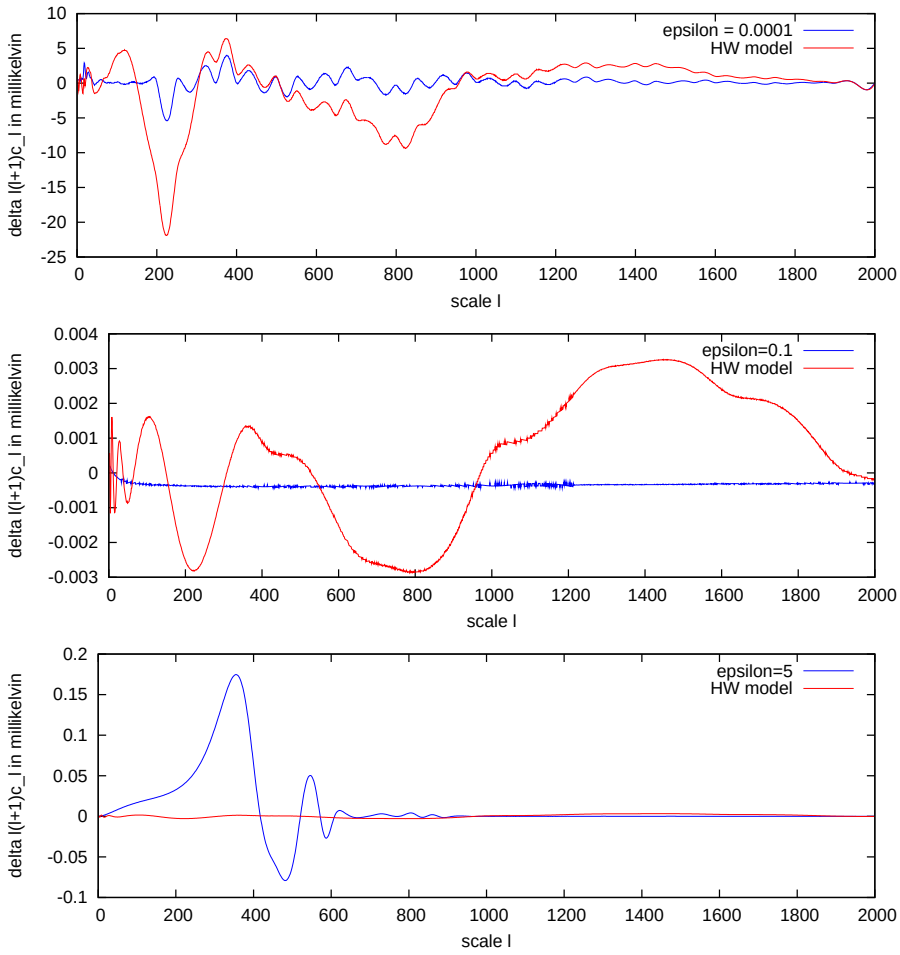

Figure 9.10: Difference between ΛCDM and the modulated model: ξ is fixed at 0.0004 while $\epsilon \in \{0.0001, 0.1, 5.0\}$. Notice the erratic behaviour of the graphs for varying ϵ.

9.4 Parameter estimation using WMAP data

Section goal 9.4.1. *To show that WMAP data does not give constraints to ξ and ϵ.*

The **Wilkinson MAP**(WMAP) experiment provides a satellite-based measurement of the cosmic microwave background. The WMAP and 3-year revised WMAP3 data are still the most important observational results for determining cosmological parameters, thus enabling us to determine which of today's theoretical model fits best with results. The ΛCDM model is still standing strong, as can be seen from standard parameter estimation [30, 31]. CosmoMC is equipped with the latest WMAP data and likelihood code, ready for use. We now modify CosmoMC to include the two auxiliary parameters ξ and ϵ, and see if WMAP data alone can give constraints on these.

9.4.1 What to expect

When plotting ΔC_l (figure 9.3) versus the error bars in the WMAP data, it is clear that the constraints on ξ and ϵ will be poor (see figure 9.11). The error bars in the WMAP data are approximately 1-2 orders of magnitude larger than the predicted modulations in the angular power spectrum. The error bars are smallest around $\log \ell = 6$ (or $\ell = 400$), but are still about 50 times larger than the predicted modulated spectrum. This should effectively rule out WMAP for detecting trans-Planckian effects especially for low ℓ in the CMB anisotropies, as supported by [7] but opposed to [1].

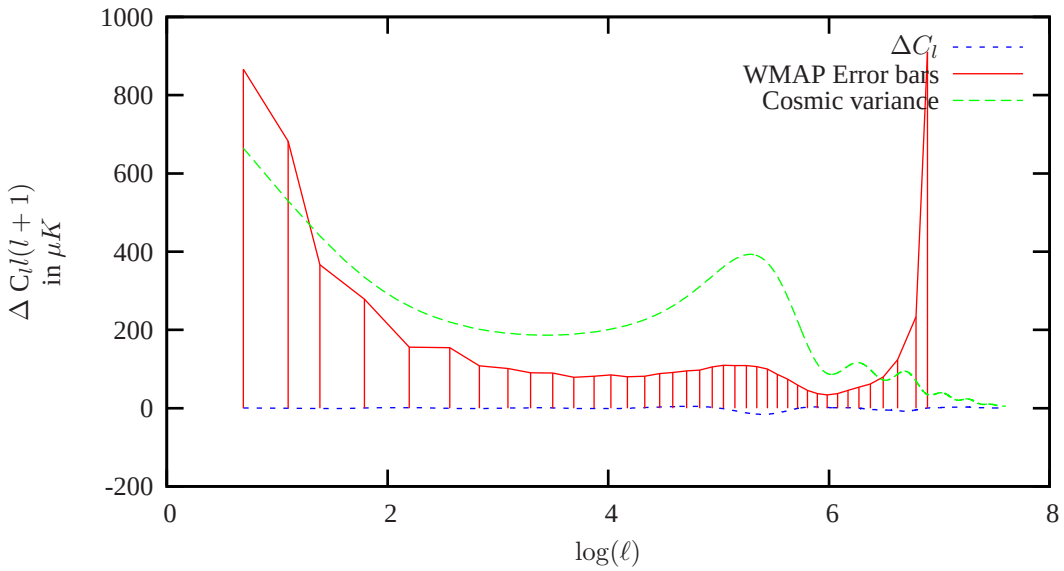

Figure 9.11: Ratio of modulated to unmodulated logarithmic power spectrum for $\xi = 0.0004$, $\gamma = 0.01$ and $\epsilon = 0.01$. The red bars are the error bars in the WMAP data, while the green graph is the cosmic variance. Notice that the modulations in the power spectrum are much smaller than either.

9.4.2 Results

We let all parameters except $w = -1$ to be allowed to vary. WMAP data was constrained with

- **HST**: Hubble Space Telescope constraint, ensuring that $H_0 = 72 \pm 8(\mathrm{km/s})/\mathrm{Mpcs}$.
- **Mpk**: Matter power spectrum constraint, using the Sloan Digital Sky Survey galaxy catalogue.
- **Age Tophat Prior**: Only models with $10\mathrm{Gyr} < \mathrm{Age} < 20\mathrm{Gyr}$ were allowed.

The convergence criterion (See the CosmoMC documentation [32]) was set to $R - 1 < 0.02$, but was never achieved: as *all* values of ξ and ϵ were allowed, no convergence occurred.

Both ϵ and ξ free

Figure 9.13 The run time was approximate 5 days, and as seen from the plot : *all* ϵ and ξ are allowed. This was already predicted in the previous section, as the variations in the modulated power spectrum were much less than the errors in the WMAP data. It is also the conclusion of [7].

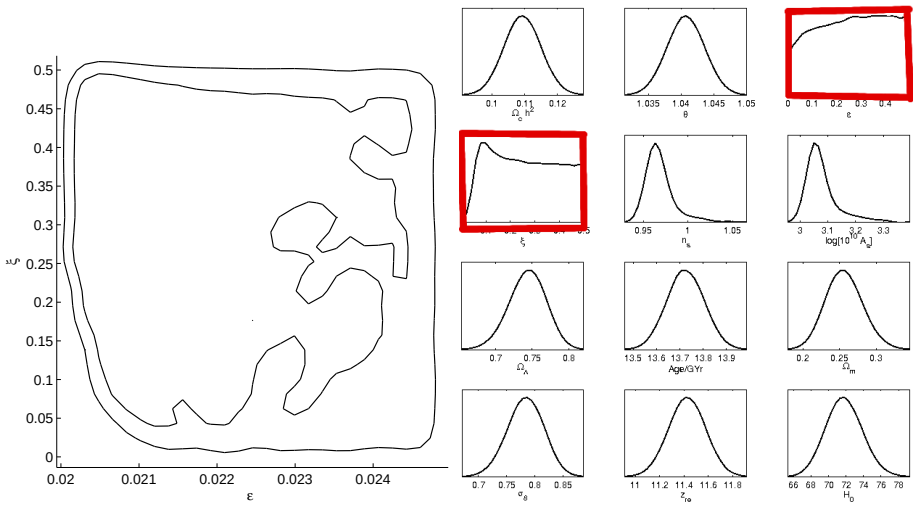

Figure 9.12: Likelihoods for ϵ, ξ. The right-hand side corresponds to 68% (inner) and 95% (outer) confidence contours. Compare with figure 7.10. Note from the right-hand figure of marginalized probabilities that all other parameters converge nicely, while ξ and ϵ remain near uniform (undetermined). Only ξ seems to have a low limit. The left-hand figure contains 68% and 95% confidence contours.

ξ free

Letting $\epsilon = 0.01$ and $\xi \in [0.0002, 0.0006]$, we see from figure 9.13 that it is not possible to determine ξ for any peak around the original input parameter $\xi = 0.0004$.

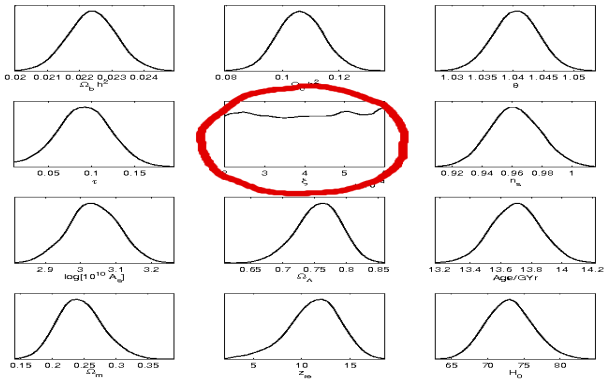

Figure 9.13: $\xi \in [0.0002, 0.0005]$ with initial value $\xi_0 = 0.0004$.

ϵ free

Letting $\xi = 0.0004$ and $\epsilon \in [0.001, 0.3]$, we see that it is not possible to determine ϵ for any value around the original peak 0.01.

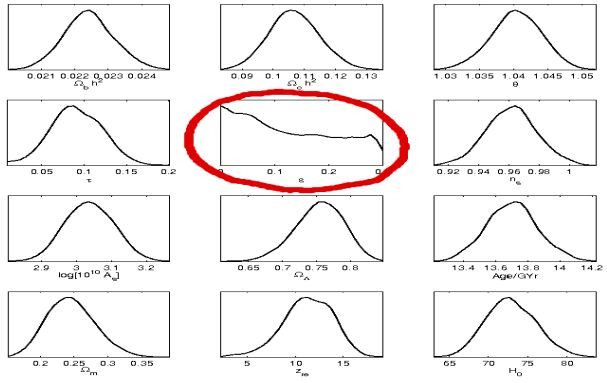

Figure 9.14: $\epsilon \in [0.001, 0.3]$ with initial value $\epsilon_0 = 0.01$.

9.5 Increasing accuracy

Section goal 9.5.1. *Enabling CAMB to perform more accurate calculations.*

In their papers [28, 29] *Martin* and *Ringeval* claim that it is necessary to increase the accuracy of the power spectrum used for deciding trans-Planckian effects. Also, the results in [7] are partly due to the inaccuracy of CMBFAST, the predecessor of CAMB. We boost the accuracy of the calculated power spectrum, increasing run time and accuracy by a tenfold. This is done by modifying the parameters in CAMB. This was not an option in the old version of CMBFAST, and was never performed in [7]. The three parameters are:

1. *accuracy_boost*: Increasing this parameter will decrease the time steps, using more k-values. Set to 2, default 1.

2. *l_accuracy_boost*: Internal variable, increasing will ensure that more terms are kept in the hierarchy evolution. Set to 2, default 1.

3. *l_sample_boost*: Increasing the variable will increase the C_ℓ values for interpolation. Set to 2, default 1.

9.5.1 Results

The parameters used to produce figure 9.18 are given in table 9.1.

accuracy_boost

Setting accuracy_boost to 2, we decrease the time steps and increase k values used. The effect on the oscillations are seen in figure 9.15. This parameter seems to modify the amplitude and general form of the modulation.

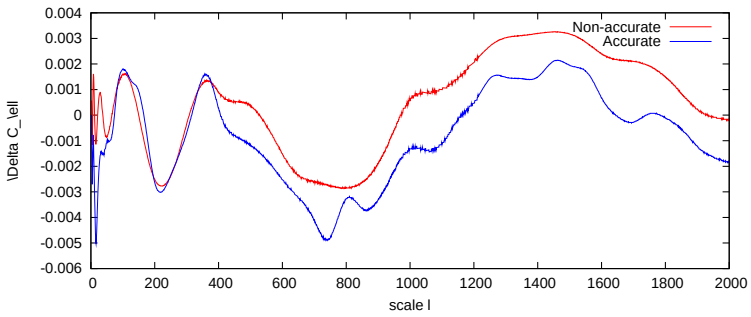

Figure 9.15: Boosting accuracy: increasing accuracy_boost.

l_accuracy_boost

Setting l_accuracy_boost to 2, we keep more terms in the hierarchy evolution. The effect on the oscillations are seen in figure 9.16. This parameter seems to have little impact on the form of the modulations, except small modifications in amplitude.

l_sample_boost

Setting l_sample_boost to 2, we increase C_ℓ-values for interpolation. The effect on the oscillations are seen in figure 9.17. This parameter seems to have a great impact on the form of the power spectrum, as the larger oscillations are composed of several smaller ones.

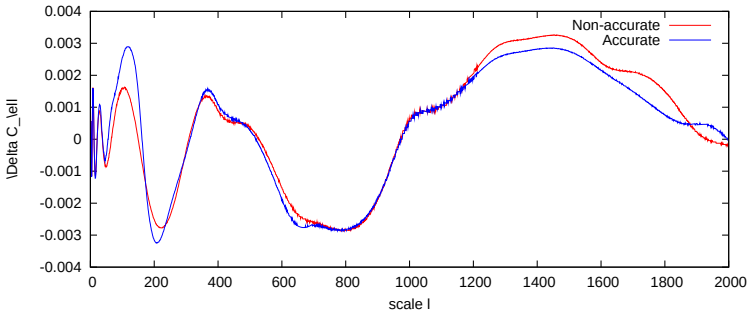

Figure 9.16: Boosting accuracy: increasing l_accuracy_boost.

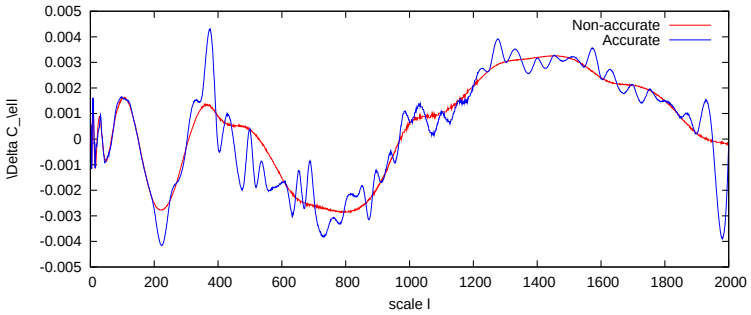

Figure 9.17: Boosting accuracy: increasing l_sample_boost.

Maximum accuracy

When let all three parameters be boosted : accuracy_boost = l_accuracy_boost = l_sample_boost = 2. The results can be seen in figure 9.18.

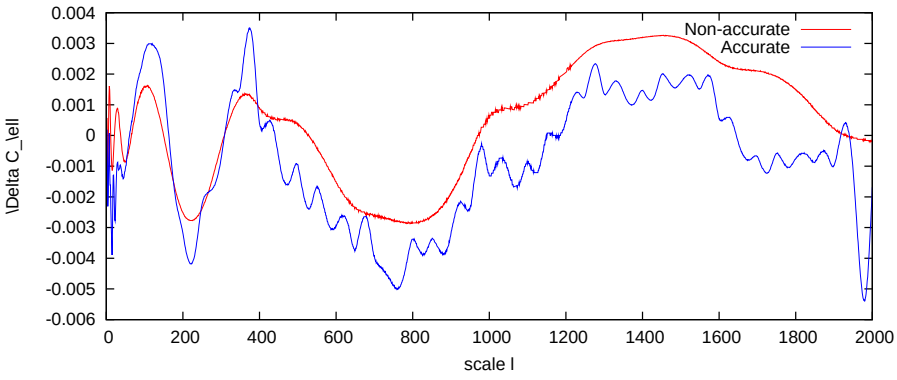

Figure 9.18: The ratio of modulated power spectrum with low and high accuracy, all 3 parameters boosted.

9.6 Parameter estimating with simulated data

Section goal 9.6.1. *Determine whether trans-Planckian effects are detectable with future data. Describe the difficulties with doing so.*

In our cosmological model, we have a set of parameters $p = \{\Omega_b, \Omega_r, w, \ldots, \xi, \epsilon\}$ where ξ and ϵ are the trans-Planckian parameters. What we now wish to do is modify CosmoMC to enable model testing against simulated data instead of the *WMAP* data. This is done by replacing the original WMAP likelihood code with modified perfect data likelihood code. The trace of this progress can be found at appendix A.

9.6.1 Adding "perfect" data to CosmoMC

In chapter 6, the algorithm for simulating a data set given a model was described. The author created a small utility *"GenerateData"*, that generates simulated data given a model power spectrum. We now wish to generate a "perfect" data set with only cosmic variance as uncertainty.

In theory, this means one must generate $N \to \infty$ simulated sample data sets before averaging, but this will only result in a sample data set that *equals* the theoretical model power spectrum. This is indeed what is done, and the resulting sample data set for the HW model is stored in "hwmodel.dat". This file is then copied into CosmoMC's WMAP directory. The parameters used for the (flat) model are given in table 9.1.

9.6.2 Verifying the likelihood code

We proceed by *removing* the WMAP likelihood code in CosmoMC. Instead, a "perfect" data set is added and likelihood code based on 7.5 is included. We run the modified CosmoMC job with fixed ϵ and ξ parameters in order to verify that the new likelihood code works. Observe from figure 9.19 that the likelihood code results in relatively good fits, with most parameters within a 2σ error. The marginalized mean values are given in table 9.2.

Notice from table 9.2 how τ is off mark, and how the amplitude A is neatly estimated. When replacing the likelihood code, we removed all data and code concerning polarization. Therefore, τ cannot be properly estimated as A and τ are degenerate (they both modify the amplitude).

Parameter	Input value	Mean value	68% interval	Status
$\Omega_b h^2$	0.022	0.229053E-01	[0.226171E-01, 0.232458E-01]	$\leq 1\sigma$
$\Omega_{cdm} h^2$	0.12	0.115912E+00	[0.113144E+00, 0.118420E+00]	$\leq 2\sigma$
τ	0.04	0.228972E-01	[0.100000E-01, 0.253712E-01]	$\leq 2\sigma$
n_s	0.99	0.100671E+01	[0.998136E+00, 0.101679E+01]	$\leq 1\sigma$
$log[10^{10} A_s]$	3.13	0.299447E+01	[0.297254E+01, 0.301722E+01]	$\leq 3\sigma$
Ω_Λ	0.71020	0.739006E+00	[0.725345E+00, 0.754143E+00]	$\leq 3\sigma$
Age/GYr	13.592	0.134236E+02	[0.133608E+02, 0.134796E+02]	$\leq 2\sigma$
H_0	70	0.729904E+02	[0.716617E+02 0.744625E+02]	$\leq 2\sigma$

Table 9.2: Results from the modified CosmoMC with fixed $\epsilon = 0.01$ and $\xi = 0.0004$.

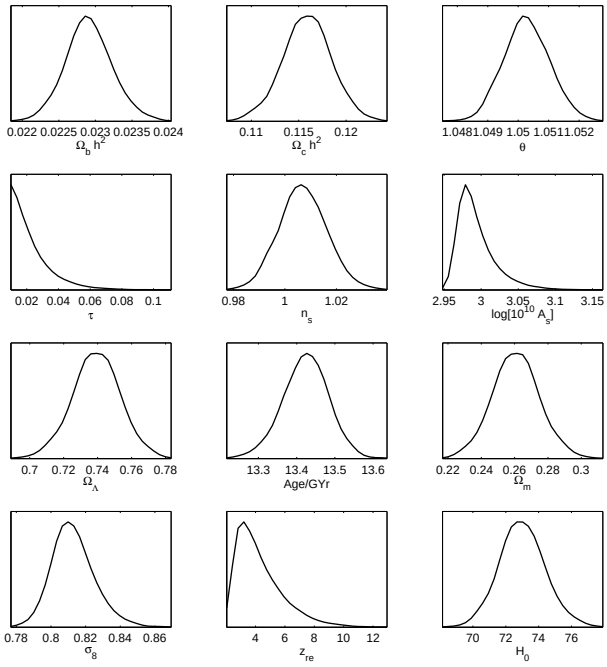

Figure 9.19: Results from the modified CosmoMC with fixed $\epsilon = 0.01$ and $\xi = 0.0004$

9.7 Estimating parameters for the HW universe

Section goal 9.7.1. *Use CosmoMC to reproduce the HW parameters with "perfect" HW data*

9.7.1 Introduction

We now wish to see if the modulations in the HW power spectrum can be detected with CosmoMC. We use a "perfect data set" created with the HW parameters and try to see if CosmoMC is able to reproduce the original parameters ξ and ϵ. This might be problematic, as the modulations are described by a rather chaotic oscillation. The convergence criteria was set to $R - 1 < 0.02$, but neither ϵ or ξ properly converged to a stationary value. We will shortly see that this is due to the nontrivial likelihood function of ξ and ϵ.

9.7.2 Setup

The following initial conditions have been set up:

- A "perfect" data set with only cosmic variance has been created in "hwmodel.dat", representing the simulated data from a HW universe model using $\xi = 0.0004, \epsilon = 0.01$. The standard model parameters used for creating the data set are listed in table 9.1.

- CosmoMC has been modified as in the previous section to use the simulated

"perfect" data for likelihood testing instead of WMAP data. All other constraints like SN data, Age Tophat etc are removed. Only the modified likelihood is used.

9.7.3 Results: ξ free

We present four different CosmoMC runs, in order to emphasize the observed effects. The initial conditions $_0$ and step length $\Delta\xi$ on ϵ and ξ are given as follows:

- Run1: Conditions for ξ are: $\xi_0 = 0.0004$, $\xi \in [0, 0.04]$, $\Delta\xi = 0.00001$.
- Run2: Conditions for ξ are: $\xi_0 = 0.0004$, $\xi \in [0.0002, 0.0006]$, $\Delta\xi = 0.000005$.
- Run3: Conditions for ξ are: $\xi_0 = 0.0004$, $\xi \in [0.0001, 0.0015]$, $\Delta\xi = 0.00005$.
- Run4: Conditions for ξ are: $\xi_0 = 0.0001$, $\xi \in [0, 0.01]$, $\Delta\xi = 0.0005$.
- ϵ remains constant with value 0.01.

First of all, notice from figure 9.20 that there is some disagreement with the correct estimation of ξ. Run2 peaks around $0.515 \cdot 10^{-3}$ with a 2σ within the input parameter, while Run2 peaks at $0.978 \cdot 10^{-3}$ and gets 3σ within the input parameter. Run3 doesn't seem to converge, while Run4 has several different peaks. The parameter estimation of ξ is severely dependent on selected initial conditions and step length. This is a major indication that ξ doesn't modulate the power spectrum in any nice way, as already seen in section 9.3. If so, then the standard MCMC method fails to converge to any stationary distribution, and becomes highly dependent on initial parameters and step length in order to converge to a local minimum. This is most likely what is observed in Run4, a step length was chosen such that the chains started converging to another minimum in the likelihood landscape.

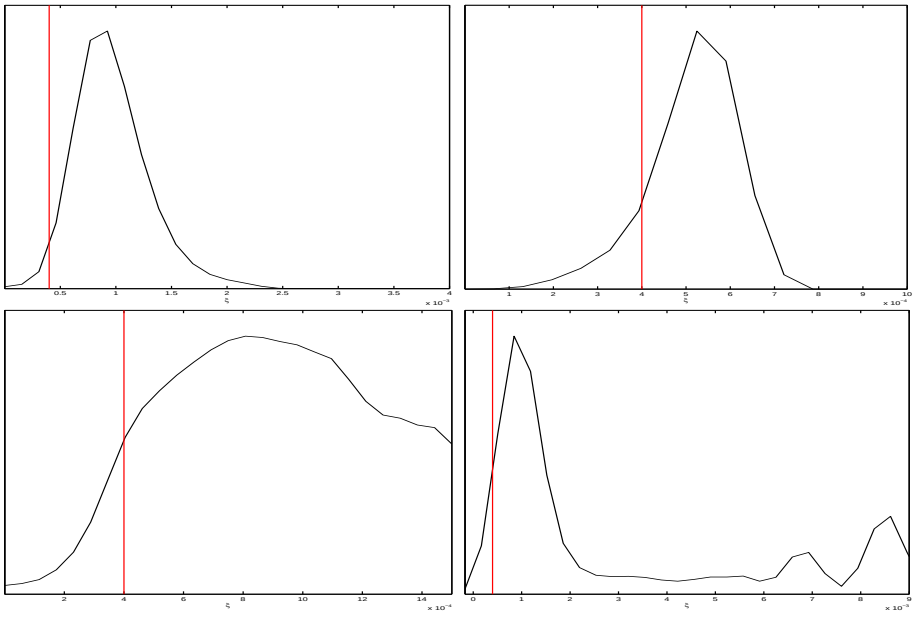

Figure 9.20: Top left: Results for Run1 with mean peak at $0.978 \cdot 10^{-3}$. Top right: Results for Run2 with mean peak at $0.515 \cdot 10^{-3}$. Bottom left: Results for Run3 with no peak, almost uniform distribution. Bottom right: Results for Run4 with several peaks. Notice how the peaks don't match, where the red line represents the original input parameter $\xi = 0.0004$ for the simulated data.

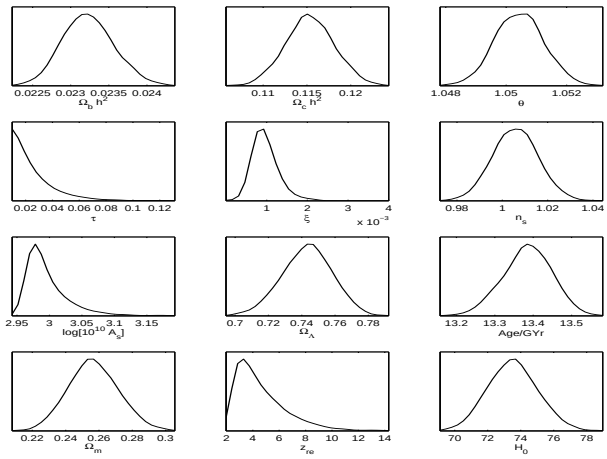

Figure 9.21: The remaining free parameters are estimated correctly. This plot shows the marginalized likelihoods for Run1

9.7.4 Results: ϵ free

We present three different CosmoMC runs, in order to emphasize the observed effects. The initial conditions ϵ_0 and step length $\Delta\epsilon$ on ϵ and ξ are given as follows:

- Run1: Conditions for ϵ are: $\epsilon_0 = 0.01$, $\epsilon \in [0, 0.3]$, $\Delta\epsilon = 0.008$.
- Run2: Conditions for ϵ are: $\epsilon_0 = 0.01$, $\epsilon \in [0, 0.05]$, $\Delta\epsilon = 0.0002$.
- Run3: Conditions for ϵ are: $\epsilon_0 = 0.01$, $\epsilon \in [0, 0.5]$, $\Delta\epsilon = 0.02$.
- ξ remains constant with value 0.0004.

Again we note that there is a total disagreement with the original input parameter and the estimated parameters. Only Run2 came within a 3σ correct estimation, all other failed by a factor of ten. The MCMC method produces different results for different chosen step lengths and parameter intervals, which again implies that the likelihood function for varying ϵ and ξ are ill-behaved.

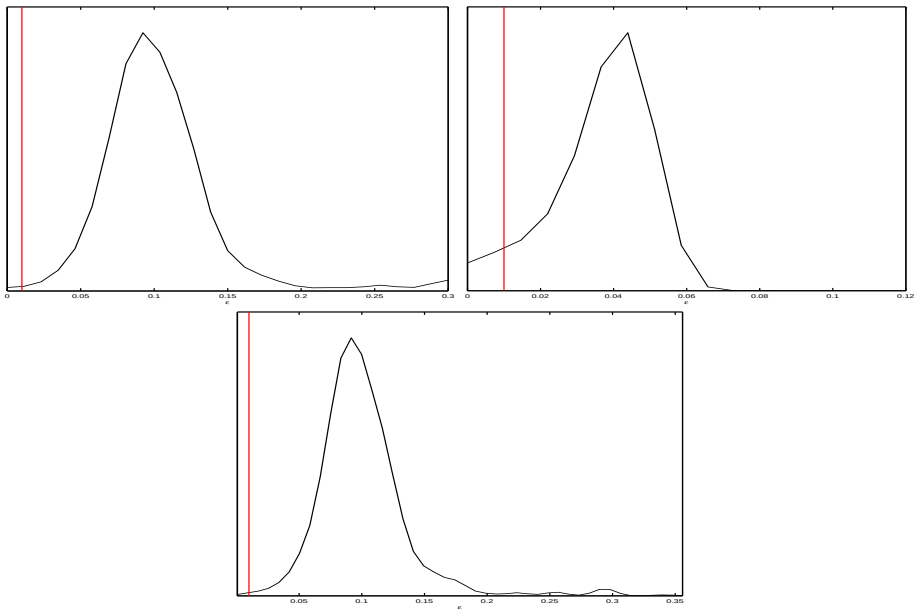

Figure 9.22: Top left: Results for Run1 with mean peak at 0.12. Top right: Results for Run2 with mean peak at 0.037. Bottom left: Results for Run3 with mean peak at 0.101. Notice how the peaks don't agree for different step lengths, where the red line represents the original input parameter $\epsilon = 0.01$ for the simulated data.

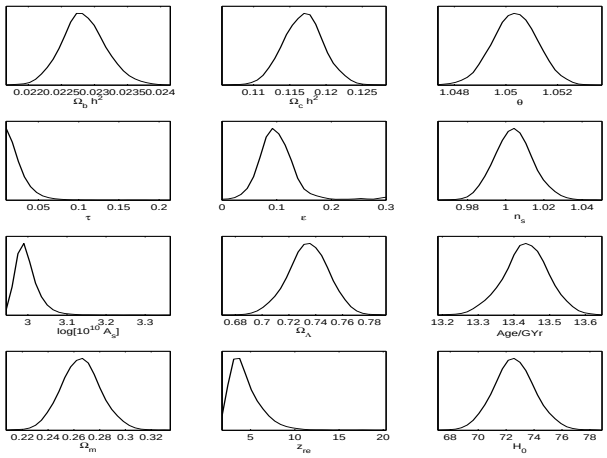

Figure 9.23: ξ is fixed at 0.0004 while ϵ varies between 0 and 0.3.

9.7.5 Results: Both ξ and ϵ free

In the simulations where both ξ and ϵ were free, no convergence occurred whatsoever. All the distributions turned out grotesque, with no apparent Gaussian likelihoods. The run time on 24 processors was aborted after 4 days, with a non-converging $R - 1 \sim 100$. See figure 9.24 for the results. This again reflects the irregular behaviour of the likelihood function for varying ξ and ϵ.

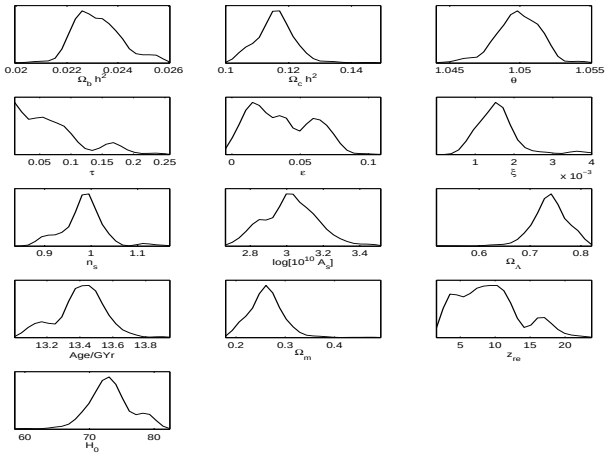

Figure 9.24: $\xi \in [0, 0.1]$ with $\Delta\xi = 0.00007$ and $\epsilon \in [0, 0.5]$ with $\Delta\epsilon = 0.02$. Notice how the distributions never converged.

9.8 Explaining the results

Section goal 9.8.1. *Determining the exact likelihood function for continuous varying ξ and ϵ. Convince the reader why the MCMC method fails.*

We have seen that parameter estimating ξ and ϵ didn't turn out quite as expected. In the first parameter estimation of ξ, we found a peak located at within a 3σ of the original input parameter. When changing step lengths, we found a new peak within 2σ. But when increasing the step length even further, we found both near-uniform likelihoods and likelihoods with different peaks. The same goes for ϵ: different step lengths results in different estimated parameters. Clearly there is something wrong with using the MCMC method here.

Earlier in this chapter, it was shown that the oscillations are highly erratic, as seen in figure 9.10 and 9.8. Recall that the MCMC algorithm is based on random walkers transversing a parameter space. Together, the walkers make up a distribution, which then is marginalized (projected) onto one dimension: the parameter distribution of interest. As a walker ambulates, it's probability to successfully move is dependent on the likelihood function. If a varying a parameter smoothly changes the corresponding graph in a well-behaved manner, the likelihood function for that parameter would most likely turn out Gaussian around the original input value. But if the parameter varies the likelihood function in a disordered manner, the likelihood function will be a landscape of local and semi-global peaks. This means that there exist several values of ξ and ϵ that will result in similar graphs as generated by the input parameters. We will show that this is indeed the case for ξ and ϵ.

9.8.1 Detailed likelihood analysis

In order to convince the reader that the MCMC method for this kind of modulations is highly incorrect, we present a "proof". What does the exact likelihood look like for the two parameters without sampling from the remaining configuration space? We created a **brute force** script program that did exactly this - varied ϵ and ξ with medium step lengths, used CAMB to determine the theoretical power spectrum and calculated the likelihood between theory and data.

The exact likelihood function for varying ξ and ϵ

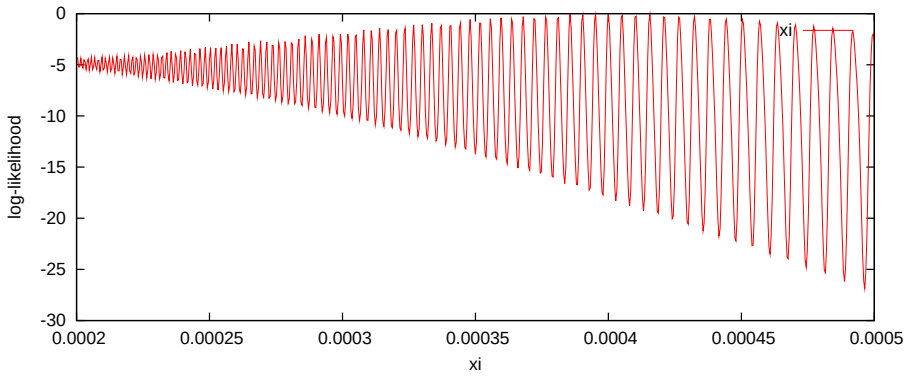

Figure 9.25: Likelihood for $\xi \in [0.0002, 0.0005]$ with correct maximum at $\xi = 0.0004$

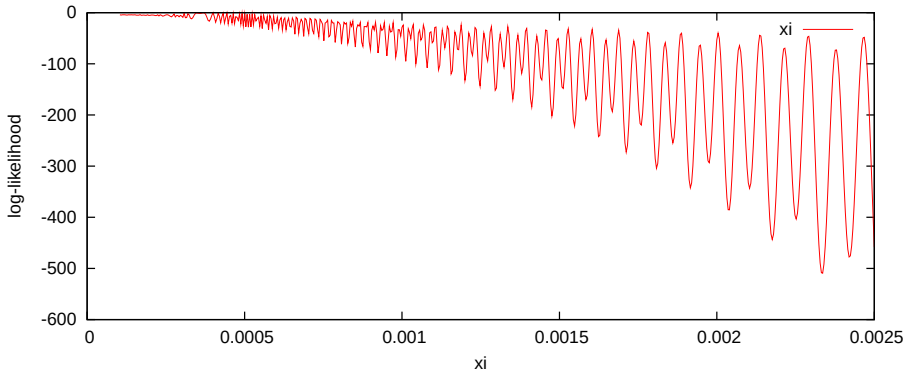

Figure 9.26: Likelihood for $\xi \in [0.0002, 0.0025]$ with correct maximum at $\xi = 0.0004$

Figures 9.10 and 9.8 show a highly irregular oscillation for varying parameters - and the exact likelihood should reflect this property. The results in figures 9.25, 9.26 and 9.27 are convincing. It is clear that the exact likelihood functions, especially for ϵ, are very hard to match exactly. In order for random walkers to give a nice distribution around the correct peak, one needs a close initial condition, a good parameter interval and a suitable step size. Without this, the walkers would be “trapped” in any of the other minima, semi-global or local.

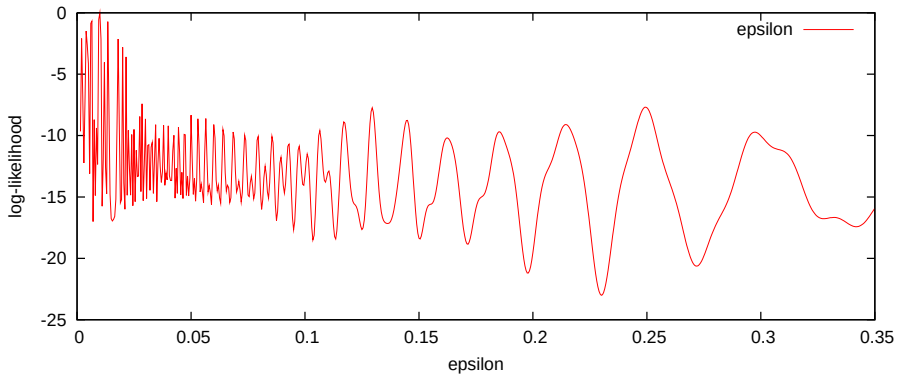

Figure 9.27: Likelihood for $\epsilon \in [0.01, 0.5]$ with correct maximum at $\epsilon = 0.01$

9.8.2 2D exact likelihood landscapes

A different version of the batch script was created to generate a two-dimensional version of the ϵ-ξ likelihood landscape. Figure 10.1.1 consists of 150×150 points, and took about 24 hours to compute on a single-processor. Figure 9.29 is a 40×40 zoom of 10.1.1, and emphasizes the ruggedness of the landscape. The correct maximum likelihood value is marked with a red circle. Both plots show $-\ln \mathcal{L}$, such that the *minimum* of the graph corresponds to a best-fit value for ξ and ϵ.

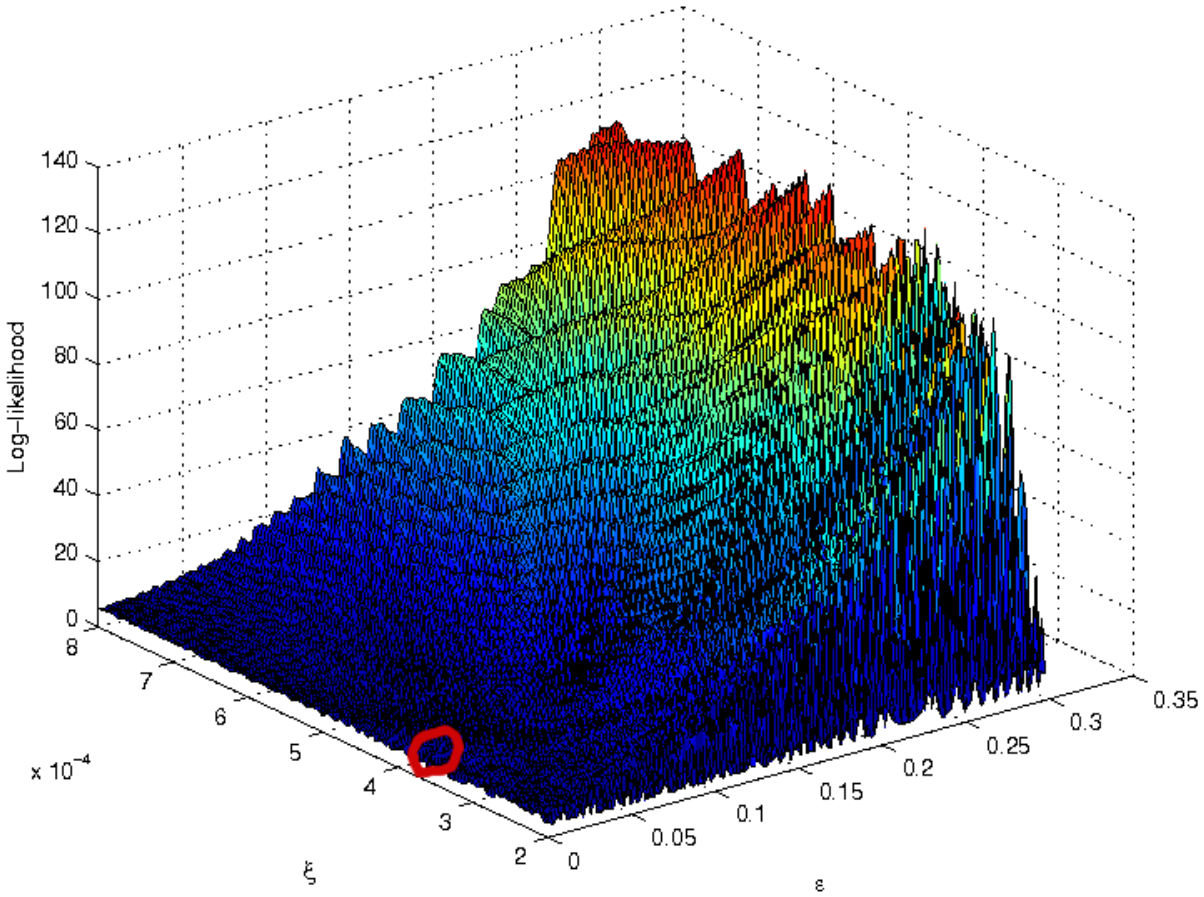

Figure 9.28: The $\epsilon - \xi$ likelihood function $-\mathcal{L}$ on a 150×150 lattice. The exact value is marked with a red circle.

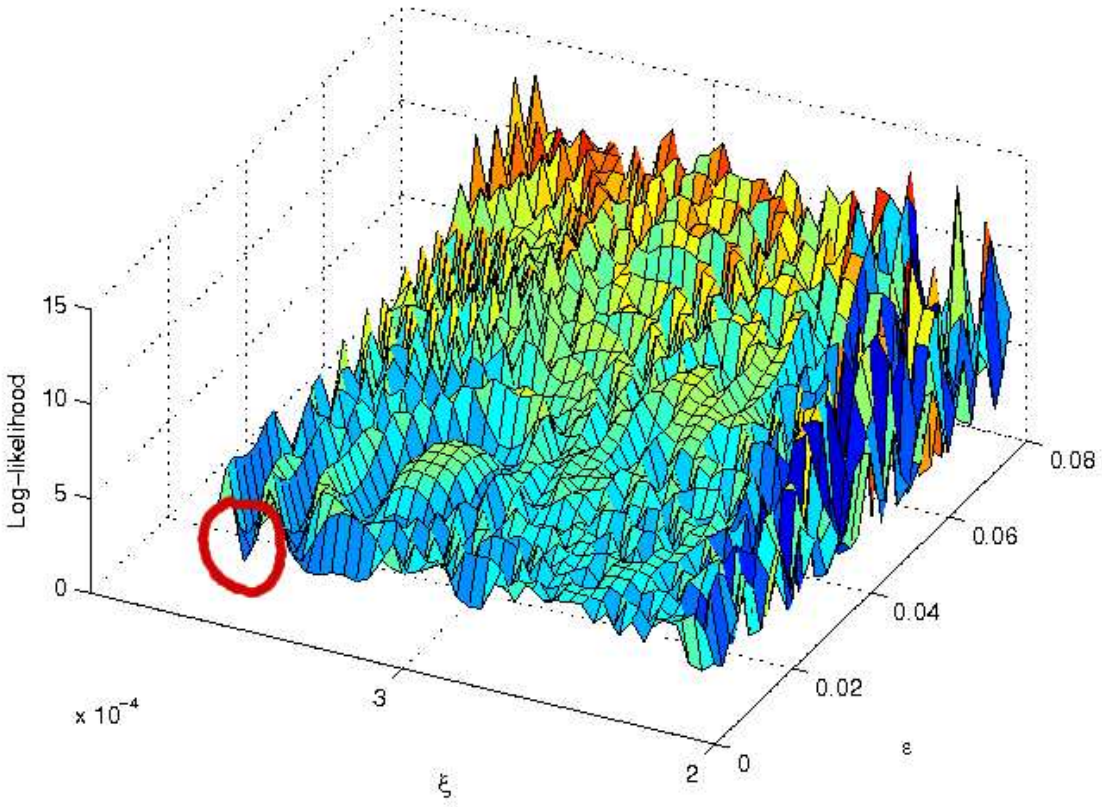

Figure 9.29: A zoom of the $\epsilon - \xi$ likelihood function $-\mathcal{L}$ on a 40×40 lattice. The exact value is marked with a red circle.

Chapter 10

Conclusions and outlook

10.1 Summary

We have investigated whether general trans-Planckian effects in the cosmic microwave background are detectable with today's and tomorrows' data. This has been done in the following manner: In chapters 1, 2 and 3 we presented a brief introduction to standard cosmology and curved spaces. The mechanics of inflation was investigated in chapters 4 and 5, before discussing post-inflationary events in chapter 6. Then in chapter 7 the angular power spectrum was introduced, the major observable that enables coupling between theory and observations. We presented tools for CMB analysis, methods for simulating data and a short guide to interpretation of the angular power spectrum. Two papers that discuss implications of trans-Planckian effects in the primordial power spectrum were reviewed in chapter 8. The papers introduced two auxiliary parameters ϵ (slow-roll) and ξ (Planck cutoff scale) that modulated the Harrizon-Zel'dovich scaling effect. We then proceeded by investigating the behaviour of these modulations in chapter 9, and reproduced the results from [7]. A simulated "perfect" data set was included into CosmoMC, and parameters were incorrectly determined. In the end, a small script utility was created in order to calculate the exact likelihood for continuous varying ϵ and ξ, without MCMC methods.

10.1.1 A comment on [1, 2]

We have seen that previous work, especially by *Jerome Martin et al.* [1, 2, 28, 29] are overly optimistic about the detection of trans-Planckian effects. Their main argument in [1, 2] is that the cosmic variance outliers in the angular power spectrum could in theory be explained by the superimposed oscillations. Following the results presented in the previous chapter, we argue that there are three reasons why this is highly improbable:

1. The oscillation frequency fluctuate too much for varying ξ and ϵ to actually fit any cosmic variance outliers. An eventual fine-tuning of ξ and ϵ would be necessary.

2. The amplitude of the superimposed oscillations is too weak (see figure 9.11).

3. The exact likelihood function makes the detection of the trans-Planckian parameters ξ and ϵ very hard, and renders the Monte Carlo Markov chain method useless.

10.2 Conclusions

In a perfect world, the author would have created the plots of the exact likelihood functions *before* futilely trying to parameter estimate ξ and ϵ. This would have saved many hours of despair in which the expression "*why, oh why doesn't the distribution peak at the correct value?*" played a major part. Unfortunately, the world doesn't operate in such manners, and the results have been presented in a time-ordered chronological order. We have reached the following conclusions:

Conclusion 10.1. *WMAP data alone does not give enough constraints on ξ and ϵ; the likelihoods are uniform and all parameters are allowed. See section 9.4 for details.*

Conclusion 10.2. *Simulated "perfect" data gives upper and lower constraints on ξ and ϵ, but the likelihood varies for different initial values and step lengths. When defining "suitable" initial conditions, the parameters are estimated within a 2σ error.*

Conclusion 10.3. *The exact likelihood function between the perfect data and models for varying ξ and ϵ is a landscape riddled with local and semi-global minima (see figure 9.27). This renders the MCMC algorithm used in CosmoMC ineffective; for different initial values and step lengths the likelihood converges to different local/semi-global minima.*

Conclusion 10.4. *Future experiments will never provide data nearly as good as the simulated data set presented in this thesis. As the exact likelihood landscape is chaotic (see figure 10.1.1), the initial conditions need to be tuned around the correct minimum with a suitable step length in order to converge properly.* ***We therefore conclude that detecting trans-Planckian effects will be difficult even with improved future data.***

10.3 Outlook

10.3.1 Additional data sets

How would additional data sets affect the detection of generic trans-Planckian effects in the CMB?

SDSS

The **Sloan Digital Sky Survey** (SDSS) [33] is a comprehensive galaxy catalogue based on continuous imaging and spectroscopic redshift surveys since the year 2000. For the detection of generic trans-Planckian effects, the galaxy catalogue would most likely not help, due to the low-accuracy of data. In addition, the CMB power spectrum is not directly observed, only the matter power spectrum is available. The matter power spectrum is smoothed by the window function, so any irregularities would be removed.

QUIET

It is uncertain whether QUIET polarization data could help on the detection of trans-Planckian effects.

SN1A

With improved super nova type 1a data, Ω_m could be determined much better. But this doesn't affect the other parameters, especially not ϵ nor ξ.

10.3.2 Additional methods

We present some additional methods that *could* be used to estimate the parameters ϵ and ξ. We also briefly explain why these methods wold fail.

Gradient method

The gradient method employs a simple solution: test the likelihood function and climb towards the nearest maximum. For a smooth, nice-behaved likelihood function, this would be an effective solution. Needless to say, when looking at the exact two-dimensional likelihood landscapes 10.1.1 and 9.29, the gradient method fails terribly unless the initial conditions are finely tuned around the correct value.

Brute force

The two-dimensional likelihood landscapes 10.1.1 and 9.29 are examples of data sets created by brute force grid integration. The parameter space was defined with rough intervals on a lattice size of 150 for each parameter. Calculating a single-dimensional lattice of size 150 took about $t \sim 10$ minutes. With two free parameters (at low resolution!), $t \sim 150 * 10 \sim 24$ hours, the time it took creating graphs 10.1.1 and 9.29 . With 11 free parameters, $t \sim 2.74 \cdot 10^{15}$ years. For few enough parameters, brute force works, but for a full parameter estimation it is virtually impossible as time scales with $lattice^d$

10.3.3 Modifying the likelihood algorithm

The exact likelihood function in figure 9.27 should convince most skeptics that any general exact parameter estimation is difficult. But a few options are available. One of the problems with the exact likelihood functions of ϵ and ξ is the local minima. An algorithm that would calculate the surrounding likelihoods and eliminate (or smooth) the local minima could possibly give a better estimation. The problem is then reduced to that of the semi-global minima, which could possible be eliminated by the following algorithm:

1. Generate random initial values for ξ or ϵ.
2. Eliminate the local minima by smoothing.
3. Find a semi-global minima, and save the lowest likelihood function value.
4. Go to 1 until a lowest likelihood function value is obtained. The distribution in which the lowest likelihood is detected will be the correct one.

However, implementing such an algorithm in CosmoMC would require time beyond the scope of this thesis.

Appendix A

Self-references

In order to separate general results from work done by the author, we present a review of independent software, code modifications and other achievements.

A.1 General notice

Even though chapters 2 to 6 contain general results from [6, 8, 17, 16, 11, 9, 15, 13, 5, 3, 14], the *representation* of the results have been independent. Chapter 3 is especially an example of this, being a mixture of several topics from the discipline of mathematics and physics. Another "special" chapter is chapter 7, which serves as a bridge between the theoretical and the experimental parts of the thesis.

A.2 Graphs and figures

All graphs and figures except figure 9.5 have been created by the author. Schematic figures were created in Xfig, and graphs were made with either Gnuplot or Matlab. Some "special" figures and graphs are mentioned:

- Figure 2.1 was created with a C++ program "TimeLine" created by the author.
- Figure 4.2 was created in Matlab using harmonical functions. The "false vacuum" was created using two two-dimensional Gaussian functions, one almost cancelling the other.
- Figure 6.5 and 6.3 were created in Matlab to illustrate the effect of diverging geodesic curves.
- Figure 7.1 is a screen shot from a C++ program that projects spherical maps onto $\mathbb{R}^2$ using the Mollweide projection. The software is written by the author.
- Figure 7.2 is a screen shot from a C++ program that calculates the spherical harmonics for a sphere, and presents the map using the Mollweide projection. The software is written by the author.
- The driven and damped harmonical oscillators in Figure 7.5 were created in a C++ program written by the author.

- All figures in chapter 9 except 9.5 are based on independent data.

- The movies mentioned in chapter 9 were made using the same script for generating the exact likelihood, " **like**". The movies were assembled in "Avidemux" for Ubuntu.

A.3 Code modification

A.3.1 Modifying CAMB

CAMB contains several files that perform various tasks. Some contain a set of subroutines, other define data structures. The primordial power spectrum is calculated in *powertilt.f90*. The original line stated:

```
lnrat = log(k/P%k_0_scalar)
ScalarPower=P%ScalarPowerAmp(in)*
            exp((P%an(in)-1)*lnrat + P%n_run(in)/2*lnrat**2)
```

or

$$P = Ae^{(n_s-1)\ln\left(\frac{k}{k_0}\right)+\frac{1}{2}n_{run}\cdot\left(\ln\left(\frac{k}{k_0}\right)\right)^2}$$

Ignoring the n_{run}, we see that

$$P = Ae^{(n_s-1)log\left(\frac{k}{k_0}\right)} = A\Big(\frac{k}{k_0}\Big)^{n_s-1}$$

is the power law behaviour. In chapter 8, the modified power spectrum (8.3) including trans-Planckian effects was defined as:

$$P_\phi = \Big(\frac{H}{2\pi}\Big)^2\Big(1-\frac{H}{\Lambda}\sin\big(\frac{2\Lambda}{H}\big)\Big)$$

We introduced a parametrized version of the power spectrum (8.6) based on two parameters ξ and ϵ, where the slow roll parameter was heavy restricted to $\epsilon \sim 0.01$ by observations in the CMB anisotropies [24]. This modified equation is basically dependent on ξ alone, and reads

$$P(\epsilon,\xi,k) = P_0(k)\Big(1-\xi\Big(\frac{k}{k_n}\Big)^{-\epsilon}\sin\Big[\frac{2}{\xi}\Big(\frac{k}{k_n}\Big)^{\epsilon}\Big]\Big)$$

Introducing

$$B = \xi\Big(\frac{k}{k_n}\Big)^{-\epsilon}$$

we can express (8.6) as

$$P(\epsilon,\xi,k) = P_0(k)\Big(1-B\sin\big(\frac{2}{B}\big)\Big) \tag{A.1}$$

A.3.2 Modifying code

CAMB was modified to include three new parameters ϵ, ξ and γ on command line, enabling batch-script running. The original data structure in *modules.f90* was also altered to include the new parameters. This makes it possible to export CAMB code directly to CosmoMC. The modified power spectrum code is

```
function ScalarPower(k,in)
real(dl) ScalarPower,k, lnrat
integer in
real(dl) B,epsilon, xi, gamma
    gamma = P%gamma
    epsilon =P%epsilon
    xi = P%xi*sqrt(epsilon)/gamma
    B = xi*(k/P%k_0_scalar)**(-epsilon)
    lnrat = log(k/P%k_0_scalar)
    ScalarPower=P%ScalarPowerAmp(in)*
      exp((P%an(in)-1))*abs(1-(B*sin(2.0/B)))
end function ScalarPower
```

where *P* is the CAMB data structure *CAMBparams*.

A.3.3 Modifying CosmoMC

The likelihood modifications were mostly done in *WMAP_3yr_likelihood.f90*. In this file, a subroutine named *PASS_COMPUTE_LIKELIHOOD* returns the computed WMAP likelihood between the current model in the MCMC chain and simulated data. Recall we found the log-likelihood for a perfect data set in equation 7.5:

$$-2\log\mathcal{L}(x_i;p_i) = \sum_\ell (2\ell+1)\Big[\ln\big(\frac{C_\ell^{theory}}{C_\ell^{sim}}\big) + \frac{C_\ell^{sim}}{C_\ell^{theory}} - 1\Big]$$

A.3.4 Likelihood code modifications

The original code has been replaced with following algorithm:

```
SUBROUTINE PASS2_COMPUTE_LIKELIHOOD(cltt,clte,clee,clbb,like)

  (Initialize variables)
  (Load the simulated HW model data file)

  ! Compute likelihood

  Likelihood = 0
  do i=ttmin,ttmax
    work = log(cltt(i)/cl_data(i)) + cl_data(i)/cltt(i) - 1
    Likelihood = Likelihood + (2*i+1) *work
  enddo

  like(2:8) = 0
  like(1) = 0.5*Likelihood ! return to CosmoMC
```

```
end SUBROUTINE PASS2_COMPUTE_LIKELIHOOD
```

where the *cltt* parameter is the model power spectrum C_l generated from CAMB that is to be tested.

A.3.5 Additional changes

Additional changes were done in the modules that call *SUBROUTINE_PASS2_COMPUTE_LIKELIHOOD* in order to prevent (log) zero likelihoods. Also, other parts of CosmoMC was modified to include the two new parameters ϵ and ξ.

A.4 Independent software

Five *independent* programs and scripts created by the author have seen use in this thesis.

- **SH** is a program that calculates the spherical harmonics for different ℓ and m, and displays them by the Mollweide projection.
- **DHO** is a small program that calculates the amplitude of a driven, damped harmonical oscillator. The software takes batch input parameters.
- **Generate** is a program that takes a CAMB CMB power spectrum as input, and outputs a simulated χ^2 data set to file. The program accepts batch input parameters.
- **TimeLine** is a small program that calculates a schematic scale factor for different universe models.
- The most important program written by the author is the *batch-script* **Like** that generated the exact $1D$ and $2D$ likelihood landscapes, as presented at the end of chapter 9.

Appendix B

A note on trans-planckian physics

Here, we present a thorough derivation of the modified power spectrum (equation 8.3, page 92) discussed in [23].

B.1 Initial conditions

Section goal B.1.1. *Derive an expression for* $|A_k|$

The author first considers the standard treatment of the fluctuations in inflation. In chapter 4 , we found that the general solution to (8.2.1) is given by

$$f_k(\eta) = \frac{A_k}{\sqrt{2k}} e^{-ik\eta}\Big(1 - \frac{i}{k\eta}\Big) + \frac{B_k}{\sqrt{2k}} e^{ik\eta}\Big(1 + \frac{i}{k\eta}\Big)$$

and

$$g_k(\eta) = A_k\sqrt{\frac{2}{k}} e^{-ik\eta} - B_k\sqrt{\frac{2}{k}} e^{ik\eta}$$

Where now A_k and B_k are different Bogoliubov coefficients. Working backwards, we find from (8.2) that

$$v_k^*(\eta) = u_k(\eta) - \sqrt{\frac{2}{k}} g_k(\eta)$$

and

$$u_k(\eta) = \sqrt{2k} f_k(\eta) - v_k^*(\eta) = \sqrt{2k} f_k(\eta) - u_k(\eta) + \sqrt{\frac{2}{k}} g_k(\eta)$$

such that

$$u_k(\eta) = \frac{1}{2}\Big(\sqrt{2k} f_k(\eta) + \sqrt{\frac{2}{k}} g_k(\eta)\Big)$$

When inserting the assumed g_k and f_k, we find

$$u_k(\eta) = \frac{1}{2}\Big(A_k e^{-ik\eta}\Big(1 - \frac{i}{k\eta}\Big) + B_k e^{ik\eta}\Big(1 + \frac{i}{k\eta}\Big) + A_k\sqrt{e}^{-ik\eta} - B_k\sqrt{e}^{ik\eta}\Big)$$

which in turns give

$$u_k(\eta) = \frac{1}{2}\Big(A_k e^{-ik\eta}\Big(2 - \frac{i}{k\eta}\Big) + B_k e^{ik\eta}\frac{i}{k\eta}\Big)\Big)$$

Similarly, we find

$$v_k^* = \frac{1}{2}\Big(B_k e^{ik\eta}\Big(2 + \frac{i}{k\eta}\Big) - A_k e^{-ik\eta}\frac{i}{k\eta}\Big) \tag{B.1}$$

From the hyperbolic identity that $|u_k|^2 - |v_k|^2 = 1$, we find that $|A_k|^2 - |B_k|^2 = 1$ Recall from the choice of vacuum (8.2.3) that $v_k(\eta_0) = 0$ at some initial moment η_0. This means from (B.1) that

$$B_k e^{ik\eta}\Big(2 + \frac{i}{k\eta}\Big) = A_k e^{-ik\eta}\frac{i}{k\eta}$$

and hence

$$B_k = A_k \frac{e^{-2ik\eta_0}}{2k\eta_0 + i} \tag{B.2}$$

Squaring this expression and using the hyperbolic identity, we find

$$|B_k|^2 = |A_k|^2|\alpha_k|^2 = |A_k|^2 - 1$$

where $\alpha_K = i/(2k\eta_0 + i)$. Solving for $|A_k|^2$ we find

$$|A_k|^2(1 - |\alpha_k|^2) = 1$$

such that

$$|A_k|^2 = \frac{1}{(1 - |\alpha_k|^2)} \tag{B.3}$$

B.2 The fluctuation spectrum

Section goal B.2.1. *Derive the expression of the modified power spectrum (8.3)*

The power spectrum in co-moving coordinates is given by

$$P_\phi = \frac{1}{a^2}P_\mu = \frac{k^3}{2\pi^2 a^2}|f_k|^2$$

We find $|f_k|^2$:

$$|f_k(\eta)|^2 = \frac{|A_k|^2}{2k}\Big|\Big(1 - \frac{i}{k\eta}\Big)\Big|^2 + \frac{|B_k|^2}{2k}\Big|\Big(1 + \frac{i}{k\eta}\Big)\Big|^2 + \Big|\frac{1}{2k}\Big(1 + \frac{1}{k^2\eta^2}\Big)\Big|\big(A_k^* B_k + A_k B_k^*\big)$$

assuming later times $\eta \to 0$, so only the second order terms of η contributes:

$$|f_k(\eta)|^2 \approx \frac{1}{2k^3\eta^2}\Big(|A_k|^2 + |B_k|^2 - A_k^* B_k - A_k B_k^*\Big)$$

The power spectrum is then

$$P_\phi = \frac{1}{4\pi^2 a^2 \eta^2}\Big(|A_k|^2 + |B_k|^2 - A_k^* B_k - A_k B_k^*\Big)$$

Using that $|B_k|^2 = |A_k|^2 - 1$ and that $\eta = -1/aH$, we get

$$P_\phi = \Big(\frac{H}{2\pi}\Big)^2\Big(2|A_k|^2{-}1{-}A_k^*B_k{-}A_kB_k^*\Big) = \Big(\frac{H}{2\pi}\Big)^2\Big(2{-}\frac{1}{|A_k|^2}{+}\frac{1}{|A_k|^2}\big(A_k^*B_k{+}A_kB_k^*\big)\Big)|A_k|^2$$

Using equation (B.3), we get

$$P_\phi = \Big(\frac{H}{2\pi}\Big)^2\Big(1 + |\alpha_k|^2 - \frac{1}{|A_k|^2}\big(A_k^*B_k + A_kB_k^*\big)\Big)\frac{1}{1-|\alpha_k|^2}$$

Finally, from (B.2) note that

$$A_k^*B_k = |A_k|^2(ie^{-2ik\eta_0})\alpha$$

and similarly

$$A_kB_k^* = |A_k|^2(ie^{2ik\eta_0})\alpha^*$$

such that

$$P_\phi = \Big(\frac{H}{2\pi}\Big)^2\Big(1 + |\alpha_k|^2 - \alpha e^{-2ik\eta_0} - \alpha^* e^{2ik\eta_0})\Big)\frac{1}{1-|\alpha_k|^2}$$

The author then does something "different": for a given k, choose η_0 such that the physical momentum corresponding to k is given by some fixed scale Λ. Λ signifies the energy scale of the new physics, e.g the Planck scale. So for $p = \Lambda$ we have

$$k = ap = a\Lambda = -\frac{\Lambda}{\eta_0 H}$$

meaning

$$\eta_0 = -\frac{\Lambda}{kH}$$

The author then makes the assumption that $\Lambda/H \gg 1$. This means $|\eta_0 k| \gg 1$, which implies early in the inflation period. Then from equation (B.3) we find that $|\alpha|^2 \approx 0$, and $\alpha \approx \frac{1}{2}\frac{H}{\Lambda}$. We then find

$$P_\phi = \Big(\frac{H}{2\pi}\Big)^2\Big(1 - \frac{H}{\Lambda}\sin\big(\frac{2\Lambda}{H}\big)\Big) \tag{B.4}$$

which is the desired result.

Appendix C

Can MAP and Planck map Planck physics?

In chapter 8 we used both familiar and new parameters to rewrite the modified power spectrum (8.3). In this section, we present the derivation of the relations between the parameters $\xi, \epsilon_{sr}, H, \gamma$ and Λ

C.1 Parameter relations

Section goal C.1.1. *Derive the relations between $\xi, \epsilon_{sr}, \gamma, H$ and Λ*

When a mode crosses the horizon ($k = aH$), H is to be *evaluated*. We differentiate and find

$$dk = Hda + adH \approx Hda$$

where we have used that H varies very little. Using that $da = \dot{a}dt = k\,dt$, we have

$$dk = kHdt$$

from slow roll condition 2 (4.4), we find dt:

$$\dot{\phi} = \frac{d\phi}{dt} = -\frac{V'}{3H}$$

$$dt = -\frac{3H}{V'}d\phi$$

and we find

$$dk = -Hk\frac{3H}{V'}d\phi = 3k\frac{H^2}{V'}d\phi$$

Using that $V \approx H^2/3M_p^2$, we find

$$dk = -\frac{k}{M_p^2}\frac{V}{V'}d\phi$$

reorganizing, we find

$$\frac{d}{dk} = -\frac{M_p^2}{k}\frac{V'}{V}\frac{d}{d\phi}$$

So, how much does H vary with respect to k?

$$\frac{dH}{dk} = -\frac{M_p^2}{k}\frac{V'}{V}\frac{dH}{d\phi}$$

using the SRA, $H \sim \sqrt{V}$ such that

$$\frac{dH}{dk} = -\frac{M_p^2}{k}\frac{V'}{V}\frac{1}{2\sqrt{V}}V' \approx -\frac{M_p^2}{k}\Big(\frac{V'}{V}\Big)^2\sqrt{V}$$

Recognizing the slow roll-parameter and H, we finally end up with a relation between H, k and ϵ:

$$\frac{dH}{dk} = -\frac{\epsilon_{sr}H}{k}$$

Integrating this separable first order differential equation, we find

$$H \sim k^{-\epsilon_{sr}}$$

This k-dependence will translate into a modulation of the power spectrum $P(k)$, with a period given by

$$\frac{\Delta k}{k} \sim \frac{\pi H}{\epsilon\Lambda}$$

Recall that the power spectrum of the co-moving curvature scalar was given by (5.17)

$$\Delta^2_{\mathcal{R}}(k) = \Big[\Big(\frac{H}{\dot{\phi}}\Big)^2\Big(\frac{H}{2\pi}\Big)^2\Big]_{k=aH} \tag{C.1}$$

Using the slow roll conditions, this may be written as

$$\Delta^2_{\mathcal{R}}(k) = \frac{1}{24\pi^2 M_p^4}\frac{V}{\epsilon_{sr}} \tag{C.2}$$

Measurements restrict this value to be

$$\frac{V^{1/4}}{\epsilon_{sr}^{1/4}} \sim 0.027 M_p \equiv \beta M_p$$

Using the Friedmann equations

$$H^2 = \frac{V}{3M_p^2} \sim \frac{1}{3}\beta^4\epsilon$$

this means

$$\frac{H}{M_p} \sim \frac{\beta^2\sqrt{\epsilon}}{\sqrt{3}} \sim 4\cdot 10^{-4}\sqrt{\epsilon}$$

Bibliography

[1] J. Martin and Christophe Ringeval. Superimposed oscillation in the wmap data? *aXiv:hep-ph/0310382v2*, 2004.

[2] Jerome Martin and Christophe Ringeval. Inflation after wmap3: Confronting the slow-roll and exact power spectra with cmb data. *JCAP*, 0608:009, 2006.

[3] Thorne K.S. Misner, C.W. and J.A. Wheeler. Gravitation, 1973.

[4] I. K. Wehus Ø. Gr. Lecture notes on general relativity, 2006.

[5] M. Nakahara. *Geometry, Topology and Physics, Second Edition (Graduate Student Series in Physics)*. Taylor & Francis, June 2003.

[6] Robert Geroch. *Mathematical Physics*. Chicago Lectures in Physics, 1985.

[7] Ø. Elgarøy and S. Hannestad. Can Planck-scale physics be seen in the cosmic microwave background? , 68(12):123513–+, December 2003.

[8] Scott Dodelson. *Modern Cosmology*. Academic Press, March 2003.

[9] Andrew R. Liddle and David H. Lyth. *Cosmological Inflation and Large-Scale Structure*. Cambridge University Press, April 2000.

[10] W. L. Freedman et al. Final results from the hubble space telescope key project to measure the hubble constant. *Astrophys. J.*, 553:47–72, 2001.

[11] G. K. Johnsen J. R. Kristiansen F. Ravndal, Ø. Rudjord. Lecture notes on cosmological physics, 2006.

[12] Francesco Lucchin Peter Coles. *Cosmology - The Origin and Evolution of Cosmic Structure*. Wiley, 2002.

[13] Michael E. Peskin and Daniel V. Schroeder. *An Introduction to Quantum Field Theory*. Perseus Books, Cambridge, Massachusetts, 1995.

[14] Morad Amarzguioui. Cosmological perturbation theory and gravitational entropy. Master's thesis, University of Oslo, 2003.

[15] N.D. Birrell and P.C.W. Davies. *Quantum fields in curved space*. Cambridge Monographs on Mathematical Physics. Cambridge University Press, Cambridge, 1982.

[16] Gorm Krogh Johnsen. Cosmological inflation with two scalar fields. Master's thesis, University of Oslo, 2006.

[17] Jostein Riiser Kristiansen. Massive neutrinos and cosmology. Master's thesis, University of Oslo, 2006.

[18] *LISA web page: http://lisa.jpl.nasa.gov/*.

[19] G. F. Smoot, M. V. Gorenstein, and R. A. Muller. Detection of anisotropy in the cosmic blackbody radiation. *Physical Review Letters*, 39:898–901, 1977.

[20] L. Verde, H. V. Peiris, D. N. Spergel, M. Nolta, C. L. Bennett, M. Halpern, G. Hinshaw, N. Jarosik, A. Kogut, M. Limon, S. S. Meyer, L. Page, G. S. Tucker, E. Wollack, and E. L. Wright. First year wilkinson microwave anisotropy probe (wmap) observations: Parameter estimation methodology. *The Astrophysical Journal*, 148:195, 2003.

[21] Antony Lewis and OPThowpublished = OPTmonth = OPTyear = OPTnote = OPTannote = Anthony Challinor, title = CAMB.

[22] Uros Seljak and Matias Zaldarriaga. A line of sight approach to cosmic microwave background anisotropies. *The Astrophysical Journal*, 469:437, 1996.

[23] Ulf H. Danielsson. A note on inflation and transplanckian physics. *Physical Review D*, 66:023511, 2002.

[24] Lars Bergström and Ulf H. Danielsson. Can map and planck map planck physics? *Physical Review D*, 66:023511, 2002.

[25] Petr Horava and Edward Witten. Heterotic and type i string dynamics from eleven dimensions. *Nuclear Physics B*, 460:506, 1996.

[26] U. H. Danielsson. Transplanckian signatures in WMAP3? *ArXiv Astrophysics e-prints*, June 2006.

[27] R. H. Brandenberger. Inflationary cosmology: Progress and problems. *aXiv:hep-ph/9910410*.

[28] Jerome Martin and Christophe Ringeval. Addendum to.

[29] Jerome Martin and Christophe Ringeval. Exploring the superimposed oscillations parameter space. *JCAP*, 0501:007, 2005.

[30] D. N. Spergel et al. Wilkinson microwave anisotropy probe (wmap) three year results: Implications for cosmology. *Astrophys. J. Suppl.*, 170:377, 2007.

[31] G. Hinshaw et al. Three-year wilkinson microwave anisotropy probe (wmap) observations: Temperature analysis. *Astrophys. J. Suppl.*, 170:288, 2007.

[32] Anthony Lewis. *CosmoMC documentation*. http://cosmologist.info/cosmomc/readme.html.

[33] *Sloan Digital Sky Surbey web site, http://www.sdss.org*.